UC San Diego

UC San Diego Electronic Theses and Dissertations

Title

Tailored Ceramics for Laser Applications

Permalink

https://escholarship.org/uc/item/5rh80881

Author

Hollingsworth, Joel Philip

Publication Date

2013

Peer reviewed|Thesis/dissertation

eScholarship.org Powered by the California Digital Library
University of California

UNIVERSITY OF CALIFORNIA, SAN DIEGO

Tailored Ceramics for Laser Applications

A dissertation submitted in partial satisfaction of the
requirements for the degree
Doctor of Philosophy

in

Materials Science and Engineering

by

Joel Philip Hollingsworth

Committee in charge:

Mark Tillack, Chair
Marc Meyers
Farrokh Najmabadi
Kenneth Vecchio
Deli Wang

2013

Copyright
Joel Philip Hollingsworth, 2013
All rights reserved.

The dissertation of Joel Philip Hollingsworth is approved, and it is acceptable in quality and form for publication on microfilm and electronically:

_____

_____

_____

_____

_____

Chair

University of California, San Diego

2013

DEDICATION

The process of carrying out research and crafting the result into a dissertation has been, among other things, a dialogue about what I am capable of.

This is dedicated to everyone who engaged in that dialogue.

EPIGRAPH

...I'll find that
Things are fine,
And they're gonna get
Much finer.
—Kathleen Hanna

TABLE OF CONTENTS

LIST OF FIGURES

LIST OF TABLES

ACKNOWLEDGEMENTS

I am deeply grateful to everyone who offered practical, conceptual, and moral support as I worked through this project. The list of people who made this dissertation possible stretches back at least as far as whatever genius in Ethiopia first noticed something special in the seeds of the coffee fruit (the notional "caffeine Eve"). I can't name them all here, but I would like to first thank them collectively, and I can at least name a few of the more direct and personal contributors.

Thomas Soules and Joshua Kuntz were early and frequent supporters in countless ways. Dr. Soules provided the opportunity and sustained the space that allowed any achievement on my part. He was also a great source of perspective on the development of transparent ceramics technology, and on important aspects of theory such as Mie scattering. Dr. Kuntz showed me the ropes in the laboratory and participated in countless technical discussions. Eric Ryerson measured Nd concentrations via electron microprobe with wavelength dispersive spectrometry, which was crucial to this work. All three were co-authors, and helped me to prepare my kinetics results for publication, along with *Optical Materials*. I am deeply grateful to everyone at Elsevier for their work to make science accessible: not only did they make it convenient for me to access and build on work that they had previously published, they have also graciously licensed my work for re-publication here. Portions of Chapters 3 and 5 are adapted from material as it appears in Joel P. Hollingsworth, Joshua D. Kuntz, Frederick J. Ryerson, and Thomas F. Soules, "Nd diffusion in YAG ceramics", *Optical Materials*, 33 (4), pp. 592-595, 2011. The dissertation author was the primary investigator and author of this paper. Section 2.1 of Chapter 2 has also been published, with some changes and additions, in the Lawrence Livermore National Laboratory internal technical report: Joshua D. Kuntz, Joel P. Hollingsworth, and Thomas F. Soules, "Transparent Ceramics for Lasers", UCRL-JRNL-237245. (12 December 2007). The dissertation author was the primary investigator and author of the content presented in this section.

The fresh perspective of Zachary Seely, combined with the wealth of experience that Richard Landingham offered, made ceramic technology much more

approachable. It was truly a joy to work alongside them. So many other colleagues at LLNL deserve mention that I am likely to forget at least one. Kathleen Schaffers, Edward Lindsey, Stephan Letts, and Alex Gash are only just the beginning. The Oakland-Livermore carpool and the long-suffering administrative staff also made this possible, as did a host of other generous people I had the privilege to work with.

Marca Doeff, among many others at the University of California and at LBNL, first encouraged me to pursue a career in scientific research, and provided a first-hand example of just how large a project could be animated by the joy of discovery. She once said that I had a "flair for research," and worked in many ways to connect me to opportunities. Since then, Prabhakar Bandaru, Mark Tillack, and Jeffrey Latkowski have also supervised my research, and each guided my development as a scientist. Much of what I learned from them has only come to my attention as my work has become more independent, and I imagine that even more will only occur to me in the course of supervising others' work.

UC San Diego has made this possible in many ways, both obvious and subtle. My committee has played the most direct role, and I'm grateful for their patient attention and ongoing effort. Charlotte Lauve has opened many doors and shown empathy and infectious determination. My classmates and colleagues also contributed in ways that have far outlasted our time together: I aspire to the attitudes of John Pulsifer and David Selby, and Kevin Sequoia raised a question that probably delayed this work but has certainly improved my understanding. Everyone who put up with me when my questions were impertinent in one or both senses of the word also deserves some credit, and quite a few such people were at UCSD. For this, as much as all the skills and information they have shared, I appreciate all the professors and teachers who prepared me for academic success.

My friends from the Irish folk dance community also contributed greatly. Among others are Elizabeth Jennings and her children Griffin and Willow, who brought me back to the work of teaching science at a crucial time; Liana Lareau, who offered indispensible help when I first got serious about typesetting; Arthur Weidmer, who helped me to work through the error and uncertainty and to arrive

at an interval of confidence (pardon the puns) as I re-examined statistics; and Suzanne Lundy, who set a challenging pace for us as she finished her own thesis and generously helped me to proofread.

Samantha Lehman and my parents, Mark and Nancy Hollingsworth, have sacrificed in a deep and sustained way for my commitment to this work and to the work that will follow it. They have met my inexplicable delays, mounting costs, and struggles of all sorts with steady and loving support of every description. I am humbled by how much they have given and emboldened by their example. I am excited to carry on giving as they have: to science, to family, and to whatever my hand finds to do.

VITA

2002	B. S. in Materials Science, University of California, Berkeley
2003-2006	Graduate Teaching Assistant, University of California, San Diego
2006	M. S. in Materials Science and Engineering, University of California, San Diego
2006-2010	Student Researcher, Lawrence Livermore National Laboratory
2013	Ph. D. in Materials Science and Engineering, University of California, San Diego

PUBLICATIONS

Marca M. Doeff, Thomas J. Richardson, Joel Hollingsworth, Chun-Wei Yuan, and Marcela Gonzales, "Synthesis and characterization of a copper-substituted manganese oxide with the $Na_{0.44}MnO_2$ structure", *Electrochemical and Solid State Letters; Journal*, 112 (1), 2002.

Tom A. Eriksson, Young Joo Lee, Joel Hollingsworth, Jeffrey A. Reimer, Elton J. Cairns, Xiao-feng Zhang, and Marca M. Doeff, "Influence of Substitution on the Structure and Electrochemistry of Layered Manganese Oxides", *Chemistry of Materials*, 15 (23), pp 4456–4463, 2003.

Marca M. Doeff, Joel P. Hollingsworth, Joongpyo Shim, Young Joo Lee, Kathryn Striebel, Jeffrey A. Reimer, and Elton J. Cairns, "Sulfur-Doped Aluminum-Substituted Manganese Oxide Spinels for Lithium-Ion Battery Applications", *Journal of the Electrochemical Society*, 150 (8), pp. A1060–A1066, 2003.

Marca M. Doeff, Joel Hollingsworth, and Jyoongpyo Shim, "Factors influencing the Electrochemical Behavior of Sulfur-doped Aluminum-substituted Lithium Manganese Oxide Spinels in Lithium Cells", Journal of The Electrochemical Society, 2003. Retrieved from:
https://community.electrochem.org/dl/ma/201/pdfs/0825.pdf

Joel P. Hollingsworth, Joshua D. Kuntz and Thomas F. Soules, "Neodymium ion diffusion during sintering of Nd:YAG transparent ceramics", *Journal of Physics D: Applied Physics*, 42 (5), 2009.

Joel P. Hollingsworth, Joshua D. Kuntz, Frederick J. Ryerson, and Thomas F. Soules, "Nd diffusion in YAG ceramics", *Optical Materials*, 33 (4), pp. 592-595, 2011.

Joshua D. Kuntz, Thomas F. Soules, Richard L. Landingham, and Joel P. Hollingsworth, "Slip Casting Nano-Particle Powders for Making Transparent Ceramics", US Patent #7,922,965, 2011.

Joel P. Hollingsworth, Joshua D. Kuntz, Zachary M. Seely, and Thomas F. Soules, "Transparent Ceramics and Methods of Preparation Thereof", US Patent #8,039,413, 2011.

Joel P. Hollingsworth, Joshua D. Kuntz, Thomas F. Soules, and Richard L. Landingham, "Compound Transparent Ceramics and Methods of Preparation Thereof", US Patent #8,329,090, 2012.

Joel P. Hollingsworth, Joshua D. Kuntz, Zachary M. Seely, and Thomas F. Soules, "Transparent Ceramics and Methods of Preparation Thereof", US Patent #8,338,322, 2012.

Thomas F. Soules, Kathleen I. Schaffers, John B. Tassano Jr., Joel P. Hollingsworth, "Method for Fabricating Apatite Crystals and Ceramics", US Patent #8,529,859, 2013.

Prabhakar R. Bandaru and Joel Hollingsworth, "Nanostructue-based Memory", U. S. Patent # 8541776, 2013.

ABSTRACT OF THE DISSERTATION

Tailored Ceramics for Laser Applications

by

Joel Philip Hollingsworth

Doctor of Philosophy in Materials Science and Engineering

University of California, San Diego, 2013

Mark Tillack, Chair

Transparent ceramics have many features that recommend them over single crystals for use as laser amplifiers. Some features, such as greater mechanical toughness and an absence of extended crystalline defects, are intrinsic to polycrystalline materials. Other advantages accrue from ceramic processing: ceramics sinter more rapidly than crystals grow from a melt, at lower temperatures. Ceramic processes are more readily scaled than Czochralski growth, facilitating larger apertures. Unlike a uniform melt, a ceramic green structure can have controlled concentration gradients, resulting in a multifunctional device upon sintering. Identifying diffusion mechanisms in a suitable host material and quantifying diffusion for a dopant with appropriate energy levels are key steps toward tailoring laser ceramics to the specifications of device designers. Toward that end, this study was the first to

identify the mechanism and rate of Nd diffusion in YAG. Grain boundary diffusion was shown to dominate Nd transport under conditions relevant to laser ceramics fabrication. Based on a definition of grain boundary width as 1 Å, this process occurs at a rate of $D_{GB} = 6.4 \times 10^5 \pm 2.0 \times 10^5 \exp(-491 \pm 64\mathrm{kJ/(mol\,K)})\mathrm{m}^2/\mathrm{s}$. Mechanism identification and the first published kinetics measurement were made possible by the introduction of a heat treatment method that isolates microstructural change from dopant diffusion: the concentration of grain boundaries was kept great enough to allow rapid diffusion, but low enough to limit the driving force for coarsening. Sintering of fine-grained and phase-pure precursor powder for 4 min at 1700 °C produced 0.8 µm grains; subsequent diffusion heat treatments at up to 1650 °C for up to 64 h caused negligible coarsening, while achieving diffusion distances of up to 23 µm.

Part I
Introduction

Chapter 1

Overview

1.1 Laser ceramic basics

Transparent ceramics are fabricated by sintering high-purity powders to form a fully-dense polycrystalline body with a cubic crystal structure. Such materials must be without significant birefringence, phase inhomogeneity, or porosity: these scatter light, and would result in a material that is translucent or opaque. Several decades of improvement, detailed in Section 2.1, have resulted in ceramics that are transparent enough to be used as gain media for lasers.

1.1.1 Advantages of laser ceramics

Transparent ceramics can match or exceed the performance of single crystals in laser applications. For instance, neodymium-doped yttrium-aluminum garnet (Nd:YAG) ceramics have been produced with scattering coefficients of less than 0.15%/cm, which is better than the 0.2-0.4%/cm observed in Nd:YAG single crystals grown by the Czochralski method[1].

Ceramic amplifiers have many advantages over single crystals, including greater mechanical toughness[2], less residual stress, better optical homogeneity[3], and fewer constraints on dopant distribution and solubility.

The increase in toughness is due to microstructure: grain boundaries within ceramics frustrate crack propagation, making the material less brittle and more

resistant to mechanical damage.

Small grains also prevent defects such as twin boundaries from extending far enough to significantly degrade optical properties, resulting in better overall homogeneity.

Another source of optical defects in single crystals is residual stress, which is intrinsic to the growth process. A temperature gradient is necessary to drive the growth of a crystal from a melt, but a temperature gradient also entails a gradient in thermal contraction across the boule. The resulting elastic strain is literally frozen into single-crystal amplifiers. Strain-induced birefringence, in turn, leads to small but significant optical effects. By contrast, a ceramic slab is sintered at a very nearly constant temperature throughout its volume, and the large volume change that occurs due to sintering allows for a nearly complete release of residual stress.

The growth of single crystals also places constraints on the distribution of optical dopants. The solute concentration profile of a single crystal grown from a melt is dictated by the segregation ratio for that particular crystal-solute pair. This ratio is only 0.18 for Nd^{3+} in yttrium-aluminum garnet (YAG)[4]. Rejection of solute into the melt causes a concentration gradient in melt-grown crystals, theoretically in the form shown in Figure 1.1. Since laser ceramics are formed without melting, they can be made with a uniform concentration. An increase in solubility below the melting point also allows Nd concentration in ceramics to be higher than is achievable in a high-quality single crystal[2].

While greater uniformity is possible in ceramics, a controlled nonuniformity of optical dopants is also an option. Of all the new opportunities facilitated by the development of laser ceramics, this might be the most exciting. A ceramic green body can have an arbitrary concentration profile and will remain solid during subsequent processing. This raises the possibility of a laser designer specifying a doping profile, and having a solid-state amplifier sintered to meet these specifications, its concentration tailored to the needs of the laser system. Subsection 2.1.5 discusses some early work toward this goal. The experiments presented in Chapters 3, 4 and 5 are focused on developing techniques for the fabrication of

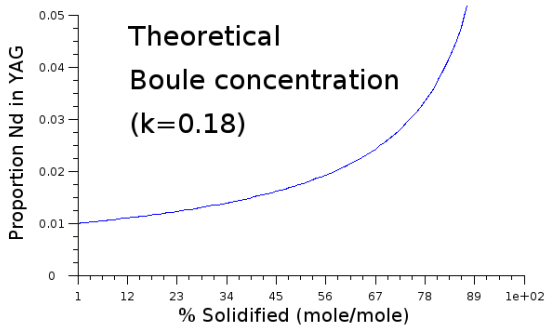

Figure 1.1: Theoretical concentration profile due to solidification from a perfectly-mixed melt, with no solid-state diffusion and a rejection ratio of 0.18.

tailored laser amplifiers, which achieve control of dopant concentration profile in ways that crystal growth does not allow.

1.1.2 Challenges to laser ceramic green-body tailoring

Several techniques for producing functionally-graded ceramics are available, but not many have been adapted to meet the demands of transparent ceramics. There have been a few successes in fabricating of tailored transparent ceramic green bodies, but the field is still under development.

Diffusion in transparent ceramics has usually only been studied for its role in sintering. With the advent of tailored laser ceramics, a non-uniform distribution of activator ions is becoming recognized as desirable, and diffusion must now be considered for its potential to re-arrange dopants in a way that affects laser performance. Some data are available on the diffusion of rare earth (RE) elements in YAG, but more study is needed before changes in dopant concentration profile can be predicted with any confidence.

This lack of predictive ability is apparent in the recent studies of engineered green structures discussed in Subsection 2.1.5. In one case, a diffusion distance larger than the intended doped region was observed[5]. That effort took into account a comparative study of RE diffusion in YAG[6]. However, it did not consider mechanisms beyond bulk diffusion *a priori*: instead, unexpectedly rapid diffusion was observed and was then explained as a result of enhanced mobility

in transient phases[5]. It is possible to design sintering processes that eliminate the possibility of transient phases, but other routes for rapid diffusion, including grain boundaries and free surfaces, present potential channels for dopant transport during any ceramic sintering process.

1.2 Scientific and engineering goals

This study addresses two particular needs: it advances research into the mechanism and rate of dopant diffusion during the sintering of transparent ceramics, and it advances fabrication technologies that allow for functionally-graded ceramics, including green body fabrication and sintering strategies.

Because diffusion had not been studied in this material system under these conditions, measurement of diffusion kinetics was a clear scientific need as this study was being planned. Efforts to quantify the rate of diffusion overlapped with efforts to identify the diffusion mechanism, which had not yet been determined conclusively. This scientific understanding developed in dialogue with advances in processing technology, which were informed by new insight while offering access to new experimental techniques.

This line of inquiry is part of a larger investigation of the new possibilities that transparent ceramics offer to the designers of optical systems, particularly the prospect of controlling the concentration profile of active species within optical devices such as solid-state amplifiers. A few potential applications of this control are listed in Subsection 2.1.5. The overall goal is to develop the field of tailored ceramics to the point that a ceramic green body can be sintered into a laser amplifier with the active ion distributed according to a practical design specification. Some parallels between ongoing developments in ceramic optics and the history of semiconductor electronics are outlined in Appendix A.

1.2.1 Choice of a model system

Nd:YAG is well-studied as a laser ceramic material, as evidenced by the body of literature cited in in Subection 2.1.4. A wide variety of techniques for

material synthesis and sintering have been published, and powder suitable for optical ceramics applications is commercially available. YAG is also the subject of a deep body of scientific literature beyond the field of optics, allowing some predictions of dopant migration during sintering to be made based on existing data.

Although the Nd:YAG system has been studied more thoroughly than other solid-state laser materials, it was clear from the outset that predicting the movement of Nd ions through a YAG ceramic over the full course of sintering would require some new data. In particular, it seemed that the field would benefit from an extension of the current knowledge of Nd diffusion in partially-sintered YAG.

The literature also offers a well-developed understanding of YAG ceramic processing and strategies to achieve transparency. This understanding should facilitate the development of appropriate fabrication techniques, but there remains the practical challenge of controling the concentration profile of dopants while maintaining the excellent optical properties of state-of-the-art transparent ceramics.

The Nd:YAG system was chosen because the literature on it was extensive enough to support further research, but still full of important opportunities. This material system is the best-developed laser ceramic material in terms of scientific understanding and technological capability, but important work remained.

1.2.2 Powder synthesis

As is apparent from a survey of the literature in Section 2.1, transparent ceramics can be rendered unsuitable for laser applications by contamination, errors in stoichiometry, or voids large enough to persist through the sintering process. Even a phase-pure sample can show poor laser performance, if local variations in composition cause the material's refractive index becomes inhomogeneous on a large enough scale[7].

YAG ceramics can be produced by sintering a mixture of pure yttria and pure alumina, and optionally, oxides of optically active elements. This mixed-oxide method has been developed thoroughly, and produces ceramics with good laser performance, so it was worth considering as a method for the fabrication of

diffusion couples. However, as mentioned in Subsection 1.1.2, transient phases that arise during sintering greatly complicate diffusion analysis. Reactions among the various oxides introduce the possibility of rapid diffusion through unstable phases and/or morphologies that are difficult to characterize and control[5]. Further, the individual powders vary in morphology, density, and surface properties, so that powder processing tends to introduce inhomogeneities in composition. Lastly, these methods require longer times at higher temperatures before the material reaches a state at which it is suitable for use as a diffusion sample. Considerations of experimental design suggested a different synthesis technique.

This work focuses on YAG synthesized by dissolving yttrium and aluminum compounds, allowing the solution to mix completely at room temperature, and then forming a powder from that solution. The focus is specifically on powders synthesized by flame-spray pyrolysis (FSP) and co-precipitation (CP). Both methods allow each particle to have nearly identical composition to its neighbors. Flame-spray pyrolysis has the additional benefit of relatively uniform composition within each powder particle[1] and of relatively fine, non-agglomerated powders. This uniformity in composition allows diffusion samples made from FSP powders to consist of a single phase (or a constant phase mixture) throughout the experiment. Non-agglomerated powders allow for a more-uniform green structure; this, along with finer powder, allows sintering to proceed relatively rapidly at a lower temperature than is possible with a mixed-oxide strategy, allowing diffusion samples to be prepared with shorter diffusion lengths, under conditions where diffusion would proceed at appreciable rates.

This choice of focus can be expected to make results more directly applicable to tailored laser ceramics derived from FSP powders than to ceramics produced by mixed-oxide methods. Further inquiry into the diffusion phenomena that operate during mixed-oxide sintering may become important to the success of tailored laser ceramics made by that method, but information on coarsening and grain boundary

[1]Powders prepared by precipitating multiple compounds display a composition gradient from the surface to the interior, or even a core-and-shell morphology, due to differences in solubility among the compounds being precipitated. If diffusion within a particle were not sufficient, these variations might complicate diffusion analysis of ceramics produced from precipitated powders.

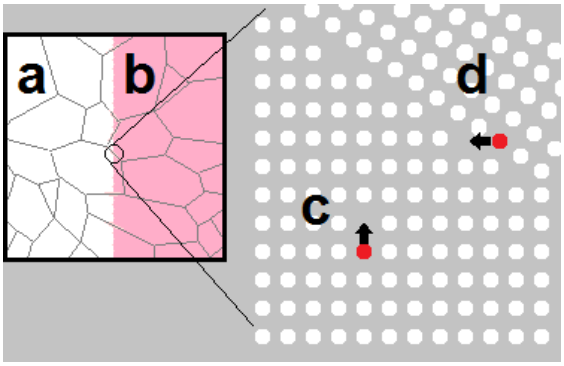

Figure 1.2: Schematic illustration of diffusion paths: At high temperature, atomic mobility is expected between un-doped (a) and Nd-doped (b) regions of YAG ceramic bodies. Among other potential mechanisms, two that can be expected to occur under a wide variety of circumstances are bulk diffusion (c), which is dependent upon vacancies within the lattice, and grain-boundary diffusion (d), which relies on extended defects between crystallites.

diffusion in phase-pure YAG is likely to apply to a wide variety of processes.

1.2.3 Nd diffusion

Diffusion conditions were chosen to be most relevant to sintering process design. The powder available as I began this work requires relatively high temperatures and long times to sinter to transparency; these conditions were chosen as the upper limit to the range of experimental conditions. Finer, FSP-derived powder became available as the research program went on. Due to its greater surface area and the concomitantly greater driving force for sintering, this powder was expected to sinter more rapidly and at lower temperature. Times and temperatures comprising the lower limit to the range of experimental condition were chosen so as to leave samples entirely opaque, even those composed of the finest powder currently available.

An initial concern was that multiple diffusion mechanisms would need to be accounted for under differing conditions. Changes in microstructure during sintering were expected to have important effects on ion mobility, potentially changing the dominant mechanism over time. The complication of enhanced diffusion due to transient phases, which had been seen in similar work by other researchers,

was expected to be much less relevant to FSP-derived ceramics. However, even the prospect of less-dramatic changes called for careful attention. In a worst-case scenario, the closure of pores and growth of grains characteristic of sintering might conceivably have made surface diffusion the dominant mechanism during the first stage of sintering, grain boundary diffusion the dominant mechanism after most pores had closed, and bulk diffusion the dominant mechanism once grains had grown larger than some threshold size. These latter two mechanisms are schematically illustrated in Figure 1.2.

Along with qualitatively identifying the mechanism or mechanisms of diffusion, it was, of course, important to quantify diffusion rates. This informed the choice of intervals between sets experimental conditions, in much the same way that the upper and lower limits were informed by established processing methods and anticipated innovations.

Diffusivity was measured by fabricating YAG diffusion couples, heat treating them, and analyzing measurements of the resulting concentration profiles across the interface between un-doped YAG and Nd:YAG. Chapter 3 focuses specifically on the development of experimental capabilities for diffusion research.

Chapter 4 revisits some of the dissertation author's preliminary work on heat-treatment and diffusion, providing a new analysis of raw data from an earlier experiment, and discussing evidence that diffusion through grain boundaries is the mechanism which controls the final Nd concentration profile under the conditions studied. These preliminary diffusion results informed the choice of experimental conditions for a further experiment, discussed in Chapter 5. This experiment was designed to more carefully manage microstructural change: all samples were sintered for a short time at moderate temperature, and samples were then separated for diffusion experiments at a range of lower temperatures and longer times.This strategy slowed microstructural change to a negligible rate, and enabled measurement of the kinetics of grain-boundary diffusion for Nd in YAG, which had not previously been published. The method of heat treatment used to obtain these results is also of interest, in that it allows sintering and dopant diffusion to be controlled independently.

The research presented in Part 2.2.3 was undertaken as part of a larger program of transparent ceramics research, in which efforts to isolate diffusion and integrate regions of different composition into devices are strongly linked to one another. However, the scope of Part 2.2.3 is limited to efforts directly relevant to diffusion rates and mechanisms.

The dissertation author's efforts to develop tailored ceramics technology, and the interplay of scientific and technological means and ends, provide additional context. Potential applications of the methods developed for diffusion research are discussed in Section 6.1. Some recent technological developments that are expected to support the field of transparent ceramics are mentioned, including work that the author participated in and selected results from other researchers whose work was carried out simultaneously are discussed in 6. Lastly, scientific and technological motivations for extending the diffusion work presented in Part 2.2.3 are briefly discussed in Chapter 7.

Chapter 2

Background

2.1 History of transparent ceramics

2.1.1 Early commercial translucent ceramics

The first commercial translucent ceramic was a fully-dense polycrystalline alumina (PCA) developed by the General Electric Company and trade-named Lucalox™. It was patented in 1962[8] and has been extensively used as the discharge envelope for high-pressure sodium lamps. Although not transparent, it diffusely transmits the sodium discharge light. More recently it is also being used as the discharge envelope for high-pressure metal-halide lamps, which, because of their high color rendition, are being used in both indoor and outdoor applications. The key to the development of nearly pore-free PCA was the addition of magnesia as a dopant to inhibit grain growth during sintering[9]. Earlier work on alumina showed that pores are closed during the final stages of sintering by material transported from grain boundaries via bulk diffusion[10, 11]. In traditional ceramics, grains often envelop pores during rapid growth, and the bulk diffusion path to remove them is too long for a practical rate of sintering to continue[12]. Lucalox PCA is fabricated by starting with a high purity alumina powder, such as that produced by Baikowski International through the ammonium alum process. The alumina powder is thoroughly blended with a suitable organic binder and a few hundred parts per million (ppm) by weight magnesia. Tubes or other parts are

extruded and, after baking out the binder at ≈ 1100 °C in air, the parts are sintered at ≈ 1800 °C in an atmosphere of hydrogen for 6 h[8]. Peelen[13] showed that PCA with quality similar to Lucalox could also be made by hot pressing alumina. Although the porosity in Lucalox PCA is very low, on the order of 0.1 % to 0.01 %, it is still too high for transparency. Soules[14] and later Peelen[15] showed through Mie scattering calculations that the optical properties of PCA can be explained by the remaining porosity. Soules also showed that the birefringence of alumina and the presence of magnesia dopants can be expected to cause rays of light to deviate, but not to contribut significantly to the reflectance of the material.

Transparent MgF_2 ceramics were first formed by vacuum hot-pressing this material. The process was patented[16] and used for making missile domes transparent in the infrared. Vacuum hot pressing of transparent CaF_2[17], LaF_3[18], MgO[19, 20], ZnO[21], ZnS[22] and other materials was developed and patented in the period between 1964 and 1968. W. F. Parsons[23] reviewed the history of optical elements made by hot pressing up to 1972.

By the late 1960s, two groups reported fabricating transparent yttria (Y_2O_3) ceramics by hot forging. Brissette *et al.*[24] thermo-mechanically deformed a pressed powder sample of yttria heated to 100 ℃ below sintering by pressing it without a die. They observed anisotropy in the grain orientation and showed higher transparency in the forged sample compared to a sample pressed uniaxially with a die. Lefever *et al.*[25] started with yttria powder ≈ 3 µm in size and milled it with 3 % to 5 % LiF by weight. The powder was first cold pressed and then subjected to a vacuum hot press similar to Brissette *et al.* When the temperature reached 850-900 ℃ and pressure 8.3 MPa, the die broke, and the forging began. The pressure was ramped to ≈ 80 MPa and held for 12 h. The workers claimed good transparency with transmission close to that of a single crystal.

Dutta and Gazza[26] also produced yttria ceramics with good transparency by hot pressing. The important processing conditions were the temperature at which pressure was applied, the heating rate and the use of a non-reactive spacer material between the anvil and the sample. Anderson[27, 28] developed Yttralox™ ceramic, a transparent yttria-based material containing also 2 % to 15 % ThO_2,

ZrO_2 or HfO_2 (mole basis). As for PCA, dopants served to inhibit the growth of grains. Yttralox ceramic was prepared by thoroughly mixing the powders, cold pressing at 70 MPa and then sintering in hydrogen in a Mo strip furnace at 2000 °C to 2200 °C for 4 h with no external pressure.

2.1.2 The first laser ceramics (1964–1975)

Fluorides

Hatch, Parsons and Weagley[29] at Eastman Kodak Company were the first to report laser amplification from polycrystalline ceramics, Dy^{2+}:CaF_2 and Dy^{2+}:SrF_2. The fluoride ceramics were prepared by first vacuum melting the desired portions of CaF_2 and DyF_2 and then pulverizing the solidified material to ≈150 μm. The ceramics were fabricated by vacuum hot pressing similar to that described in the references above. The ceramic Dy^{2+}:CaF_2 was transparent and exhibited laser oscillation at cryogenic temperatures. However, performance was not as good as for single-crystal Dy^{2+}:CaF_2 lasers. Lower efficiency was attributed to scattering by very fine inclusions of perhaps CaO.

Yttria

The first polycrystalline oxide laser was Yttralox, with ≈ 10 % ThO_2 as a grain growth inhibitor and 1 % Nd_2O_3 as the optically-active dopant ion, reported by Greskovich and Chernoch[30] in 1973. Appropriate amounts of the nitrates were dissolved and dripped into a solution of oxalic acid to co-precipitate a mixed oxalate salt, which was washed and calcined to form an oxide powder. The powder was cold pressed, then sintered in dry hydrogen (dew point 70 ℃) for 6 h at 2170 °C[31]. The authors' discussion of their results emphasizes the importance of ball milling the powder before sintering, relating this processing step to decreased porosity in the finished parts. Pore densities were measured by counting pores observed under an optical microscope and were typically less than one to a few ppm[32]. Unfortunately, laser slope efficiencies were much lower than expected and laser thresholds were higher. They attributed the low laser efficiency to local variations

in the material's index of refraction[7].

Subsequently, a number of other methods were published with the goal of achieving transparency using a second phase during sintering. Additives studied included BeO[33], Al_2O_3[34], ceMgO[34], La_2O_3[35, 36], and LiF[37]. Some of these were chosen to be transient phases, which would influence the sintering process and subsequently evaporate or re-dissolve.

2.1.3 Transparent ceramics (1975–1995)

Following the work of Greskovitch and Chernoch there is a period during which few, if any, reports were published of transparent ceramic materials being applied to lasers. In this period, which lasted until 1995, the field of transparent ceramics would develop in ways that impacted laser applications only indirectly, by introducing and developing processing techniques that would late become influential.

AlON

The optical anisotropy of non-cubic materials, such as α-alumina, will distort a beam of light passing through randomly oriented grains. However, the addition of aluminum nitride was found to stabilize the cubic γ-phase of alumina to form a material known as AlON or nitrogen-stabilized cubic alumina. There is a relatively wide range of compositional stability centered at $5\,AlN \cdot 9\,Al_2O_3$[38]. To make transparent AlON ceramics, α-alumina was ball milled with AlN in ethanol for 12 h. It was then isostatically cold pressed and pre-reacted at 1200 °C for 24 h. Sintering was carried out at 1975 °C in a BN-covered crucible. McCauley and Corbin[38] carried out a systematic study of phase equilibria for the AlN-Al_2O_3 system in flowing N_2, and, in the process, produced a translucent material. The Raytheon Company significantly improved the transparency of AlON ceramics by optimizing the process and adding a small amount of yttria ($\approx$ 600 ppm) and $\approx$ 100 ppm boron from crucibles[39]. Raytheon's ALON®ceramic has been made

in large pieces for use as missile windows and transparent armor[1].

Spinel

Another important transparent ceramic material considered for infrared missile windows and transparent armor is spinel, $MgAl_2O_4$. The first reports of translucent spinel are from 1974. Bratton[40] calcined a Mg/Al hydroxide CP powder at 1100 °C for 4 h. The powders were screened (approximately 200 mesh), ball milled and calcined at 1100 °C. A small amount of calcium, 0.5 % to 1.0 % by weight, was added by mechanically blending the powder in a calcium nitrate, sulfate or chloride salt solution, drying and again calcining to remove the volatile anions. Sintering was carried out first at 1500 °C in a vacuum and then 1750 °C to 1850 °C in a vacuum or an Ar atmosphere.

Since these early studies, numerous syntheses of spinel have been reported. In addition to using different high purity sources of Mg and Al, different sintering and compacting techniques have been used. Hot pressing[41] achieved better results than those quoted above for sintering without pressure. Hot pressing of transparent spinel generally requires adding a small amount ($\approx$ 2 % by weight) of LiF as a sintering aid[42]. Villalobos *et al.*[43], at the Naval Research Laboratory, claimed that reproducible fabrication of high-transparency spinel requires a homogenous distribution of LiF in the precursor material. LiF must also volatilize out of the material, which can limit the thickness of a finished ceramic body.

Sample preparation by Li *et al.*[44] began with co-precipitation of a mixed carbonate. An aqueous solution of high-purity aluminum and magnesium nitrates was added drop-wise to a 0.15 M solution of NH_4HCO_3 with stirring at 50 °C. The solution was aged for 12 h and then suction filtered, washed, rinsed with ethanol and dried. The powder was isostatically pressed and vacuum sintered for 2 h. Shimada *et al.* used commercial spinel, magnesia and alumina powders, ball milled together for 16 h to 64 h, isostatically pressed, sintered, and further densified in a hot isostatic press (HIP)[45, 46]. HIPing was relatively new to ceramic fabrication

[1]The lowercase letter in "AlON" is consistent with chemical notation for aluminum; for purposes of this dissertation, this spelling denotes a generic compound. "ALON®", with all capital letters, is used to denote a particular brand name product based on this compound.

at that time. In order to prepare for this process, the green structure was sintered in a high vacuum to $\approx 92\,\%$ of theoretical density. Once a closed-pore structure was achieved, the sintered part was placed in a high-pressure vessel, and the vessel was heated and filled with Ar gas. High hydrostatic pressure [2] was applied to this cas, in order to close residual porosity.

Bickmore *et al.*[47] developed an FSP technique for making various ceramic raw materials. For spinel, a double alkoxide metal-organic is prepared by heating a suspension of the Al and Mg oxides or hydroxides in triethylamine and ethylene glycol at 200 ℃. After complexation, the solution is mixed with alcohol and fed into an oxygen-natural gas flame. The result is spherical $< 30\,\text{nm}$ sized non-agglomerated particles that are collected by means of an electrostatic precipitator. This type of precursor will be discussed in more detail in a later section. Due to its high surface area and non-agglomerated nature the powder is "active" in sintering. This attribute, combined with a high-pressure, low-temperature sintering, was what allowed the development of a transparent material with grains less than 100 nm in size[48].

Yttria

Vacuum-sintering followed by HIPing was also applied to yttria, producing $80\,\%$ in-line transmission without the need for any sintering aid. However, even when the initial vacuum sintering was kept to as short a time as possible, some reduction of the oxide occurred, and annealing in air was necessary to recover transparency[49]. This process was refined to include a grog of oxides, such as ZrO_2, to prevent reduction in the HIP vessel[50]. Hot pressing at lower temperatures, followed by a slightly higher-pressure HIPing step, yielded better-quality yttria without any reported reduction of the oxide[51]. In a very recent attempt at second-phase sintering, Belyakov[52] used $6\,\%$ (mole basis) HfO_2 to pin grains during the sintering of yttria. An in-line transmission of $64\,\%$ was achieved via vacuum sintering. Raytheon has developed yttria, spinel, and ZnSe windows large

[2] Discussion with Joshua Kuntz and other colleagues suggest that pressures of 200 MPa to 400 MPa are not uncommon in such a process.

enough for missile domes and other government applications[53]. The yttria windows were made by starting with 99.99 % Y_2O_3 powder, milled so that there were no agglomerates and an average particle size of 1 µm to 2 µm, and formed in a Teflon-coated mold placed in an isostatic press. The green body was heated to 1350 °C to 1450 °C to drive off volatile substances such as dispersants. It was sintered at a temperature of 1800 °C to 1900 °C to achieve closed porosity and then HIPed for 0.5 h to 10 h at 1700 °C to 1900 °C and under 170 MPa to 200 MPa of uniaxial pressure. The sample was later annealed in air at 1400 °C to 1800 °C to remove discoloration due to reduction[49].

ZnSe and other windows

ZnSe is the most commonly used optical window for infrared radiation with $\lambda = 5\,\mu m to 20\,\mu m$. Transparent ceramic ZnSe parts are commercially available, and are prepared by reacting H_2Se with zinc vapor in a chemical vapor deposition (CVD) process. Certain other materials, for example SiAlON[54, 55, 56, 57, 58, 59], LiAlON[60], aluminum magnesium oxynitride[61, 45] silicon nitride[62, 63] and aluminum nitride[64, 65, 66, 67] have been made translucent to transparent for potential window applications.

Scintillators—Eu^{3+}-doped rare-earth sesquioxides

Since the early 1980s, transparent ceramic scintillators have been progressively replacing single crystals in modern digital detectors, such as those on X-ray computer aided tomography (CAT) scanners and positron emission tomography (PET) scanners. Ceramics have many advantages over single crystals for scintillators. They provide much broader range of materials and are easier to fabricate. Scintillators for tomography absorb X-rays or gamma rays throughout a bar approximately 1 cm to 3 cm long and approximately 2 mm^2 in cross section, which serves as one pixel. The ionizing radiation excites luminescent dopant centers throughout the bar and is converted to a wavelength suitable for a silicon or other detector, via a process of relaxation and emission. The emitted radiation must be effectively transmitted by the bar to the detector at one end, but

some amount of scattering can be accepted (attenuation coefficients $< 100\,\%\,\mathrm{cm}^{-1}$). General Electric developed a transparent scintillator material with composition $Y_{1.34}Gd_{0.6}Eu_{0.06}Pr_{0.0001}O_3$[68] for its CAT scan systems. Gadolinia forms a solid solution with yttria up to $\approx 40\,\%$ (mole basis) while keeping the cubic bixbyite structure, and is added for its higher X-ray stopping power compared to Y. Eu^{3+} is the luminescent dopant or activator. It has near-unity quantum efficiency in yttria-gadolinia, and emits in a single narrow band at 611 nm. This emission spectrum is a good match to a silicon detector. Pr^{3+} or certain other dopants are added in small amounts to suppress afterglow, which is important since the detector bar will be addressed in every pass of the X-ray beam. This scintillator ceramic was developed over several years. According to the patent, it is fabricated by blending high purity yttria and gadolinia submicron powders with the desired rare-earth activators in the form of oxides. Alternatively, the inventors claim that the powder can be prepared by dissolving the appropriate amount of the nitrates in water and then adding this to a solution of oxalic acid, 80 % saturated at room temperature. The co-precipitated oxalates are washed, neutralized, filtered and dried in air and then calcined at 800 °C for 1 h. The powder is then ball milled or fluid-energy milled to break up aggregates that would cause porosity in the final product. The green structure is prepared by cold pressing the powder and then isostatically pressing to further increase the green density. The green body is sintered at 1800 °C to 2100 °C in a vacuum or in wet hydrogen (dew point 23 °C) for 1 h to 30 h. Alternatively, the powder may be pre-sintered at 1500 °C to 1700 °C to achieve closed porosity at 93 % to 98 % of its theoretical density and then HIPed at 1750 °C[69]. The resulting ceramic is black due to reduction but is rendered transparent by heating in air at 1200 °C for 32 hour. Yttria-gadolinia scintillators can also be prepared by hot pressing. If the oxalate precipitate is further refined by agitating an aqueous suspension while admixing an effective amount of ammonium hydroxide to increase the pH to 8 to 10, then it is possible to prepare the scintillator material by pressureless sintering at 1800 °C to 2100 °C in wet hydrogen[70, 71]. Lu_2O_3:Eu^{3+} was studied as a highly efficient scintillator for digital radiography and fluoroscopy, to on the grounds that its X-ray stopping power is even greater

than yttria-gadolinia [72]. Both laser and scintillator materials were produced by co-precipitation of rare-earth nitrate solutions using oxalic acid. After washing and calcinations, the green structure was hot pressed and then heated in air for 2 h at 1200 °C to remove reduction discoloration.

Scintillators—gadolinium oxysulfide:Pr^{3+}

Transparent ceramic $(Gd_0{\cdot}999\,Pr_0{\cdot}001\,Ce_0{\cdot}0001)_2O_2S$ was developed by the Siemens Company for X-ray tomography about the same time as yttria-gadolinia. Because it is not cubic there is some refraction, reflection and birefringence at grain boundaries. However it can be made transparent enough for the CAT scanner. The oxysulfide is prepared starting with a water suspension of the appropriate amounts of the oxides. One mole of sulfuric acid is added per mole of rare earth ions. The reaction is carried out at a temperature around 70 °C to 100 °C for 5 min to 200 min. The precipitate, a rare-earth oxysulfate, is washed, filtered, dried and calcined. Then the material is reduced, transforming the oxysulfate into an oxysulfide by firing in an atmosphere of hydrogen, carbon monoxide, or other reducing gas at 500 °C to 1000 °C[69]. According to the inventors, the transparent ceramic can be produced by uniaxial hot pressing, HIPing or sintering without pressure. Matsuda[73] suggests sealing the green structure in a flexible metal envelope made of tantalum or niobium before performing HIP at 1300 °C to 1800 °C. A good review of scintillator materials including a comparison between ceramic scintillators and single crystals up to 1997 is given by Greskovich and Duclos[1].

High energy ceramic scintillators

Recently there has been considerable interest in scintillators for high energy gamma rays and positron emission tomography (PET). These scintillators must have very short decay times and recovery times. Ce^{3+} is the activator of choice because it efficiently luminesces in several hosts and because the allowed d-f transition has a lifetime on the order of tens of nanoseconds, depending on the host. In 1996, General Electric patented a method for making ceramic garnet scintillators with the chemical formula $A_3B_5O_{12}$ including gadolinium gallium garnet ($Gd_3Ga_5O_{12}$),

gadolinium scandium gallium garnet ($Gd_3Sc_2Ga_3O_{12}$), and gadolinium scandium aluminum garnet ($Gd_3Sc_2Al_3O_{12}$)[74] with Cr^{3+} or Ce^{3+} or Nd^{3+} ions as activators. To prepare these ceramics, the oxides were dissolved in hydrochloric acid and then precipitated as hydroxides by drop-wise addition of ammonia until the pH was 7.8 to 8.3. The precipitate was washed, rinsed with alcohol, dried, calcined at 900 °C, cold pressed and isostatically pressed. The green structure was sintered in an oxygen atmosphere at 1400 °C to 1600 °C. These ceramic scintillators showed more loss than single crystals. This loss was attributed to the transfer of energy to defects, perhaps at grain boundaries[74]. Lutetium aluminum garnet ($Lu_3Al_5O_{12}$, or LuAG) is a promising scintillator host having high X-ray and gamma ray absorption due to the high atomic number and density of Lu. Lutetium silicate (Lu_2SiO_5) doped with Ce has also been sintered as a scintillator[75]. Very transparent ceramic slabs of LuAG materials have been produced by using a carbonate precipitation similar to that discussed for laser ceramics in Subsection . Lutetia is dissolved in nitric acid and added to a solution of aluminum nitrate. The mixed nitrate solution is added at $2\,\mathrm{mL\,min^{-1}}$ into 2 M ammonium hydrogen carbonate solution under mild stirring. The resulting precipitate is filtered, washed, dried and calcined as above and isostatically pressed into a green structure. Sintering is carried out at 1850 °C for 6 h in a hydrogen atmosphere. The carbonate precipitate displays smaller particle size and less agglomeration than is seen for comparable hydroxides, resulting in quite transparent parts[76]. Ce-doped LuAG was also made via reactive sintering, by ball milling very pure lutetia, alumina and ceria in the correct proportions in alcohol and then sintering the pressed blended oxides in a vacuum at 1760 °C for 10 h, followed by annealing at 1450 °C for 20 h[77].

Kuntz[78] compared the reactive sintering method of Li *et al.*[77] with LuAG produced via FSP. Both materials were vacuum sintered for 8 h at 1800 °C. The FSP route led to significantly improved optical properties. Today, cerium-doped YAG with very good transparency can be purchased commercially.

Transparent ceramic electrooptics

Another area of interest in lasers is optical switching. Transparent ceramic electrooptic materials have been studied for more than 40 years. These materials are perovskite-phase solid solutions of lead zirconate, lead titanate and lanthanum zirconate (PLZT, or $(PbLa)(ZrTi)O_3$).[79, 80, 81]. Transparent ceramic PLZT has advantages over competing technologies, such as liquid crystals, in simplicity of construction and speed of response. A disadvantage is the relatively high electrical potential required for switching. PLZT is fabricated either by blending and ball milling appropriate amounts of the high-purity oxide powders, PbO, ZrO_2, TiO_2 and La_2O_3 (a mixed oxide (MO) process), or by an organometallic process. The latter process involves starting with high-purity liquid tetrabutyl zirconate and tetrabutyl titanate, which are mixed with lead oxide in a high-speed blender and then precipitated by adding a water solution of lanthanum acetate. The slurry is dried, calcined, wet milled and cold pressed prior to sintering[82]. Haertling and Land[80] were the first to achieve transparency in ferroelectric ceramics. This group achieved 80 % transmittance in an 8 % La sample via hot pressing, with a refractory powder such as magnesia around the part to prevent reaction with surrounding materials, at 1100 °C to 1300 °C and 14 MPa for 10 h. Snow[83] showed that excess PbO_2 could be used to create a liquid phase during sintering, allowing translucent materials to be fabricated by a pressureless sintering process. This required a sintering atmosphere rich in O_2 and PbO_2 vapor, and a controlled rate of PbO_2 evaporation from the finished product to allow closure of the pores left by removal of the second phase. Results were not quite as good as for hot-pressing, with transmission of only 50 %.

More recently, several other compositions have been reported based on using lead niobate in place of lead zirconate and a divalent cation to balance the charge in the perovskite structure[84]. $Pb(Mg_{\frac{1}{3}}Nb_{\frac{2}{3}})O_3$-$PbTiO_3$ (PMN-PT) has been developed, and it has much less hysteresis than PLZT. It also has an isotropic cubic perovskite structure, which can be easily distorted by applying an electric field, producing birefringence that varies quadratically with the field. The electrooptic effect is 2 to 5 times higher that that of PLZT and 100 times higher than

$LiNbO_3$. Nanosecond modulation has been achieved[85]. PMN-PT can be prepared by either the MO or CP process but the co-precipitation process is preferred for higher purity and a more homogenous material. Powder preparation is most important to the transparency. The transparency achieved in OptoCeramic™PMN-PT at Boston Applied Technologies, Incorporated matches or is slightly better than PLZT, $\approx 3\,\mathrm{dB\,cm^{-1}}$ attenuation at a wavelength of 1.5 µm. PLZT has also been studied as a laser host material. Spectroscopic studies were carried out by de Camargo *et al.*[86] for ceramics doped with Nd, Er, and Yb. The following year, stimulated emission was observed in Nd-doped PLZT[87].

2.1.4 Laser ceramic gain media (1995-2005)

Laser quality ceramic Nd:YAG

Nd:YAG is probably the most commonly used solid-state laser material. Single crystals are grown using the Czochralski (Cz) method. Translucent YAG ceramic was first made using SiO_2 to aid sintering or MgO to inhibit grain growth. These findings emphasized the importance of smaller, more-uniform powder grains, and recommended silicon-based additives over magnesia[88].

In 1995, Ikesue *et al.*[89] demonstrated transparent ceramic Nd:YAG samples with an attenuation coefficient at 1000 nm (measured by using the slope of the log of the transmitted intensity versus sample thickness) of $0.9\,\%\,\mathrm{cm^{-1}}$. This was a dramatic improvement over the transparencies of any of the ceramics discussed above, providing impetus to subsequent development of transparent ceramics for commercial lasers. Ikesue also showed a comparison of the lasing power of ceramic YAG with 1.1 % Nd (dodecahedral site basis) versus a single crystal doped at 0.9 % Nd as a function of input pumping power. The ceramic had a comparable threshold for lasing, $\approx 300\,\mathrm{mW}$, and comparable lasing efficiency, $\approx 28\,\%$. Ikesue also showed the pore structure and the change in density during heating by interrupting heating of samples at different temperatures. A comparison of properties of the sintered ceramic versus the single crystal showed a Vickers hardness, refractive index, room and higher temperature thermal conductivity, and optical properties to be essentially the same as those of the single crystal.

In the same year, Ikesue *et al.*[90] reported on Cr^{3+}/Nd^{3+} co-doped YAG. Cr^{3+} absorbs radiation throughout the visible region of the spectrum, making it a good absorber for flashlamps and perhaps for sunlight. The energy is then transferred non-radiatively to Nd^{3+} for lasing at 1064 nm[3]. Ikesue *et al.*[3] prepared samples by first synthesizing the oxide powders by alkoxide precipitation of Al from solution, pyrolysis of $Y(OH)_2Cl$, and oxalate precipitation of ceNd. After calcinations, the Al_2O_3, Y_2O_3 and Nd_2O_3 powders were blended and ball milled using high-purity alumina balls for 12 h in alcohol mixed with 0.5 % (by weight) tetraethyl orthosilicate (TEOS). They claim that both the small addition of silica (measured at 320 ppm in the final part) and the preparation of the raw material powders are key to obtaining their transparency. They indicate that their raw material powders are all at least 99.99 % pure and have median particle sizes of 60 nm to 500 nm. The slurry was dried using a spray drier with the atomizer rotation speed adjusted to give granulated spherical particles < 100 µm in diameter. Spray drying conditions can also be used to control porosity. The granulated powder was isostatically pressed into disks. Sintering was carried out for 20 h to 50 h under a vacuum of 1.3×10^{-3} Pa. Porosity, as measured by microscopy, was ≈ 150 ppm. Cooling after vacuum sintering was carried out at $> 600\,^{\circ}\mathrm{C\,h^{-1}}$; the authors found that a slower rate of cooling can allow silicon-rich precipitates to form. Ikesue *et al.*[92] showed that increasing the silica content and decreasing the cooling rate results in a silica-rich grain boundary phase, which decreases laser efficiency by increasing scattering in otherwise-homogeneous, low-porosity samples. Ikesue *et al.*[93] also tried adding a HIPing step to their process. A series of experiments were performed varying the TEOS content and HIP conditions. The results showed increased porosity due to argon being dissolved in the silicate grain boundary phase and then being released as argon gas bubbles when the pressure was released and the sample cooled.

In 1995-1996, Ikesue *et al.*[94] demonstrated that the Nd^{3+} concentration could be increased from 1.1 % to 2.4 % and 4.8 % of dodecahedral sites in their ceramic samples. These higher concentrations are not possible in the single crystal

[3] Ueda suggested that this approach might potentially be practical for a solar pumped laser[91].

because of the low accommodation coefficient for Nd in the YAG boule. The 1.1 % and 2.4 % samples show a somewhat higher threshold for lasing than the 0.9 % single crystal and higher slope efficiencies. The 4.8 % sample shows lower efficiency due to concentration quenching. However, the high concentration of Nd^{3+} is potentially useful for microchip laser applications and Ikesue *et al.*[95] show that for such applications, the higher Nd concentration can be up to 4 times as efficient as a 1 % Nd single crystal. Lupei *et al.*[96] studied the high-resolution spectral properties of Nd:YAG ceramics made by the above process up to concentrations of 9 % Nd. The spectra are consistent with Nd ions occupying only the D2 sites of YAG similar to perfect flux-grown single crystals. With increasing concentration, satellite peaks are consistent with a statistical distribution of Nd-Nd next-nearest neighbor pairs, and at higher concentrations some statistical triads of three Nd ions on near-neighbor D2 lattice sites. Emission decay curves of the 1 % ceramics are very similar to the single crystal. Decay curves at higher concentrations can be explained by energy transfer and cross relaxation with some energy migration. At higher Nd concentrations, absorption increases and the absorption bands widen, allowing Nd ions to be pumped at 885 nm rather than the usual 808 nm. 885 nm pumping can be expected to reduce the quantum defect heating of the lasing medium by $\approx 30\,\%$[97].

Even before the Ikesue paper in 1995, a second group in Japan[98] had achieved attenuation coefficients of $2.5\,\%\,\mathrm{cm}^{-1}$ to $3.0\,\%\,\mathrm{cm}^{-1}$ for Nd:YAG ceramics using a different approach to the synthesis. Their approach was to first carefully prepare 1M solutions of YCl_3, $AlCl_3$, $NdCl_3$, and $(NH_4)_2SO_4$. These solutions were mixed in the ratio of 50-x/30/x/30 where x was chosen to determine Nd^{3+} doping in the final oxide. Next, 72 g of urea and 0.003 g of colloidal silica were added to the solution. The temperature was raised to 95 °C and held for 2 h, during which time the urea hydrolyzed and coprecipitated all the cations as amorphous hydroxides. The precipitate was washed, filtered, and calcined. The resulting oxide was pressed into disks and vacuum sintered at 1700 °C. Said group measured absorption and emission spectra of the samples with different Nd concentrations and, except for the background attenuation from scattering, the spectral features were

found to be the same as for the single crystal. The calculated induced emission cross section was $\approx 49 \times 10^{-20}\,\mathrm{cm}^2$, in reasonable agreement with values obtained from laser measurements in the single crystal. Precipitation techniques continued to improve, further reducing the level of porosity. In 2000, Li *et al.*[99] emphasized the importance of precipitate agglomeration, and compared two methods of precipitation. A solution of pure yttrium and aluminum nitrates in distilled water was divided and added to two separate solutions, one of ammonium hydrogen carbonate and one of ammonium hydroxide. The hydroxide precipitate was gelatinous and more difficult to process than the carbonate precipitate. The two precipitates were calcined in oxygen, isostatically pressed, and vacuum sintered under comparable conditions. The YAG from carbonates sintered more completely and with less agglomeration than YAG from mixed hydroxides. Using carbonate co-precipitation methods later that year, Lu, *et al.*[100, 101] claimed a porosity of ≈ 1 ppm, in agreement with the theoretical calculations by Soules and two orders of magnitude less than observed by Ikesue in his transparent ceramics. Unfortunately, it is not clear how the measurement techniques should be compared. Lu *et al.*'s method of preparation of the starting powder is described in two Japanese patents [102, 101]. In the first patent, aqueous solutions of 1 M YCl_3 and 1 M $AlCl_3$ were carefully prepared and mixed together in a 3:5 volume ratio, and concentrated sulfuric acid was added in molar ratio of 0.75 SO_4^{2-} per metal ion. 2.5 M ammonium hydrogen carbonate solution was added drop-wise to the acidic metal ion solution to achieve a pH of 4.8 (adding the precipitant to the metal salt solution is known as the normal-strike precipitation). The solution was allowed to age for 12 h and then ammonia was added until the pH reached 7.5. By this time all metal ions had precipitated. Six rounds of filtering and washing were carried out, until the anion content of the effluent was < 2000 ppm. After drying and calcining at ≈ 1200 ℃, a fine, well-dispersed powder was obtained, which was uniaxially and isostatically pressed and then vacuum sintered at 1650 °C for 3 h. In the second patent the precipitation order is reversed (the reverse strike method). Solutions of 0.5 M yttrium and aluminum nitrate were prepared and mixed in the proper ratios and then the metal ion solution was added drop-wise with stirring to a 2 M solution

of ammonium hydrogen carbonate, keeping the pH between 7.5 and 11 with ammonia. The solution was aged until the pH stabilized between 7.5 to 11, and then filtered, washed, dried and ball milled for 24 h, before being pressed and sintered as before. Lu *et al.*[100, 103] obtained 72 W of laser output from a Nd:YAG ceramic rod produced by the group at Konoshima Chemical Co., Ltd. At the time this was the highest output achieved in a Nd:YAG laser. Over the course of the next four years, decreased scattering led to further improvements in slope efficiency from 58.5 % to 62 %[104] and corresponding increases in laser output power. In 2002 Lu *et al.*[105] discussed the properties of Konoshima ceramic Nd:YAG, pointing out that stimulated Raman scattering and highly efficient laser oscillation suggested that this material would be an excellent alternative to Nd:YAG single crystals. Instead of cold pressing the powder, Konoshima ball milled the powder for 24 h in alcohol and binders and poured it into a gypsum mold (slip casting). After drying, the slip-cast sample was removed from the mold, heated to remove organic binders and then sintered at 1750 °C. that may occur during cold pressing.

Laser quality ceramic Nd:YSAG and other garnets

Yttrium scandium aluminum garnet (YSAG) has a mix of Sc and Al in the octahedral sites. This variety of ion environments causes inhomogeneous broadening of the Nd emission and absorption lines, making possible a tunable laser. A ten-fold increase in the width of the Nd spectral line allows 10 ps pulses to be produced[106]. Nd:YSAG can be made transparent using the mixed oxide synthesis discussed above for YAG[107]. Lasers have been made from Nd- and Yb-doped ceramic YSAG[1], showing significantly broader emission peaks.

Terbium aluminum garnet (TAG) and terbium gallium garnet (TGG) have also been made by Konoshima as Faraday rotators, a possible magneto-optical switch. TGG has one of the highest Verdet constants for a Faraday rotator and it is 40 times higher at low temperatures[108].

Laser quality ceramic yttria, Y_2O_3

Unlike YAG, where a slight imbalance of metal ions can easily produce secondary phases, yttria does not have a second metal ion component. Several precipitation methods have been used to prepare laser quality yttria. Ikegami *et al.*[109] precipitated yttrium hydroxide from a solution of $Y(NO_3)_3 \cdot 6\,H_2O$ by adding a 2 N aqueous ammonia solution at $10\,mL\,min^{-1}$ and 0.36 g per 100 mL of ammonium sulfate. The precipitate was aged at 10 °C, 50 °C and 100 °C. After aging, the cold precipitate was observed to contain thin flakes arranged as houses of cards. The sulfate ions were found to reduce anisotropy and result in more-spherical particles, which is reportedly essential to achieving good transparency. In 2007, Fukabori *et al.*[110] published a continuation of Ikegami's earlier work starting with a 0.3 M $Y(NO_3)_3$ and $Nd(NO_3)_3$ solution and adding ammonia while stirring to precipitate $Y(OH)_3$, aging, then adding a 0.05 M $(NH_4)_2SO_4$. The slurry was aged, washed and calcined as usual. They found that the sulfate should be driven off as completely as possible without forming large particles by calcining at 1080 °C to 1100 °C. Urea precipitation was used successfully by Lu *et al.*[111] to fabricate Nd:Y_2O_3 and a working laser slab in 2002[112], 2003[113], and 2004[114]. The 2002 paper briefly describes the fabrication method that was presumably used in all these efforts. As in the urea precipitation discussed above, urea was added and the solution was heated to near boiling. The resulting precipitate was filtered and washed repeatedly, after which it was dried for two days. The precursor powder was then calcined at 1100 °C and ball milled for 24 h. The milled slurry was then slip cast. After organic components were removed by calcining, the green body was vacuum sintered. Saito *et al.*[115] described the fabrication of transparent yttria ceramics using a carbonate precipitation method. Yttrium nitrate hexahydrate (99.99 % pure) was dissolved in deionized water. A 2.5 M solution of ammonium hydrogen carbonate was dripped into the yttrium nitrate solution at a speed of $2\,mL\,min^{-1}$ (normal strike). The precipitated slurry was then aged for two days, during which time the amorphous spherical carbonate crystallized and a 0.05 % (by weight) ammonium sulfate solution was added. The precipitate was filtered and washed repeatedly, and the filtered cake was dispersed in acetone and dried to

prevent aggregation. The powder was calcined at 1100 °C for 4 h. It was then cold pressed and sintered at 1700 °C in a vacuum of 10×10^{-3} Pa. In-line transmission at 1000 nm was $\approx 50\,\%$, compared to 80 % for a single crystal.

Laser quality ceramic scandia, Sc_2O_3

Scandium oxide has the same bixbyite crystal structure as yttria, but higher thermal conductivity. Like yttria, Sc_2O_3 has been fabricated from several precursors. Li *et al.*[116] thermally pyrolyzed scandium sulfate, $Sc_2(SO_4)_3 \cdot 8\,H_2O$ at 1200 °C, resulting in ultra-fine Sc_2O_3 powder with good dispersion. Transparent ceramics obtained had in-line transmittance of 56 % to 58 % in the visible. After trying several other precipitation methods, Li *et al.*[117] obtained the best results by precipitating the basic sulfate, $Sc(OH)SO_4 \cdot 2\,H_2O$, by mixing a 0.4 M scandium nitrate solution and an equi-volume solution of ammonium sulfate. The precipitate was washed repeatedly with distilled water until free SO_4^{2-} was no longer detected with $Ba(NO_3)_2$. The powder was calcined at 1000 °C, and was quite transparent after vacuum sintering at 1700 °C. The urea precipitation method discussed above, followed by slip casting and vacuum sintering at 1700 °C for 5 h, was used by Lu *et al.*[118], who showed that the spectral properties of Yb:Sc_2O_3 are quite similar to those of Yb:Y_2O_3, and produced a laser output of 0.4 W.

Laser quality ceramic lutetia, Lu_2O_3

Lutetia is also similar to yttria both in crystal structure and chemistry. However, the lutetium ion Lu^{3+} is very close to Yb^{3+} in both size and mass, so that the addition of Yb^{3+} has little effect on the thermal conductivity. This gives Yb-doped lutetia the highest thermal conductivity of any of the oxide laser materials. Lu *et al.*[119] fabricated Nd:Lu_2O_3 using the urea process and demonstrated laser action. The spectroscopy is very close to Nd:Y_2O_3 with just a small shift, approximately 1.5 nm, due to the different crystal field and slightly narrower line widths. Kaminskii *et al.*[120] demonstrated efficient lasing using Yb:Lu_2O_3 ceramic samples presumably obtained using the same urea process. They also analyzed phonon transmission and scattering at grain boundaries using the heat-pulse technique at

liquid helium temperatures.

Recent work on fluoride laser ceramics

Fluorides have certain advantages as laser gain media due to their large band gap and low non-linear optical coefficients, high quantum efficiency due to low phonon coupling and relatively low-energy phonons, and long rare-earth laser lifetimes. These advantages must be traded against difficulties in sintering transparent fluoride ceramics. Fluorides may be contaminated by water or oxygen impurities from the air, and so are typically purified under fluorine or anhydrous hydrofluoric acid. This also makes normal methods of slip casting unworkable. Although they sinter at lower temperatures than oxides, they have a significant vapor pressure at sintering temperatures and so cannot be vacuum sintered without a loss of much of the material. Recently, Aubry *et al.*[121] reported on the synthesis of ceramic CaF_2 powder via several techniques to prepare the starting powders, including reverse micelle precipitation, hydrofluoric acid precipitation, and mechanical alloying of crushed single crystals. All three methods produced a powder that was phase pure by X-ray diffraction, but sintering revealed traces of zirconia in the powder prepared by mechanical milling and organic impurities in the reverse micelle samples. Translucent parts were fabricated using uniaxial hot pressing, spark-plasma sintering and vacuum sintering followed by HIPing.

T. T. Basiev *et al.*[122] reported on ceramics and single crystals of a solid solution, Yb^{3+}:$(_1-x)CaF_2-(x)SrF_2$ ($x = 5\,\%$). They argue that, being near a eutectic composition of $\approx 25\,\%$ SrF_2, this solid solution can have better crystallinity, higher pump light absorption, and narrower spectral peaks. They report $0.9\,\%\,cm^{-1}$ loss in the ceramic sample and laser slope efficiency $\approx 80\,\%$ that of the single crystal.

Laser quality ceramic zinc selenide, ZnSe

Cr^{2+}:ZnSe ceramics were recently prepared by mixing CVD ZnSe and CrSe (1 % by mole) and hot pressing. Efficiencies of 10 %, 5 % and 3 % were achieved for low and high doping densities. This materials system potentially offers tunable

mid-IR laser light[123].

2.1.5 Engineered laser ceramics (2005–present)

As mentioned in Subsection 1.1.1, one advantage that transparent ceramics offer the laser designer is the ability to tailor ceramics to meet the needs of the laser. Recent advances outlined below have brought greater public attention to this advantage.

Co-sintered parts

Composites have been fairly recently fabricated by bonding partially-sintered ceramics. The approach is to partially sinter several parts, then polish the sides to be bonded to $\frac{\lambda}{10}$ flatness, with no defects under 10 × magnification. The parts are then placed in contact and held under pressure during the next sintering step. Konoshima has successfully used this technique to produce Nd:YAG amplifiers clad in pure YAG. Kracht *et al.*[124] designed a composite cylindrical rod in which only the core was doped. The cladding internally reflected pump light and distributed it uniformly over the doped region. The rod and cladding also served as a thermally self-focusing wave guide. The design was modeled and optimized for optical absorption efficiency using a ray tracing code. By water-cooling the outside of the rod they were able to achieve 144 W of output power from 290 W of input power (*i.e.*, 64 % optical-to-optical efficiency). Strasser[125] showed that beam clipping at the aperture could be avoided by the use of undoped cladding, using core-doped rods by Konoshima in a side-pumped configuration. Dong *et al.*[126] co-sintered a short rod of Cr^{4+}:YAG to Yb^{3+}:YAG to produce a single-piece Q-switched laser with a pulse energy of 125 mJ, a pulse width of 1.2 ns, and a repetition rate of 105 kHz.

Engineered green structure

Tailoring the powder compact before sintering could potentially allow additional flexibility in the design of monolithic transparent parts. As a proof of

this concept, a concentration gradient of Nd in YAG was achieved by cold-pressing successive layers of powder with different concentrations of dopants[1].

Wisdom[5] identifies four potential design goals for activator profile tailoring, each with progressively less-stringent requirements for profile control: Longitudinal mode control, wave guide construction, thermal management, and transverse mode control.

Longitudinal mode control is the strategy of selectively amplifying certain modes of oscillation, with heavier doping at the peaks of standing waves and lighter doping at the nodes. To reap the full benefits of such a tailoring strategy would require that the spatial control of doping achieve an accuracy finer than the wavelength of emitted radiation.

Wave guides could be constructed by exploiting the effect of activator doping upon refractive index, with the goal of confining light to a thin layer for greater amplification efficiency. This would require composition control at a length scale on the order of or slightly larger than one wavelength.

Thermal management of end-pumped rods could be accomplished by balancing the active material's absorption to the expected intensity of pump light. This would allow for uniform heating of the rod, even as different portions of it are exposed to different amounts of energy. This improved uniformity of thermal load would reduce the risk of thermal shock. This strategy calls for control of ion concentrations and gradients on a length scale of several millimeters.

Lastly, large-aperture slabs may benefit from transverse mode control, which would be accomplished in much the same way as longitudinal mode control. However, the length scale of intended transverse modes is several orders of magnitude greater, allowing this goal to be met even if doping can only be controlled on a length scale of centimeters. One laser application seems particularly well suited to this strategy: edge-pumped amplifier slabs. A uniformly-doped slab will absorb more pump light at its edges than at its center, since the pump light will be dimmed by its passage through the material. This means that the edges of such a slab receive the most pump energy, energy that is wasted amplifying the edges of the beam. If tailored ceramics can be made with well-controlled concentration

gradients, then edge-pumped amplifier slabs can be made so that each point absorbs only as much pump light as is needed to amplify that portion of the beam by the desired amount.

Wisdom fabricated a waveguide structure by reactive sintering, with higher-index Nd:YAG sandwiched between lower-index undoped YAG ceramics. His design called for a 400 µm wide doped region, which was predicted to be achievable based on the bulk diffusivity of Nd in YAG. However, the observed Nd diffusion distance was approximately 250 µm. Additionally, some regions showed pronounced differences in Nd concentration near grain boundaries vs. near the center of grains, which indicates the action of a high-mobility path. He attributed this rapid diffusion to the presence of transient phases that had not yet fully reacted to form YAG, based partly on the observation that a much lower diffusivity is observed during the final stage of sintering: samples sintered for 10 h, 50 h and 125 h showed identical concentration profiles.

Messing[127] presented a similar idea, using tape casting to build up layers of different concentrations of Er:YAG as a means of thermal management. Each layer is ≈ 100 micrometers in thickness. These initial efforts have shown promising optical quality. The Er diffusion distance was on the order of 0.2 mm, and, as for Wisdom, some non-uniformity of concentration was observed when mapping fluorescence[5].

Single crystal growth in polycrystalline ceramics

Scott *et al.*[128] first observed "solid-state crystal conversion" (SSCC) in Lucalox grade polycrystalline alumina with low MgO concentration. He showed that $\approx \frac{1}{3}$ of a PCA tube with an OD of 5 mm could be converted to sapphire by soaking at 1880 °C for 18 h. In an article discussing a number of experiments in engineering transparent ceramics for lasers, Ikesue discusses the conversion of ceramic YAG to a single crystal by polishing both a ceramic and a single crystal, putting them in contact and soaking at high temperature. Abnormal grain growth reached $1.7\,\mathrm{mm\,h^{-1}}$ at 1840 °C. The importance of this work is that an optical-quality single crystal is obtained, and one can produce a Nd:YAG single crystal

with heavier doping than is possible by melt-growth methods such as Cz.

2.2 Atomic mobility in YAG ceramics

The wide range of applications for YAG have prompted many investigations of diffusion in this particular material. These studies offer insight into both the process of sintering itself and the diffusion of dopant ions in the material, although they stop short of providing diffusion data sufficient to design heat treatment methods for tailored Nd:YAG ceramic optical devices.

2.2.1 Microstructure evolution during sintering

Models of sintering generally separate the process into three stages. In the first stage, necks form between particles, which lowers the system's energy by replacing free surface area with grain boundary area in the necks. In this first stage, the contact area between any two grains is too narrow to allow any coarsening. In the second, some coarsening occurs. Pores become tube-shaped, and shrink as the material densifies. As this process continues, these tube-shaped pores break up due to Rayleigh instability. In the final stage, isolated pores with a roughly spherical shape are filled in by diffusion from grain boundaries[12].

Coble[12, 9] tested a wide variety of analytical models against the observed behavior of alumina and found that the functional dependence of density and grain size as a function of time were consistent with the model of Kingery and Berg[129], and with the work of Burke[11]. Kingery and Berg's model assumes that a bulk diffusion mechanism controls the early stages of sintering, while Burke's work strongly suggested that pore closure during the final stage of sintering depends upon bulk diffusion from grain boundaries to pores. As mentioned in Subsection 2.1.1, Coble's work to develop this theoretical understanding was closely linked to the development of a practical technique: his strategy of preventing grains from enveloping pores allowed the first commerical applications of transparent ceramics[8]. While these models provide a good overall description of the observed microscopic behavior of ceramics during sintering, they describe neither sub-microscopic phenomena,

nor the details of observed diffusion processes.

2.2.2 Grain boundary grooving in YAG: First and second stage sintering

In the first two stages of sintering, as described by Coble, a single continuous void percolates through the entire sample. The end of the second stage of sintering is marked by the closure of pores, which is expected after a shrinkage of approximately 6 % to 10 %[10].

The work of Peters and Reimanis[130] measured the rate of material transport by annealing bicrystals of YAG and measuring the rate at which grooves form at grain boundaries. As for first stage sintering, this process is driven by surface energy and allows the free surfaces near a grain boundary to reach a more stable contact angle. Experiments show that the controlling mechanism in grain boundary grooving of YAG is bulk diffusion of oxygen. They observed an activation energy of $(330 \pm 75)\,\mathrm{kJ\,mol^{-1}}$ for diffusion from grain boundaries to nearby surface sites, which is consistent with results from oxygen tracer studies[131]. Since Y transport does not control this process, as would be expected from its much lower bulk diffusivity rate, they conclude that Y transport during grain-boundary grooving operates by some more-rapid mechanism, such as surface diffusion.

2.2.3 Diffusion of rare-earth ions in YAG: final stage sintering

During the final stage of sintering, pores cease to connect distant grains, and so the available routes for diffusion are expected to be grain boundaries and the bulk of the sample (*i.e.*, the interiors of grains). For this reason, data on material transport in single crystals and dense polycrystals is relevant to efforts to predict dopant diffusion and microstructural evolution during the final stage of sintering.

The diffusion of rare-earth (RE) elements in single-crystal YAG was studied by Cherniak as a stand-in for Y tracer diffusion. Y atoms, or similar atoms in the

dodecahedral sites of the garnet structure, are described as limiting the rate of creep because they diffuse more slowly than do metal atoms in octahedral sites (typically Al) and much more slowly than oxygen atoms. Reported diffusion activation energies were similar for all RE elements studied. La, Nd, and Yb activation energies show a systematic variation with ion size. For example, the diffusivity of Nd was found to be

$$D = 0.163 \exp\left(\frac{(-576 \pm 15)\, kJ/mol}{RT}\right) m^2/s,$$

and that of Yb was found to be

$$D = 0.015 \exp\left(\frac{(-540 \pm 26)\, kJ/mol}{RT}\right) m^2/s.$$

Since the ionic radii of Nd and Yb bracket that of Y, and all have similar chemical properties, Cherniak presents measurements of RE ion diffusion as a means of estimating Y diffusion kinetics.[6]

There were no published studies of Nd diffusion in polycrystalline YAG when this study began, but the observed similarity in RE diffusion kinetics mentioned above suggests that published work on other RE elements is relevant. Yb diffusion in the grain boundaries of YAG was measured by Jimenez-Melendo, Haneda, and Nozawa[132], as a means of estimating Nd transport rates during final stage sintering. This study showed a bulk Yb diffusivity of

$$D = 0.087 \exp\left(\frac{(-565 \pm 85)\, kJ/mol}{RT}\right) m^2/s,$$

which is comparable to Cherniak's results, as well as a grain boundary diffusivity of

$$D = 2100 \exp\left(\frac{(-530 \pm 190)\, kJ/mol}{RT}\right) m^2/s,$$

given an average grain size of $\approx$ 2 /micro /meter. A selection of observed RE diffusivities of RE ions in YAG are plotted together in Figure 5.2.2, illustrating comparisons between new and previously-published diffusivity data in a manner directly inspired by similar comparison plots[6, 132].

The results Wisdom[5] obtained when sintering waveguide structures called for investigation of diffusion in single-phase YAG. This led to the construction of

diffusion couples by bonding together phase-pure YAG ceramics with 1 µm grains. The results were not interpreted in terms of grain boundary diffusivity directly, but in terms of a fitting parameter, κ. Given that $\kappa t^{0.3} = \exp\left(\frac{E_\Lambda}{RT} - A\right)$, measurements from diffusion couples at three temperatures in the regime of negligible grain growth were fit by parameters $E_\Lambda = 314\,\mathrm{kJ\,mol^{-1}}$ and $A = 21.22$.

Section 2.1 of Chapter 2 has also been published, with some changes and additions, in the Lawrence Livermore National Laboratory internal technical report: Joshua D. Kuntz, Joel P. Hollingsworth, and Thomas F. Soules, "Transparent Ceramics for Lasers", UCRL-JRNL-237245. (12 December 2007). The dissertation author was the primary investigator and author of the content presented in this section.

Part II
Experimental Program

Chapter 3

Powder consolidation

Ceramic processing methods were investigated for two main reasons: to advance tailored ceramic technology and to enable diffusion research under conditions that are expected to be relevant for the production of optical devices. This section presents developments in processing technology that achieved the latter goal by enabling the work reported in Chapters 4 and 5. Further developments of processing technology, carried out more collaboratively and without any immediate impact on diffusion research, are beyond the scope of this chapter and are briefly outlined in Chapter 6.

Powders synthesized by two different means were explored as potential diffusion couple materials. For reasons outlined in Subsection 1.2.2, attention was focused on FSP and, to a lesser extent, on aqueous precipitation methods such as CP, as sources of YAG. Multiple methods of powder synthesis were pursued in case the properties of one or the other powder proved unsuitable based on the nature of the synthesis process, but also in anticipation of a need to study the effect of powder size on dopant diffusion during the first two stages of sintering (see Subection 2.2.1 for a definition of the three stages of sintering).

FSP produces powder via the combustion of tiny droplets of a solution of metalorganic compounds[133, 134]. This technique is capable of producing particles of very small and uniform size, with relatively little agglomeration. FSP powder was available doped to specification, due in part to its active, ongoing development as a commercial product.

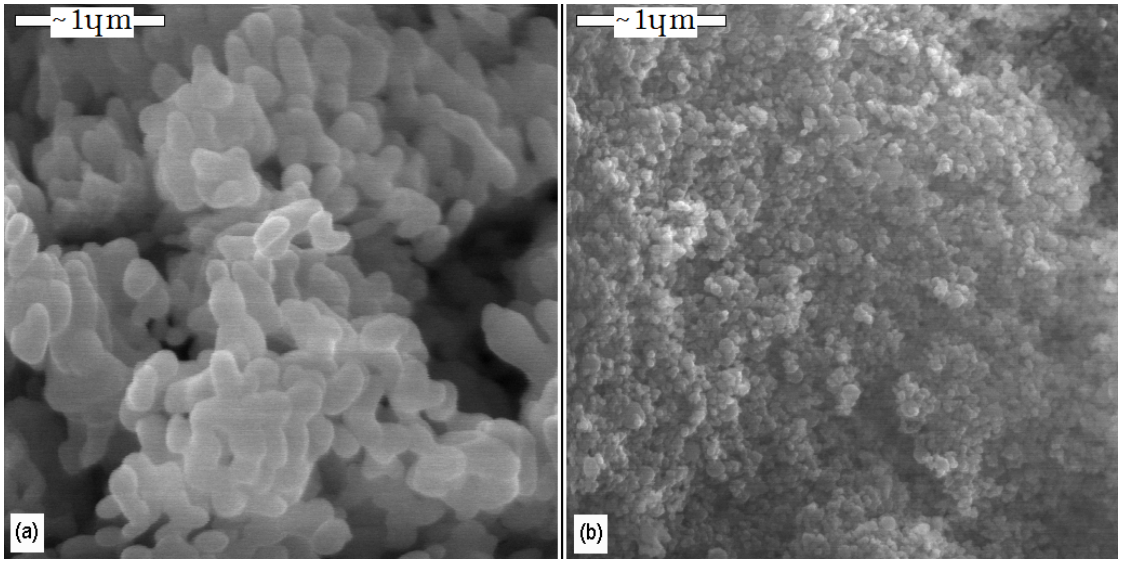

Figure 3.1: Scanning electron micrographs of green body fracture surfaces: a) slip-cast precipitated powder from Shin Etsu, and b) cold-pressed FSP powder from Nanocerox

Nanocerox uses flame-spray pyrolysis to produce YAG powder noticeably finer than can be sythesized by CP. The LLNL transparent ceramic research group used powder from this supplier in a range of experiments, some of which are described in Chapter 6.

Precipitation methods begin with an aqueous solution of metal ions, and form particles of insoluble compounds (typically hydroxides or carbonates) via chemical changes in the solution. After drying and filtration, these compounds are calcined to form oxides. This is a mature commercial technology: whether because of the constraints of economies of scale, or merely the tendency of precipitation to segregate different compounds, there is little or no commercial offer of custom compositions of precipitated powder. See Section 2.1 for extensive references to powder synthesis via precipitation.

Shin-Etsu offers a CP YAG powder, which had previously been slip-cast and sintered into highly-transparent ceramics at LLNL. Comparable Nd-doped powder was not available commercially; the development of methods to incorporate Nd into the material was undertaken in order to allow its use in the fabrication of diffusion couples.

3.1 Diffusion couple fabrication development

In order to obtain precipitation-derived Nd:YAG powder, a method of mixed-nitrate doping was developed. Neodymium nitrate (Rare Earth Products Ltd., A. R.) and aluminum nitrate (Aldrich, $\geq 98\,\%$) were dissolved in deionized water, with a ratio of three Nd^{3+} ions for every five Al^{3+} ions. This solution was then added to YAG powder (Shin-Etsu lot RYAG-OCX-076) and the resulting mixture was dried at 60 °C and ground in a mortar and pestle. Dry, nitrate-coated powder was then calcined at 1050 °C for 2 h to produce a mixed oxide.

Conventional slip-casting techniques were extended by casting a thin layer of one composition into a mold, followed by another layer of a different composition. As is typical for slip casting[2, 108], a gypsum mold was filled with a slurry of ceramic particles in water (slip). These particles remained in the mold as the water was drawn into the gypsum. In discussing this method, Joshua Kuntz emphasized that a green body so formed necessarily has a continuous, percolating pore structure that allows the passage of fluids through it (personal communication, *ca.* 2009). Such a structure can be expected to trap gas to less of an extent than would structures with enclosed pores. A procedure for slip casting diffusion couples is illustrated schematically in Figure 3.2.

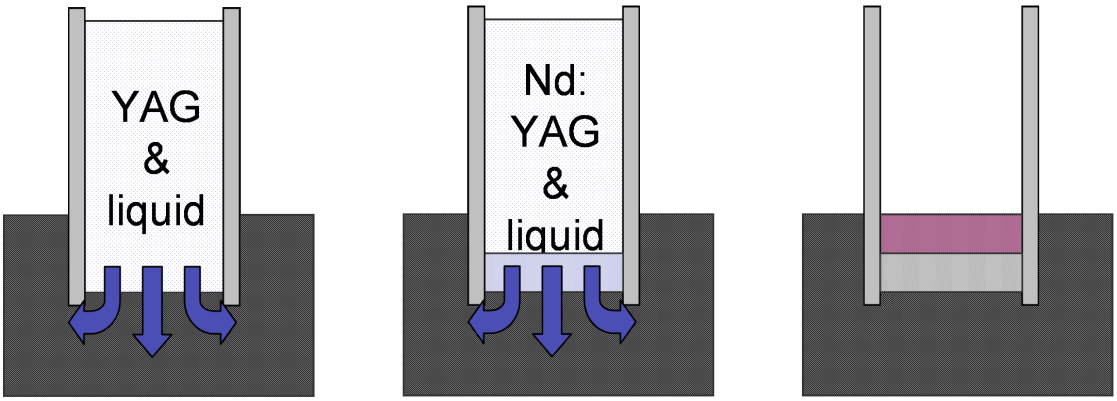

Figure 3.2: Schematic illustration of slip casting. To fabricate diffusion couples, a slurry of un-doped YAG was first poured into a gypsum mold (a). When the liquid from this first slurry had flowed into the gypsum, a slurry of Nd-doped YAG was added (b). Liquid from this second slurry continued to flow into the gypsum, resulting in the finished green structure (c).

Powders resulting from the mixed nitrate technique were slip cast along with as-manufactured powder to produce a green structure with a step function Nd concentration profile, designed to have a nominally planar interface between a region with 1 % Nd and a region of un-doped YAG. This experiment was repeated using powders that had been ball milled in alcohol, using alumina milling media, for 8 h.

By contrast with CP powder, FSP powder was available in custom compositions from a commercial supplier. Such powder was obtained with a doping of 1 % Nd (relative to dodecahedral sites, *i.e.* Y sites) and separately without any intentional rare-earth doping. Bboth compositions were used for the fabrication of diffusion couples.

Cold pressing techniques for tailored ceramics were adapted from a prior procedure that LLNL had developed for uniformly-doped parts. The procedure for uniform parts began with the loading of loose powder into a die. The die was then vibrated to allow the powder to settle into a flat layer at tap density. Pressure was applied with a punch to consolidate the material, as illustrated schematically in Figure 3.5. To prevent gas from becoming trapped in the green body as the powder was compressed, a rotary vane vacuum pump was used to maintain a reduced air pressure within the sample during pressing.

Two methods of cold pressing multi-functional ceramics were explored, which differ as to the stage of the process in which powder of a different composition is introduced. The first method, shown in the upper flow chart of Figure 3.3, was to press a half-thickness green structure of uniform composition, remove it from the die, load powder of a different composition along with the pressed structure, and press the loose powder and pressed structure together into the final structure. The second method, shown in the lower flow chart of Figure 3.3, was to achieve tap density in a first layer via agitation, then add loose powder immediately, agitating the die again to achieve tap density in the second layer before pressing both layers simultaneously.

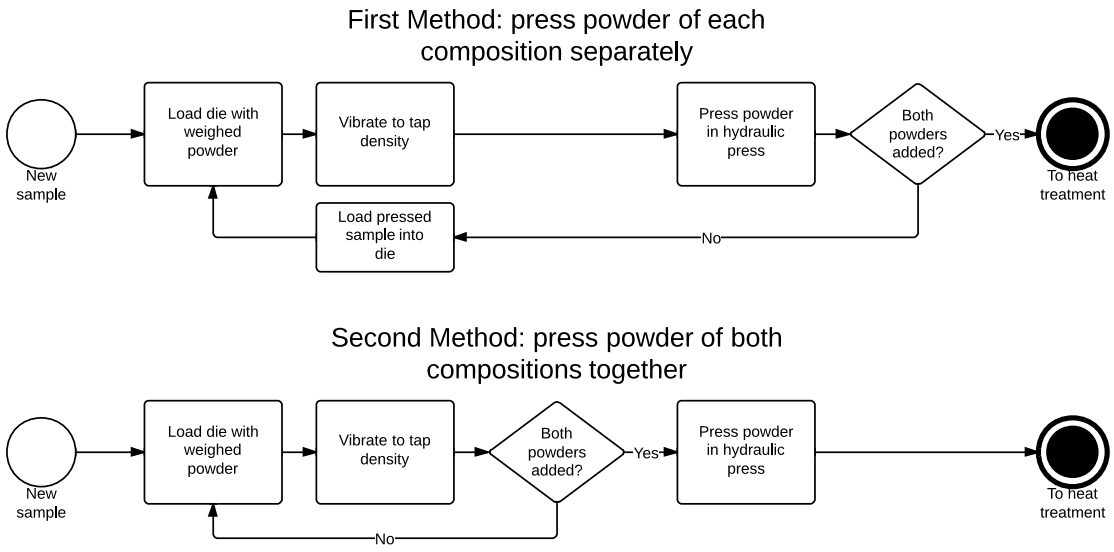

Figure 3.3: Flow charts representing two methods of producing diffusion couples via cold pressing. The first method, represented in the upper flow chart, was to press each composition of powder separately. The second method, represented in the lower flow chart, generated the diffusion interface in tap density powder, and pressed all powder for a given sample at one time.

3.1.1 Results and Discussion

Layered slip-cast samples were subject to an unintentional curvature due to a greater rate of flow near the edges of the sample. As illustrated in Figure 3.2, flow of the liquid component of slip tended to diverge at the bottom of the mold. Portions of the mold with a shorter fluid path to dry gypsum (*i.e.*, the edges of the mold) saw a greater flow rate and a concomitantly greater rate of powder accumulation, especially during earlier stages of slip casting, when the mold was relatively dry. This effect led to noticeable distortions in both the overall sample shape and the shape of the interface between doped and un-doped layers, as seen in Figure 3.4.

Mixed-nitrate doping resulted in uniform incorporation of Nd into the YAG powder: Figure 3.4 shows ceramics sintered from this powder. The resulting ceramics had optical quality consistent with a small amount of second-phase precipitates. This suggests that there is room for improvement in stoichiometry control. More importantly, hard agglomerates were among the results of mixed-nitrate process-

ing. Surface energy considerations would theoretically cause new garnet material to form preferentially at points where particles touch, which welding existing particles together into larger bodies; this would explain the formation of agglomerates.The largest of these agglomerates were visible in the dregs of the slip, but enough agglomerates seem to have remained suspended through the casting process to result in a non-uniform green structure, such that the sintered transparent ceramic displays scattered large pores (see Figure 3.4) and is unsuitable for use as a laser amplifier.

Efforts to break these agglomerates apart via ball milling also broadened the particle size distribution, which complicated the process of slip casting and degraded the sinterability of the resulting green structure. Milled slip exhibited slower drainage than was seen during the casting of un-milled slip, and the resulting ceramic parts were opaque upon sintering.

Layered samples fabricated via cold pressing showed dramatic differences in structural integrity according to the details of fabrication. No usable green structure resulted from the first method (*i.e.* that of pressing half of the powder before adding a second composition) . All such samples were destroyed by the fabrication process. The second method (*i.e.* that of bringing each layer to tap density prior to pressing) produced solid green structures, which sintered to form usable diffusion couples. Sections of sintered samples produced via this second method are shown in Figure 3.4.

Some cracks, visible toward the outside edge of each cold-pressed sample shown, seem to have been the result of rapid rarefaction as pressure was released from the hydraulic press. While they seem far enough from the center of the samples to have a negligible effect on diffusion measurements, such cracks would make a ceramic slab unsuitable for laser applications. A minor refinement of cold-pressing methods for layered samples was implemented in order to prevent cracking in subsequent samples, as described in Subsection 3.2.1.

When two compositions of powder are present in a die that is undergoing agitation, and neither powder has been pressed to form a cohesive mass, mechanical mixing of the two powders is hypothetically possible. If it were to occur

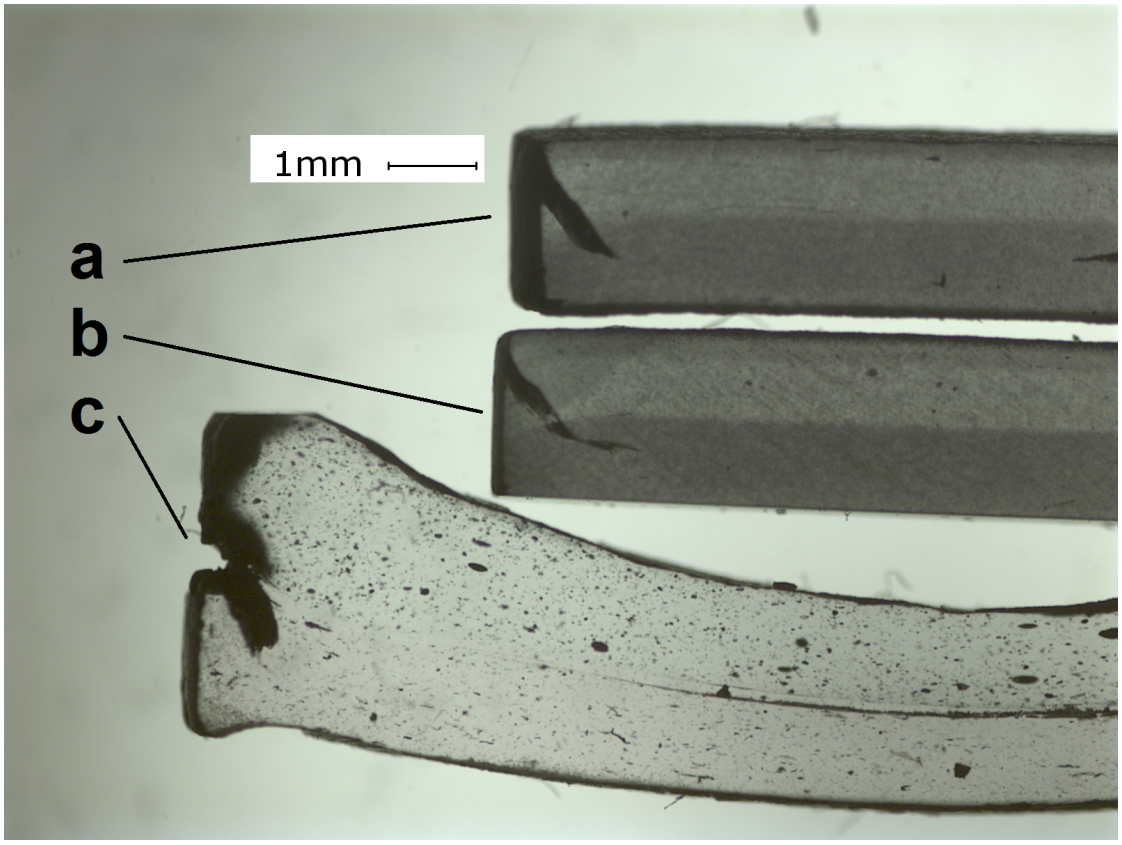

Figure 3.4: Sections of layered transparent ceramic samples, prepared by cold-pressing FSP powder (a, b) and by slip casting precipitated YAG powder and Nd:YAG powder doped by the mixed nitrate process (c).

during the preparation of diffusion couples, significant mixng would result in an Nd composition gradient before sintering even began, as opposed to a step function in concentration. Measurement of such mixing in control samples was therefore important to the interpretation of results. In order to test the hypothesis that powders mixed within the die, and as a means of controlling for unforeseen errors, concentration profiles of un-sintered control samples were measured as a continuation of this experiment. These profiles are reported in Section 3.2.1.

3.2 Production of couples for diffusion research

All controlled diffusion experiments discussed in Chapters 4 and 5 were carried out on samples fabricated in the same fashion, building on the results of

Subsection 3.1.1.

3.2.1 Experimental procedure

Diffusion couples were cold pressed from powders of un-doped YAG and YAG doped with 1 % Nd (dodecahedral site basis). Powders were prepared via flame-spray pyrolysis (FSP) by Nanocerox. The powders used had a surface area of approximately $30\,m^2\,g^{-1}$ as determined by BET, and a purity of 99.99 % as determined by glow discharge mass spectrometry.

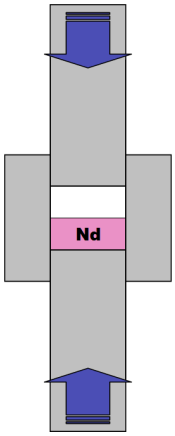

Figure 3.5: Schematic illustration of cold pressing. To press diffusion couples, doped powder (labeled Nd) and un-doped powder were added in layers.

To fabricate each diffusion couple, 0.3 g of un-doped YAG was first added to a 13 mm diameter vacuum die and vibrated to achieve a flat surface at tap density. 0.3 g of 1 % Nd powder was then added, the die was again vibrated, and a punch was installed. The layered structure was then placed in a hydraulic press, and a rotary vane pump was used to evacuate the sample volume. The hydraulic press was used to apply a maximum pressure of approximately 67 MPa. In order to minimize rarefaction cracking, the release valve of the hydraulic press was opened gradually and with great care, such that the pressure applied to the powder declined at a rate no greater than one MPa every three seconds.

The resulting pellet was calcined according to the manufacturer's instructions to remove volatile impurities. Discussions with Joshua Kuntz revealed that 1050 °C was chosen as the final soak temperature in order to convert any metastable

defect perovskite phase formed during FSP to the more stable garnet structure (personal communication, *ca.* 2009). Sintering was then carried out in a vacuum furnace with tungsten heating elements (Thermal Technologies). After outgassing at 1050 °C, each sample was sintered for a time and at a temperature prescribed by the experimental design. The furnace atmosphere was maintained at a pressure of less than 0.3 mPa during sintering; in some cases, it was necessary to pause at moderate temperatures to allow volatiles to escape from the sample. Samples were allowed to cool from the processing temperature at a rate of 5 °C/min.

As a baseline for further diffusion measurements, it was necessary to measure the Nd concentration profile of cold-pressed green structures. This was done in order to account for Nd redistribution due to powder mixing and due to diffusion during calcining, to allow such effects to be subtracted from diffusion results. A calcined sample and a control sample (as-pressed, *i.e.* not heat-treated) were both potted in epoxy resin under vacuum. A diamond saw was used to prepare sections of the samples, including sintered samples and epoxy-infused control samples. These sections were then mounted in a stainless steel ring using epoxy and polished in preparation for electron microprobe measurements. Figure 3.6 is a photograph of the samples as they were presented to the EMP operator.

Electron microprobe measurments quantified the intensity of X-ray fluorescence at wavelengths characteristic of Nd, Y, and Al at each of approximately one hundred evenly-spaced points in each sample. Calibration samples of known concentration were also supplied to the equipment operator, allowing the instrument to be calibrated so that x-ray brightness could be interpreted as atomic concentration.

Measurements were requested along a line perpendicular to the initial interface between doped and un-doped material in order to reveal any migration of Nd across this boundary. SEM voltages are not high enough to excite Nd K_α x-rays, so the comparatively dim L_α line is the best available signal. [1]

[1] One initial experimental plan had called for concentration profiles to be taken via energy-dispersive spectrometry (EDS). However, at Nd concentrations of less than 1 %, the signal from the brightest available line characteristic of Nd is of a magnitude similar to the noise inherent in EDS. For this reason, it was necessary to use wavelength-dispersive methods.

Figure 3.6: Sintered diffusion couples mounted in epoxy and polished to allow EMP measurements.

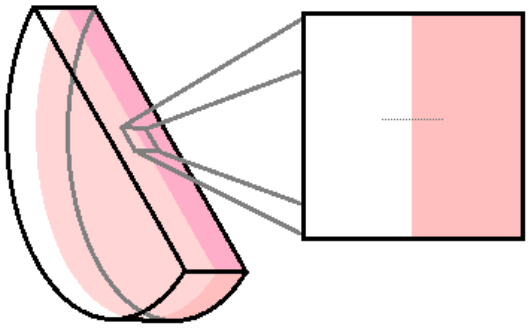

Figure 3.7: Schematic illustrating electron microprobe measurements to determine Nd concentration profiles of diffusion couples.

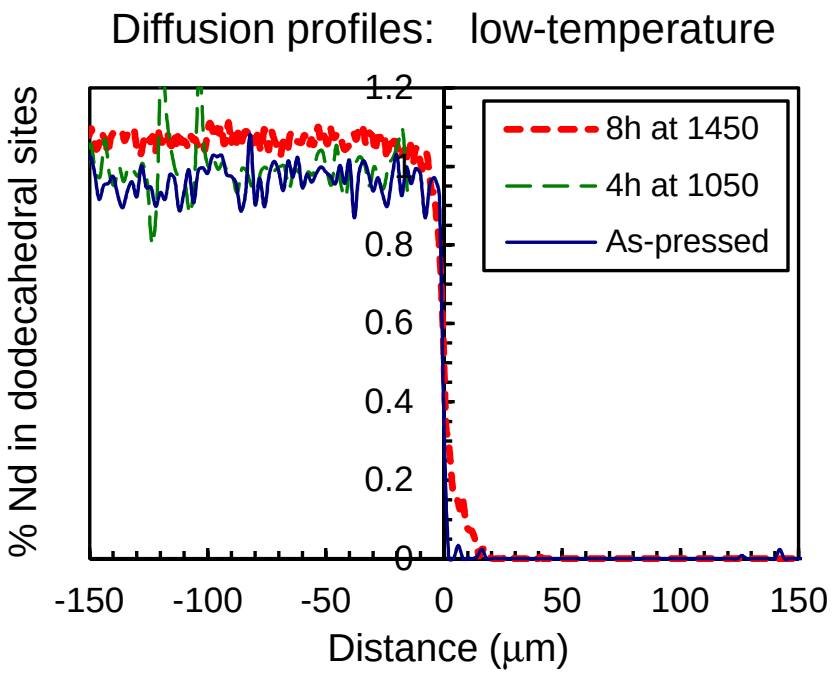

Figure 3.8: EMP measurements of concentration as a function of location, for sample pellets as-pressed (solid line), and after heat treatments in air at 1050 °C for 4 h (thin dashed line) and at 1450 °C for 8 h (thick dashed line).

3.2.2 Results and discussion

Cold-pressed samples made with a slow rate of pressure release, some of which are shown in Figure 3.7, were revealed upon sectioning to be without any cracking of the sort seen in Figure 3.4. Samples made by this method had robust green structures. Each sample sintered from such a green structure displayed a nearly-planar interface between regions of different composition.

EMP results are shown in Figure 3.8. These suggest a resolution of green body fabrication finer than or approximately equal to 1 µm. This length is at the limit of features resolvable by EMP: it corresponds to approximately the diameter of the sample volume which is excited to x-ray fluorescence by the focused electron beam. In the course of studying characterisation methods with Ronald Gronsky (verbal communication, *ca.* 2001) an in-depth description was given of the teardrop-shaped volume of sample approximately 1 µm in diameter, in which an electron beam deposits energy. The EMP operator, Frederick Ryserson, confirmed

that the phenomenon of electron scattering within the sample places a practical limit on the spatial resolution of the instrument, and that this limit is approximately 1 µm (verbal communication, *ca.* 2009). The fitting parameter which best matched this curve corresponded to the distance between points of measurement, and so should be regarded as an upper bound on fabrication resolution observable via EMP, rather than an estimate of the fabrication resolution achieved.

The low-temperature heat treatments necessary to calcine the sample and to drive off adsorbed gases prior to vacuum sintering are also not expected to contribute significantly to solute diffusion: the measured concentration gradient of a sample heat treated for 4 h at 1050 °C was indistinguishable from the sharp gradient of an as-pressed sample. Figure 3.8 presents these two concentration profiles in comparison to the lowest-temperature heat treatment for which significant diffusion was observed.

Sintered samples exhibited some dishing, which was attributed to slight differences in sintering rate among different parts of the sample. The radius of curvature produced by this effect was at least of the order of centimeters. This radius is many orders of magnitude greater than the greatest observed diffusion distance (see Table 5.1), and so curvature is expected to have only a negligible effect on the final concentration profile.

On the basis of these results, the two diffusion experiments discussed in Chapters 4 and 5 were carried out using the exact method of sample fabrication discussed in Subsection 3.2.1. Evidence that the sample preparation method achieved a sufficiently sharp boundary was especially important to this decision: from EMP results, it follows that powder mixing and diffusion at temperatures less than or equal to 1050 °C have a negligible effect on the measured composition profile of such samples.

The method described in Subsection 3.2.1 and the data presented in 3.2.2 are discussed in previous publications[135, 136]. Portions of Chapter 3 are adapted from material as it appears in Joel P. Hollingsworth, Joshua D. Kuntz, Frederick J. Ryerson, and Thomas F. Soules, "Nd diffusion in YAG ceramics", *Optical Materials*, 33 (4), pp. 592-595, 2011. The dissertation author was the primary investigator

and author of this paper.

Chapter 4

Initial sintering and diffusion experiments on Nd:YAG

The sample preparation and heat treatment methods presented in Chapter 3 allowed experimentation with sintering conditions. In planning heat treatments, the criteria outlined in Section 1.2 were important, as was consideration of theoretical descriptions of the dependence of diffusion processes on time and temperature. The former criteria suggested an exploration of processing conditions that incorporate the range of anticipated manufacturing methods, while the latter suggested that sets of conditions within that range be distributed at intervals which facilitate mathematical analysis.

An initial experiment was published separately by the dissertation author: Joel P. Hollingsworth, Joshua D. Kuntz and Thomas F. Soules, "Neodymium ion diffusion during sintering of Nd:YAG transparent ceramics", *Journal of Physics D: Applied Physics*, #42, 5 February 2009, 052001. For that study, thirty-six diffusion couples were fabricated and sintered using methods described in Subsection 3.2.1. Two samples were subjected to each set of sintering conditions, at temperatures that ranged from 1600 °C to 1781 °C and for times that ranged from 4 min to 480 min. A decline in apparent diffusivity with time and temperature suggested that high-diffusivity paths were made unavailable by some ongoing, thermally-activated process. This effect was explained by the theory that diffusion through grain boundaries is the dominant mechanism of Nd mobility, and that coarsening

eliminates these grain boundaries. A heuristic model based on this explanation was constructed and the data were fit to it, but this method could not distinguish between the activation energy of coarsening and that of diffusion, and so could not quantify sintering kinetics[135].

The initial experimental design called for sintering at 1600 °C for 240 min, but surprisingly rapid sintering at low temperatures raised the possibility that interesting phenomena would be observable only during early stages of sintering. In an effort to capture such phenomena, the samples and furnace time originally intended to be sintered under those conditions were re-assigned to a heat treatment at 1450 °C.

4.0.3 Theoretical and empirical concentration functions

Because Nd concentration was maintained at 1 % or fewer (as a proportion of dodecahedral sites on the YAG lattice), and because of its chemical similarity to the Y for which it substitutes, Nd diffusivity was assumed to have a negligible dependence on Nd concentration. The initial profile intended for these samples was a Heaviside step function; concentration measurements, shown in Figure 3.8, indicate that the concentration profiles of samples as fabricated were a good approximation of this function.

The textbook solution to the diffusion equations for these initial conditions is a concentration profile described by the error function[137]. More elaborate models are available, which account for interactions between diffusion through grain boundaries and diffusion through the bulk of grains, but the dissertation author has achieved a good fit to observed concentration profiles using the error function[135].

In addition to the empirical utility of fitting these profiles with error function fit, there is some theoretical justification that profiles of such a shape are to be expected. Familiar diffusion equations can be applied to polycrystals by defining an "effective diffusivity" D_{eff} as a weighted average of bulk and grain boundary diffusivities. This simplification applies best under conditions where a typical atom interacts with several grain boundaries, because in such circum-

stances, iso-concentration lines remain relavely flat, even as they cut across grain boundaries. In mathematical terms, the approximation has been shown to be rigorous for diffusion parallel to grain boundaries a distance a apart when the bulk diffusion distance $\sqrt{D_b t} \gg a$[138].

For some samples the dissertation author has analyzed, this simplification is justifiable via a straightforward calculation: one set of conditions from the experiment described in Chapter 5, for example, is 64 h at a temperature of 1600 °C. Based on published values for $D_b(T)$[6], the diffusion distance for Nd during such a heat treatment works out to 7.6 µm, which is several times greater than the final grain size of 0.8 µm observed following this heat treatment. However, final grain size was not measured for all samples in the initial sintering experiment, and so a less direct but more general justification is in order: YAG crystallites in the initial powder had a diameter of only a few tens of nm[1], constrained by powder particle surfaces. Even if the bulk diffusion distance were negligibly small, a typical atom would have interacted with many grain boundaries due to coarsening: a typical volume of the sample must have had many grain boundaries sweep through it in order for samples to attain a grain size of the order of µm.

Concentration profiles of diffusion couples were taken to have the following form:

$$c = \frac{1}{2} c_0 \mathrm{erfc}\left(\frac{x}{\sqrt{4 D_{eff} t}}\right) + c_b, \tag{4.1}$$

where c is the local concentration of Nd, c_0 is the difference between minimum and maximum concentrations, erfc is the complimentary error function, x is the distance from the diffusion interface, $D_{eff} = (1 - \frac{\delta}{a}) D_b + \frac{\delta}{a} D_{GB}$, and c_b is the background concentration of Nd observed in the nominally un-doped sample.

4.1 Analysis and discussion

Published results were based on a preliminary analysis, in which only the signal from Nd fluorescence was interpreted. A re-examination of the raw data,

[1] Individual FSP powder particles can be seen in Figure 3.1. A particle diameter of approximately 50 nm is consistent with both SEM images of this sort, and BET results of approximately $30\,\mathrm{m^2\,g^{-1}}$.

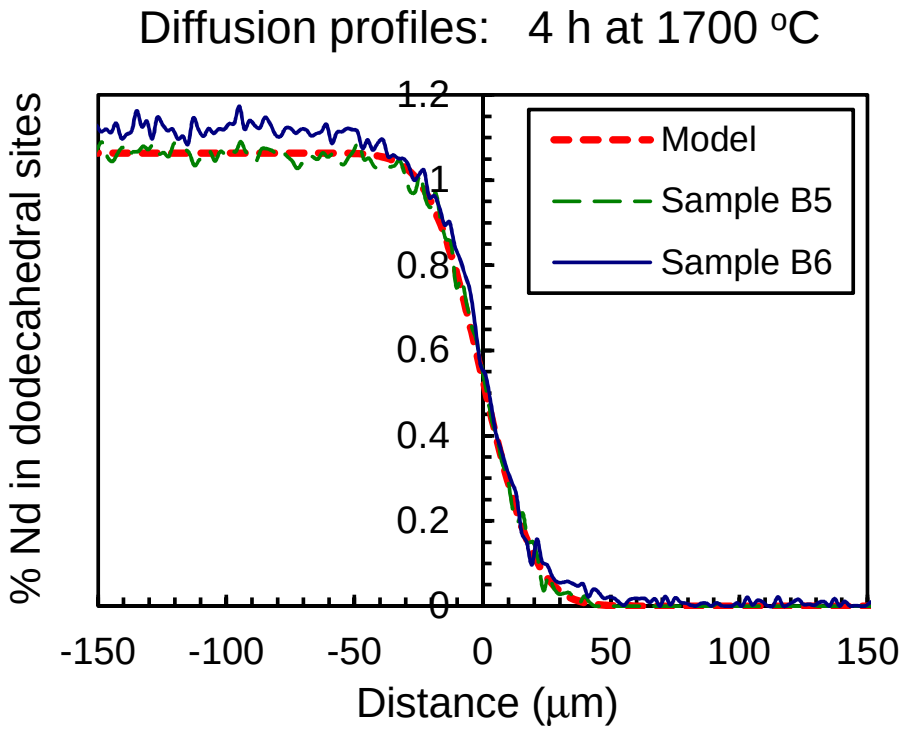

Figure 4.1: Concentration profiles of diffusion couples sintered at 1700 °C for 4 h. Electron microprobe measurements of the concentration of Nd^{3+} ions as a function of distance from the diffusion interface are shown for two different samples, one of which is shown as a solid curve, and the other, as a dashed curve. A best-fit curve from the regression model described here is plotted on the same axes for reference.

including measurements of Y and Al fluorescence, follows.

Calibrated measurements of the concentration of Y, Nd, and Al agreed well with the intended composition. Assuming enough O to balance charge, the total signal at a typical location was $(100.3 \pm 2.1)\,\%$ of the theoretical mass. The observed ratio of rare earth ions to aluminum ions was 0.609 ± 0.018, which agrees well with the theoretical ratio of sites appropriate to Y and Al in the crystal structure of garnet (0.6). To compensate for surface irregularities, concentration measurements were normalized according to a total concentration of $100\,\%$. Examples of normalized concentration profiles can be seen in Figure 4.1.

Each concentration profile was then subjected to three phases of regression analysis. First, an initial effort was made to estimate two parameters that are not expected to change due to diffusion. These estimates were then applied using a linearization function, so that two further rounds of regression could be carried out on a linearized set of concentration profiles.

The goal of the first round of regression analysis included the minimum and maximum concentrations of Nd, as observed at points far from the diffusion interface. As expressed in the nomenclature of Equation 4.1, these quantities are c_b and $c_0 - c_b$, respectively. For most samples, c_b was not significantly different from zero[2], and regression produced the fitting parameters directly. In cases where a signficant background signal was present in the data, c_0 was easily calculated by subtraction.

Using these concentration parameters, the data were linearized via the probit function, which is the inverse of the error function; this strategy has some similarity to the technique of probit analysis[139]. Each concentration measurement $c(x)$ was linearized to $\text{probit}(\frac{c(x)-c_b}{c_0-c_b})$. Because $\text{probit}(x)$ is only defined for $0 < x < 1$, and because most data points are clustered around c_0 and c_b, most data points did not produce a meaningful linearized value. This is to be expected,

[2]GDMS measurements on the un-doped powder agreed with the majority of EMP measurements in suggesting that negligible Nd was present in un-doped powder from Nanocerox. For purposes of diffusion measurements, it would not matter if c_b were a physical background concentration; however, in many applications, it would of course be preferable if Nd concentration were as low as specified. The opinion of the dissertation author is that c_b here is not physical, but rather that very small errors in instrument calibration were responsible for the background signal reflected in this fitting parameter.

because the majority of measurements were taken at points in the sample where the concentration of Nd was not significantly influenced by diffusion.

Linear regression was performed on the largest contiguous set of meaningful linearized data points for each sample. The results of this initial linear regression process were taken as a rough estimate of $\sqrt{Dt}$, and of the distance from the diffusion interface to the first concentration measurement. However, fluctuations in the concentration data introduce some bias under this analysis method: instances of noise which increase the difference between the measured value and the concentration at the diffusion interface will tend to place data points outside the domain of the linearization, while instances of noise which result in mesurements more similar to that concentration will place other data points inside of that domain. Using the standard error estimates from the first round of regression and the model from the second round, it was possible to identify which data points were most likely to be biased in this way. Data points whose distance from the inferred diffusion interface corresponded to a Nd concentration within two standard deviations of either c_0 or c_b were omitted from the third round of regression analysis. The results of this final round of linear regression are presented in Table 4.1[3].

Diffusivities observed at each temperature are shown in Figure 4.2, along with diffusion results from the literature. The initial publication of this experiment includes some preliminary discussion of these same raw data, but space constraints and the fact that work was ongoing at the time of publication limited the scope of the analysis. An expanded analysis and discussion is presented here in order to facilitate future work on the topic.

The diffusion rate observed in the initial experiment was far too rapid to be explained by diffusion through the bulk[6], and so a high-diffusivity path is implicated. The observation of negligible Nd diffusion during calcining, as reported in Subsection 3.2.2, and of continued diffusion following pore closure, suggests that both diffusion along free surfaces and transport via evaporation and condensation can be ruled out. This agrees with theoretical models suggesting that such mechanisms interfere with densification[12], and with the observation that sam-

[3]Note that samples 153B5 and 150F were each measured twice. The duplicate measurements, with confidence intervals, are presented together in the table.

Table 4.1: Observed diffusion distances for samples sintered at 1600 °C to 1781 °C for 4 min to 480 min. Diffusion distances are listed with a 99 % confidence interval from regression performed on each sample's EMP concentration profile.

Sample	T (℃)	t (min)	$\sqrt{D_{\mathit{eff}}t}$ (µm)
154A5	1450	480	6.54 ± 0.12
154A4	1600	4	6.82 ± 0.12
154A2	1600	4	7.29 ± 0.15
154A1	1600	480	13.5 ± 0.2
154A3	1600	480	13.5 ± 0.2
152B9	1650	4	8.81 ± 0.19
151C	1650	4	9.40 ± 0.20
153B2	1650	240	16.5 ± 0.2
153B1	1650	240	18.6 ± 0.2
152B8	1650	480	17.4 ± 0.1
152B7	1650	480	19.9 ± 0.1
153B5	1700	4	11.2 ± 0.2, 11.3 ± 0.2
153B6	1700	4	12.0 ± 0.2
152B5	1700	240	16.8 ± 0.1
152B6	1700	240	20.1 ± 0.1
152B4	1700	480	20.2 ± 0.1
152B3	1700	480	23.0 ± 0.3
152B1	1750	4	13.9 ± 0.2
152B2	1750	4	16.2 ± 0.1
151B	1750	240	21.7 ± 0.2
150E	1750	240	23.1 ± 0.3
153B3	1750	480	23.8 ± 0.3
153B4	1750	480	24.5 ± 0.3
150F	1781	4	16.1 ± 0.2, 18.1 ± 0.1
150D	1781	240	27.2 ± 0.8
139B	1781	480	29.0 ± 0.7
150B	1781	480	29.1 ± 0.4

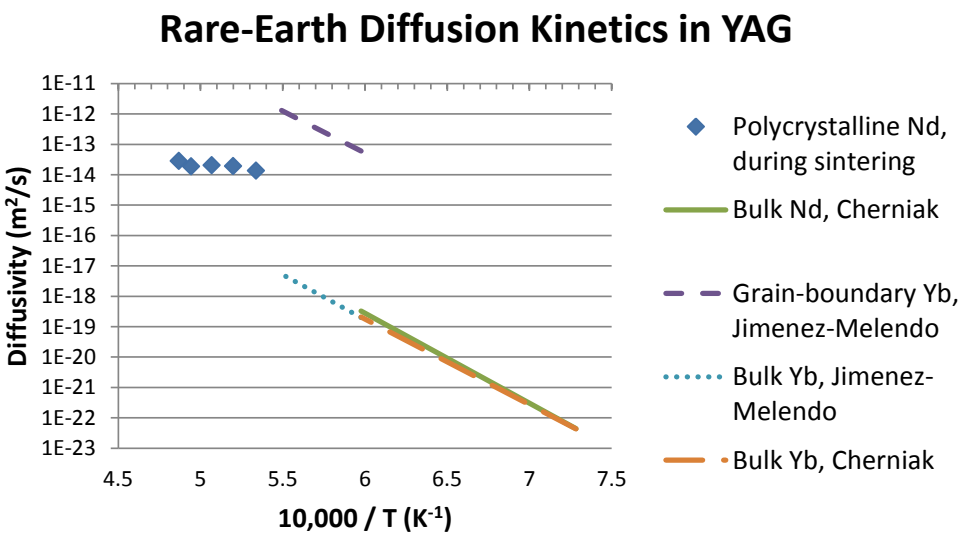

Figure 4.2: Rare-earth diffusivity in YAG as a function of temperature. Published values for the diffusivity of Nd through the bulk[6], and of Yb both through the bulk[6, 132] and via grain boundaries[132], are plotted as lines. Variation observed during sintering (diamonds) is attributed to coarsening of the grain structure, in addition to thermal activation of diffusion. Note that Yb grain boundary results have been normalized to the grain boundary concentration, but the dissertation author's results for Nd have not been normalized, and so the two sets of diffusivity data are not directly comparable.

ples rapidly became more dense. The large unit cell of the garnet structure gives YAG a high energy of dislocation formation, and dislocations are not significant to the rate of creep[140], suggesting that diffusion via dislocations is unlikely to contribute significantly to Nd mobility. The evidence points more to grain-boundary diffusion than to any other potential mechanism.

In agreement with published conclusions[135], the dissertaion author anticipates that the results published here can be applied to typical applications of YAG ceramic devices with tailored Nd doping. The maximum doping of 1 % Nd (dodecahedral site basis) is consistent with published dopant concentrations for ceramic Nd:YAG amplifiers (see Section 2.1.4 for a review of relevant literature). Micrographs such as the one shown in Figure 4.3 show no difference between the microstructure of the doped and the undoped regions of these samples, which suggests that differences in atomic mobility due to these small concentration differences were not great enough to result in visible differences in coarsening or

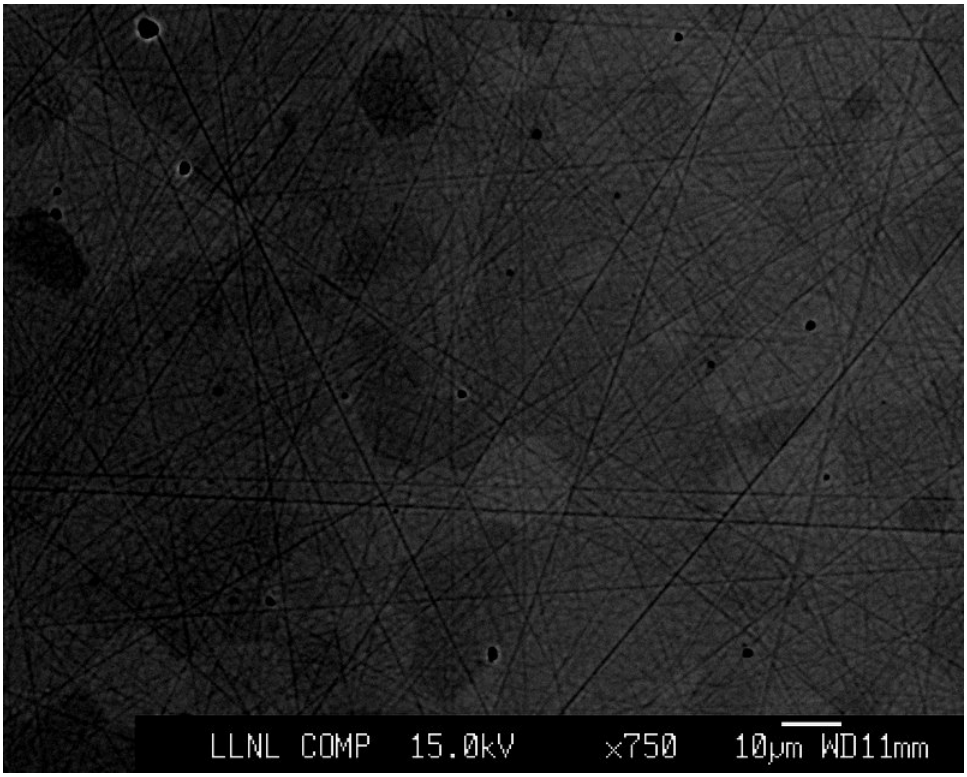

Figure 4.3: Electron backscatter image of the sintered interface between un-doped YAG and Nd:YAG

densification rates.

The original study cautions against applying its results too broadly. The dissertation author stands by these statements: studies of dilute Nd:YAG offer no guarantee that diffusivity will remain independent of concentration at high Nd concentration, and additional care may be necessary if conditions are found wherein Nd doping and grain growth interact significantly[135].

Chapter 5

Iso-structural intergranular diffusion

To isolate the kinetics of Nd diffusion from the kinetics of grain growth, a two-stage sintering method was developed, allowing diffusion to occur without significant grain growth. The strategy was to first sinter all samples for a short time at relatively high temperature, then to carry out subsequent heat treatment at significantly lower temperatures. The intent of the initial heat treatment was to cause a controlled and uniform amount of coarsening in all samples, reducing the grain boundary concentration and therefore the driving force for further coarsening. This reduced driving force, in turn, was expected to reduce variations in grain size due to variation in diffusion heat treatment, with a greatly reduced rate of coarsening at temperatures lower than the initial sintering temperature. Design of this method was greatly informed by previous work on yttria [141].

5.1 Experimental procedure

Diffusion couples were pressed, calcined, and sintered following the methods described in Subsection 3.2.1. Sintering conditions were chosen in order to achieve a relatively stable microstructure while maintaining a relatively short Nd diffusion distance. The set of measurements presented in Table 4.1 were consulted in search of the highest sintering temperature that would still allow for a sufficiently short

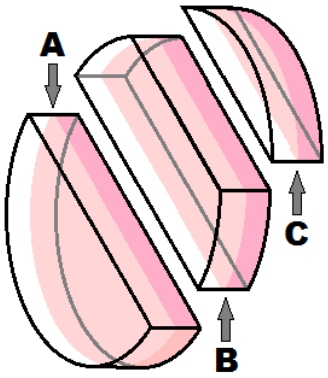

Figure 5.1: Illustration of diffusion couples after sectioning via diamond saw. A: section prepared for electron microprobe measurements (cf. Fig.3.1) ; B: section prepared for thermal etching and grain size measurement; C: section heat treated via HIP (samples P and Z only).

diffusion distance; a diffusion distance of approximately 10 µm was not expected to interfere with the measurement of subsequent diffusion.

Samples were sintered at 1700 °C for 4 min. As shown on the right side of Figure 5.5, the samples were translucent after sintering, due to some residual porosity.

Duplicate samples were subjected to each set of diffusion conditions. Diffusion temperatures were chosen to be significantly less than the sintering temperature in order to minimize grain growth: 1500 °C, 1550 °C and 1600 °C, for times of 4 h, 16 h and 64 h. Two control samples, which did not undergo any heat treatment beyond sintering, were also included in the analysis.

After diffusion was carried out, samples were sectioned into three parts using a diamond saw, as illustrated in Figure 5.1. One part of each diffusion couple was prepared for microstructural analysis, and another, for concentration profile measurements. In the case of samples P and Z, the remainder of each sample was then processed in a hot isostatic press (HIP) at 200 MPa and 1650 °C or 1750 °C for 4 h. Two un-cut control samples also underwent HIP, one at each temperature.

In order to reveal microstructure, a surface cut from near the center of the original sample was polished and thermally etched in a vacuum at 1450 °C for 2 h. Prepared samples were mounted for SEM imaging, which was carried out by a

microscopist. Images of the grain structure were overlaid with a randomly-placed grid, and intersections between this grid and grain boundaries were counted in order to measure the concentration of grain boundaries.

The facing surface was mounted and polished, and prepared for electron microprobe analysis, which was then carried out by a specialist. The procedure, technician, and equipment were the same as for the work reported in Subsection 3.2.1.

5.2 Results

5.2.1 Microstructure

An SEM secondary electron image of a typical microstructure can be seen in Figure 5.2. Pore edges were used to aid the microscopist in adjusting the instrument. This procedure produced images with a greater concentration of pores than would have appeared in micrographs framed at random. Density, as measured by the Archimedes method, suggests that the pore volume fraction is no greater than 5 %.

A grid of known length was overlaid on each of two images from each sample, and the number of intersections between the grid and any grain boundary was counted. At least one hundred such intersections were observed per sample, allowing average grain size to be measured with an uncertainty (95 % confidence interval) of between 0.3 µm to 0.05 µm for each sample (listed in Table 5.1). Analyzing the variance among grain size measurements, grain boundary concentration measurements were divided into groups of four images, each corresponding to a particular heat treatment. Variance among these groups of images was 0.0026 as great as variance among the 36 individual images, suggesting that grain size did not vary significantly: testing for significance under a hypothesis that coarsening occurred yields $p > 0.99$. The mean grain size observed across all samples was (0.83 ± 0.02) µm.

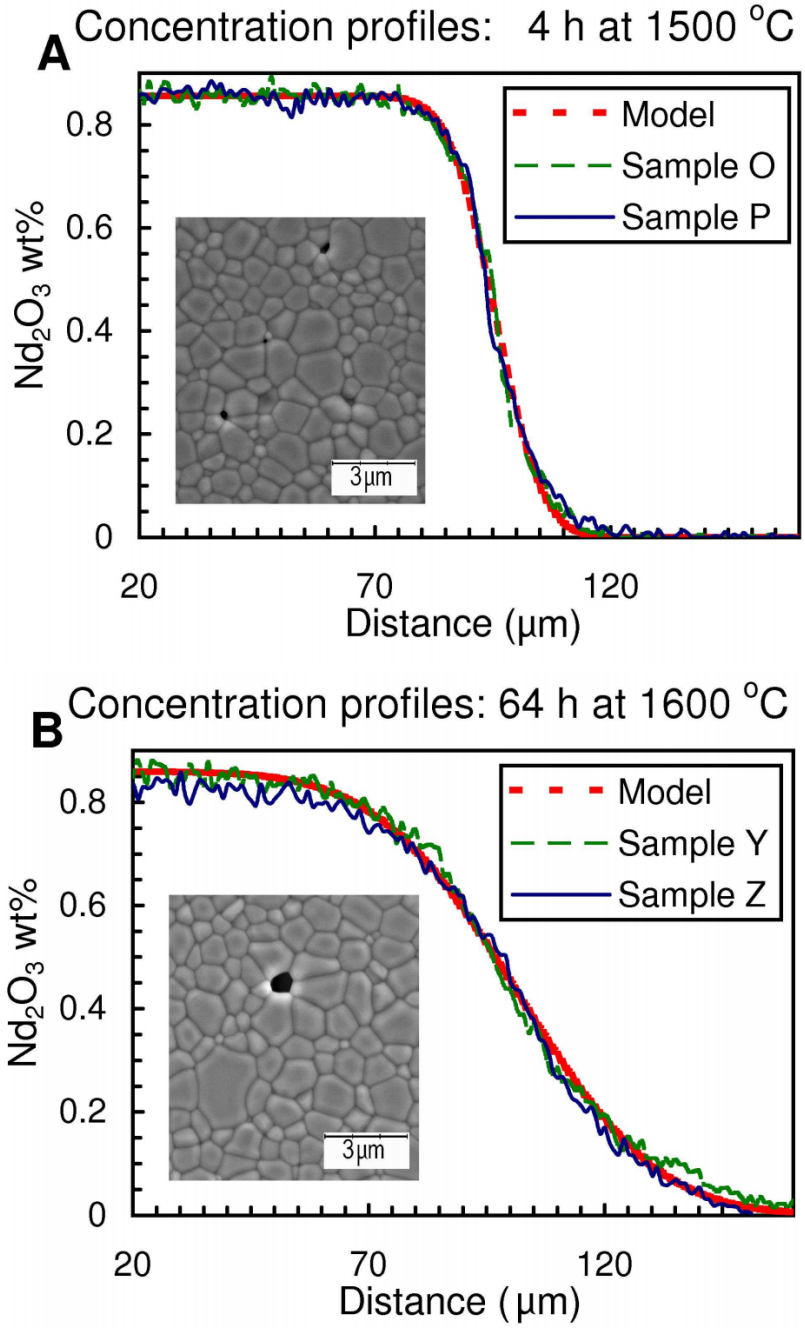

Figure 5.2: Electron microprobe profiles of YAG/1 % Nd:YAG diffusion couples, showing duplicate samples and a complimentary error function fit of one sample's data for each set of conditions. Inset: SEM images of thermally-etched surfaces after diffusion heat treatment. A: 4 h at 1500 °C. B: 64 h at 1600 °C.

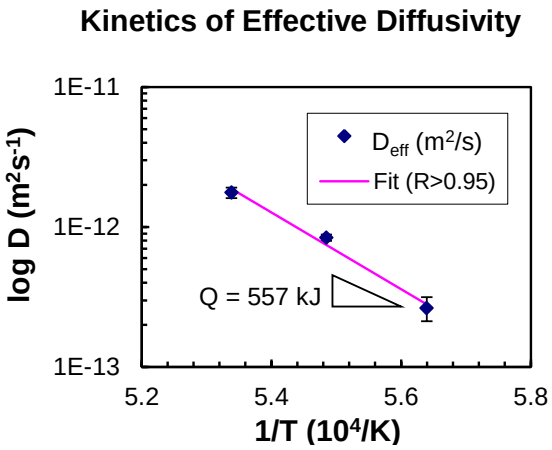

Figure 5.3: Effective diffusivity of Nd in polycrystalline YAG at 1500 °C, 1550 °C and 1600 °C. Regression produced a diffusivity and standard error for each temperature, which were used to generate a normally-distributed set of random points with which the activation energy was estimated.

5.2.2 Diffusion

As was the case for composition data presented in Subsection 3.2.2, calibrated measurements of the concentration of Y, Nd, and Al agreed well with the intended composition. The normalization of concentration measurements was carried out as before. Examples of normalized concentration profiles are shown in Figure 5.2. The examples chosen were the extremes of measured conditions, including two concentration profiles produced by a 4 h soak at 1500 °C (A) and two produced by a 64 h soak at 1600 °C (B). The full set of concentration profiles is included in Appendix C.

A model was fit to these normalized concentration profiles using the three-stage regression method described in Subsection 4.1[1]. Following the same reasoning discussed in Section 4.0.3, an error function, $c = \frac{1}{2}c_0\text{erfc}(\frac{x}{\sqrt{4D_{\mathit{eff}}t}})$, was used as the basis of the diffusion model, with $c(x)$ the local concentration of Nd as a function of distance from the diffusion interface, c_0 the concentration at $x = -\infty$, D_{eff} the effective diffusion coefficient, and t the soak time. This model described observed

[1]Previous publication of these results used the least-squares method. A more rigorous analysis was possible using linearized concentration data and excluding data points from locations where little diffusion ocurred. This additional rigor was particularly useful in the estimation of confidence intervals.

Table 5.1: Observed diffusion distances and grain sizes for samples sintered at 1700 °C prior to diffusion heat treatment. Diffusion distances are listed with a 99 % confidence interval from regression performed on each sample's EMP concentration profile, heat treatment conditions, and grain size measured by SEM of a thermally-etched cross-section.

Sample	T (℃)	t (h)	$\sqrt{D_{eff}t}$ (µm)	grain size (µm)
F	N/A	0	9.18 ± 0.07	0.773±0.05
G	N/A	0	N/A	0.820±0.05
O	1500	4	9.04 ± 0.07	0.732±0.09
P	1500	4	9.33 ± 0.08	0.856±0.09
H	1500	16	10.25 ± 0.10	0.800±0.23
I	1500	16	10.38 ± 0.07	0.835±0.23
Q	1500	64	12.96 ± 0.10	0.765±0.09
R	1500	64	11.58 ± 0.09	0.782±0.09
S	1550	4	10.22 ± 0.10	0.861±0.18
T	1550	4	9.94 ± 0.07	0.752±0.18
K	1550	16	11.09 ± 0.11	0.850±0.04
L	1550	16	11.51 ± 0.10	0.791±0.04
W	1550	64	17.56 ± 0.07	0.895±0.07
X	1550	64	17.00 ± 0.07	0.805±0.07
U	1600	4	10.95 ± 0.08	0.825±0.07
V	1600	4	11.58 ± 0.10	0.840±0.07
M	1600	16	15.20 ± 0.09	0.895±0.09
N	1600	16	14.58 ± 0.08	0.820±0.09
Y	1600	64	24.61 ± 0.08	0.850±0.03
Z	1600	64	22.38 ± 0.05	0.845±0.03

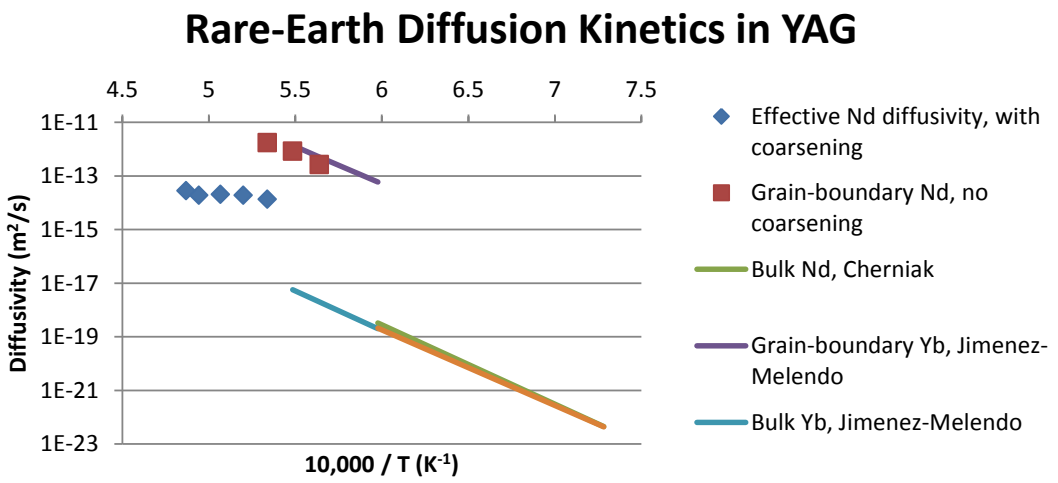

Figure 5.4: Rare-earth diffusivity in YAG as a function of temperature. Published values for the diffusivity of Nd through the bulk[6], and of Yb both through the bulk[6, 132] and via grain boundaries[132] are plotted as lines. Effective diffusivity observed in a previous experiment (diamonds) exhibits some super-exponential curvature, attributed to coarsening. Coarsening has been prevented in this experiment (squares) via maintenance of a constant grain structure, allowing the first publication of kinetics for Nd diffusion in polycrystalline YAG.

concentration profiles well enough that the final regression of linearized concentration profiles achieved $R > 0.97$ for all concentration profiles. Error function curves are plotted with parameters that best fit samples O and Y, on the same axis as the normalized data for those samples, in Figure 5.2. The fitting parameters c_0 were $(0.85 \pm 0.02)\,\%$ by weight, which is consistent with $1\,\%$ Nd doping (theoretically, $0.848\,\%$ Nd_2O_3 by weight), and parameters Dt are listed in Table 5.1.

For each temperature studied, linear regression was carried out on the square of diffusion distance as a function of time, in order to estimate D_{eff}. Similar to Figure 4.2, the resulting point estimates of diffusivity are presented in comparison to published diffusivitiy kinetics for rare-earth elements in YAG in Figure 5.2.2. Three values of D_{GB} are plotted as a function of temperature; these values and their activation energy are comparable to published kinetics for Yb grain-boundary diffusion.

In order to estimate the dependence of diffusivity on temperature, several random values for D_{eff} were generated for each temperature, using a normal distribution with a mean equal to the point estimate and a standard deviation based

Table 5.2: Variation of diffusivity model parameters with temperature. Estimation of diffusivity was based on a different number of DOF at each temperature, because greater diffusion distances resulted in a larger number of meaningful data points. This variation is reflected the number of diffusivity data points generated to estimate diffusion activation energy via the Arrhenius equation. The mean and standard error of each normal distribution are shown for D_{eff} and for $D_m athit GB$.

Temperature (℃)	1600	1550	1500
$\sum DOF$	399	308	259
Points generated	40	31	26
D_{eff} ($\mathrm{m^2\,s^{-1}}\times10^{-12}$)	1.76 ± 0.15	0.841 ± 0.042	0.264 ± 0.051
D_{GB} ($\mathrm{m^2\,s^{-1}}\times10^{-8}$)	1.47 ± 0.13	0.701 ± 0.035	0.220 ± 0.043

on the standard error of regression. In order to give appropriate weight to the data from various temperatures, the number of points generated for each temperature was determined in proportion to the total number of degrees of freedom (DOF) available from linearized data points corresponding to that temperature. Table 5.2 lists the number of DOF used to determine diffusion distance at each temperature, the number of data points generated for each temperature, and the values of diffusivity defining the distributions from which these points were drawn.

Regression analysis on these ninety-seven values of D_{eff}, illustrated in Figure 5.3, produced a fit of $D_{\mathit{eff}} = (6535 \pm 591)\,\mathrm{m^2\,s^{-1}} \exp(\frac{-(557 \pm 12)\,\mathrm{kJ\,mol^{-1}\,K}}{\mathrm{R}T})$. Based on the concentration of grain boundaries, subtracting bulk Nd diffusion at the rate reported in the literature[142], and following the convention that the width of a YAG grain boundary is 1 Å[132], this same method of regression analysis was carried out on corrected values of diffusivity to determine that grain boundary diffusivity is $D_{GB} = (6.37 \pm 2.01) \times 10^5\,\mathrm{m^2\,s^{-1}} \exp(\frac{-(491 \pm 64)\,\mathrm{kJ\,mol^{-1}\,K}}{\mathrm{R}T})$.

5.2.3 Final densification

HIP densification at temperatures lower than the sintering temperature was found to greatly improve the transparency of samples. Creep was rapid enough at 1650 °C to produce fully transparent samples within 4 h, which can be attributed to relatively fine grain structure compared to that produced by typical YAG sintering

Figure 5.5: Effects of hot isostatic press treatment. Left: 1750 °C for 4 h at 200 MPa. Center: 1650 °C for 4 h at 200 MPa. Right: as-sintered.

conditions.

Full samples are shown before and after HIP in Figure 5.5. Portions of samples P and Z were similarly transparent after HIP, suggesting that heat treatment for Nd diffusion did not interfere with densification in a way that degraded optical quality. This is expected, based on the negligible coarsening observed during diffusion.

5.2.4 Discussion

Polycrystalline YAG can be fabricated with a relatively small (approximately 0.8 µm) grain size, and this fine-grained microstructure can be retained while heat treatments are carried out to accomplish significant solute diffusion (diffusion distances through approximately 23 µm). Further, high temperature, high vacuum sintering is necessary only during the short first stage of heat treatment, which can decrease the demands this process places on vacuum furnace equipment. Further refinement of this processing strategy may allow even greater isolation of heat treatments undertaken for their effect on microstructure, from

processes undertaken to relax dopant concentration gradients. Greater independence between these two processes would reduce the need to compromise between ceramic processing considerations and the concentration profile specifications of laser system designers.

Portions of Chapter 5 are adapted from material as it appears in Joel P. Hollingsworth, Joshua D. Kuntz, Frederick J. Ryerson, and Thomas F. Soules, "Nd diffusion in YAG ceramics", *Optical Materials*, 33 (4), pp. 592-595, 2011. The thesis author was the primary investigator and author of this paper.

Part III
Impact

Chapter 6

Ongoing development of tailored ceramics technology

6.1 Controlled diffusion with laser amplification

The implications of the methods presented in Chapter 5 go beyond the measurement of atomic mobility: they also point the way toward greater control of processing. Methods of rapid sintering are, of course, important: they save costs in their own right, and loosen constraints on subsequent processing methods. A lack of observed coarsening during dopant diffusion may be the more important result though, because it suggests that multi-stage heat treatment of this sort can allow independent control of concentration gradients and of microstructure.

As the results presented in Chapter 4 were being compiled for publication, the research group was excited by the ease with which vacuum sintering of FSP powder resulted in transparent parts. Diffusion couples for that study achieved transparency after relatively mild sintering treatments: as little as 4 min at temperatures of 1700 °C and greater, and temperatures as low as 1600 °C when sintering was carried out for at least 8 h. However, the need to also control dopant diffusion suggests that perhaps transparency is not the wisest goal during the initial sintering process.

The practical constraints on laser amplifiers go beyond mere transparency,

as work at the Lawrence Livermore National Laboratory (LLNL) has shown. In order to verify that the consolidation and sintering methods presented here were suitable for the fabrication of laser amplifiers, the author's colleagues[1] fabricated amplifier slabs via the same methods used to produce diffusion couples and compiled oscillation data to be presented alongside these diffusion results[135]. The performance of these samples was promising, and suggested that further development of the methods described in Subsection 3.2.1 could produce laser amplifiers with a tailored dopant concentration profile. However, this method is limited to concentration gradients aligned with the direction of pressing, and subject to the slab size limitations inherent to cold pressing of ultrafine powders. However, these experiments show that even the small pore volume retained after sintering for eight hours at 1781 ℃ results in more scattering than is acceptable in laser applications. HIP was necessary for the production of useful laser amplifiers, and the processing regimen used in this experiment might even benefit from some refinement. This suggests that sintering should be understood as a preparation for HIP rather than as a means of achieving transparency.

To prepare a sample for HIP, the most important goal to achieve is closure of pores. Another important consideration is sample plasticity: a greater concentration of grain boundaries is expected to enhance creep[140] and to allow HIP to proceed more rapidly. The optimum sintering procedure, according to these criteria, is one that achieves closed porosity without excessive coarsening.

The initial heat treatment carried out on diffusion couples for Chapter 5 was a step in the right direction. It showed that Nd:YAG ceramics can be sintered to a state of closed porosity while maintaining sub-micron grains and only modest diffusion of Nd. This result ccan likely be built upon by developing heat treatment routines in which pores close but even less coarsening occurs. This would require less time, and a lower maximum temperature.

The result that followed is closely related: subsequent heat treatment at temperatures less than the sintering temperature was shown to allow a wide range

[1]Joshua Kuntz pressed and sintered 0.6 % Nd:YAG ceramic rods. After HIP by an external vendor, the rods were polished, and used as amplifiers in a laser cavty operated by an on-site technician. See the full publication[135] for additional details of this experiment.

of dopant diffusion distances without significant change of microstructure. This latter result has the same potential for exension: any milder sintering conditions will result a higher concentration of paths for rapid diffusion and will reduce the time necessary to achieve a specified concentration gradient.

The same experiment also showed that HIP processing at temperatures less than the sintering temperature can achieve transparency, at least in the case of YAG with an average grain diameter of 0.8 µm.[2] Finer grains, though still coarse enough not to drive rapid coarsening during subsequent heat treatment, are expected to enhance the benefits of isolating processing steps intended to alter microstructure from steps intended to allow dopant diffusion, thereby enabling a broader range of achievable concentration gradients within the limited conditions required to achieve transparency.

More generally, consolidation research can be de-coupled from dopant diffusion research: the effects of powder particle size and of green density are expected to have only a simple impact on diffusion once the second stage of sintering is complete. Changes in consolidation method are expected to impact coarsening rates[60], but measurements of coarsening rates should then allow predictions of grain-boundary diffusivity. The dissertation author is not currently aware of any mechanism by which variations in green density or initial grain size can directly affect Nd transport during the sintering of YAG ceramics for tailored laser amplifiers. Bulk diffusivity is a relatively minor and predictable contribution to Nd transport, and other mechanisms are not expected to contribute significantly, for reasons discussed in Section 4.1. Grain boundary diffusivity measurements reported in Chapter 5 are therefore expected to inform the design of heat treatment programs for tailored Nd:YAG ceramics even if processing conditions are significantly different.

Because grain boundary diffusion is the major mode of transport for Nd

[2]It may be necessary to account for enhanced atomic mobility due to the disorder introduced by this final densification step. If the rate-limiting process is a movement of Y vacancies from pores to grain boundaries, the vacancies so released must make a random walk over a distance proportional to grain size, and so the effect of these vacancies on the final composition profile must vary in proportion to the volume fraction of pores removed during HIP and to the square of the average grain size of the ceramic.

(see Section 4), the interface between doped and un-doped YAG in such a device would show roughness on the order of the size of a grain boundary; Nd alters YAG's refractive index, and so the material would need to have grains finer than the wavelength of the amplified light in order to avoid undue scattering from this interface.

6.2 Supporting technologies

As the experiments reported in Chapters 3, 4, and 5 were being carried out, a broader research effort was underway, at LLNL and elsewhere, whose results also support tailored ceramic technology. The new technologies produced by that effort, especially the invention of gel casting, may facilitate the production of multi-functional optical ceramics for a broader range of applications, and thereby extend the impact of the diffusion results presented here.

6.2.1 Concurrent work at other institutions

Efforts undertaken outside LLNL include those referenced in Section 2.1.5. Among other important contributions, a series of studies by the Byer research group advanced methods to design concentration profiles suitable for high-power ceramic lasers[143] and introduced an elegant strategy for measuring the concentration of active laser dopant species via stimulated emission[144].

A study by the Messing group brought attention to the promise of tailored Er:YAG ceramics, by demonstrating laser oscillation from a tape-cast amplifier with a sintered boundary between pure YAG and Er:YAG. This result supports an extension of tailored ceramics research beyond Yb and Nd. It also introduces into the transparent ceramics literature a method which meets the stringent quality criteria of laser amplifier applications while also offering the capability to fabricate multi-functional ceramics[127].

6.2.2 Resolving conflict between transparency and multi-functionality

The difficulty of developing tailored ceramics methods can be partly understood as arising from conflicting needs for uniformity and non-uniformity. On the one hand, the green structure needs to be extremely uniform, in most ways, in order for the sintered product to be transparent. On the other hand, multi-functional ceramics require the introduction of controlled variations of composition: otherwise there can be no variation in function. This fundamental tension can be partly resolved by designing a processing procedure that ensures significant atomic mobility, capable of removing significant non-uniformities from the green structure. For example, reactive sintering induces rapid dopant diffusion, which is understood to be a result of a high atomic mobility in the transient phases that occur as pure oxides transform into garnet[5].

While this has benefits in terms of microstructural uniformity, it does so at the expense of any ability to control dopant diffusion. There would be some benefit from developing means of densification and microstructural homogenization that could be carried out more independently of dopant diffusion, such that independent parameters could be varied in order to meet both concentration profile specifications and microstructural requirements. As discussed in Section 6.1, the maintenance of fine grain structure seems likely to facilitate such a development.

A complimentary strategy for resolving this tension is to minimize non-uniformity at interfaces within the green structure; ideally, interfaces between regions of various composition would not be special to consolidation processes, such that no light-scattering non-uniformity would ultimately be introduced into the sintered product. This is challenging due to the surface-driven nature of most consolidation processes: for example, pressure is applied to the powder surface by a punch in pressing processes, or water is drawn out of the slip at the mold surface in slip casting.

6.2.3 Greater surface area: Flame-spray pyrolized powder

FSP powder is made up of particles that are typically smaller than the particles that make up precipitated powders, and are of a more uniform size, as can be seen from Figure 3.1. Powder with a greater surface energy is desirable, as it tends to drive more-rapid sintering. The author and others at LLNL found that this same small particle size also causes aqueous suspensions of this powder to be especially reactive in comparison to coarser powders: in particular, methods of slip casting that work reliably for co-precipitated powder were found to be entirely unsuitable for FSP powder. The highly reactive FSP particles produce a less stable aqueous suspension with a tendency to flocculate. The rate of liquid flow into the mold was found to decrease rapidly following the addition of slip, likely due to some combination of infiltration of pores by the fine powder and pozzolan-like chemical reactions between the powder and the gypsum. A goal to produce larger-aperture laser amplifiers from FSP powder motivated further exploration of aqueous methods of powder consolidation. The research program was able to address many of the difficulties presented by this material, and has applied for patents on some of the resulting methods[145].

By slowing the flow rate, interactions between the powder and the mold also revealed problems due to interactions among powder particles themselves. Green densities were much lower than had been observed for larger particles, and in some cases, reserved portions of slurry solidified before the liquid level in the mold fell enough to accommodate them. Despite their low density, some of the resulting green structures were found to sinter to a translucent state.

6.2.4 Gel casting

The observation of translucency from un-intentionally consolidated parts led to the development of a novel fabrication method. This method resembles slip casting, but calls for a non-porous mold. Early results suggested that the strength of particle-particle reactions might be sufficient to produce a green structure that could be handled, and the result would be dense enough to sinter. A method of encouraging and harnessing gelation was developed on this basis, and was then

patented[146].

While it offers many advantages, the patented gel casting technique is not yet suitable for the casting of tailored ceramics. The rate of gelation and total degree of shrinkage due to gelation are highly sensitive to parameters of FSP powder that are not currently subject to strict control in manufacturing. Since different levels of doping in FSP powder are only available as different batches, variations in gel behavior from batch to batch greatly complicate the casting of tailored parts. Variations in shrinkage have caused de-lamination of gels along the boundary between compositions, and uncertainty over the timing of gelation has resulted in turbulent mixing at the boundary.

Among the many consolidation techniques on which the author participated in experiments, published and unpublished, gel casting was found to be the most appropriate for large parts. For example, it set a size record for transparent ceramic slabs sintered at LLNL (150 grams). The lack of constraints on mold material and configuration relative to slip casting also promises greater versatility in terms of shape and composition. These strengths especially recommend this method for use in applications calling for pulses of high energy, where larger apertures are called for, and gains in efficiency due to tailored doping are expected to ease other constraints on system design.

Future work could include a more fundamental investigation of the mechanisms of gelation, which would allow for greater control of gelation timing and rate. There are also practical questions that can be answered by empirical study. Developments in FSP synthesis have continued in this period, and any or all of these developments could extend gel-casting capability in terms of aperture size, optical quality, or suitability to the fabrication of devices with tailored doping profiles.

Chapter 7

General implications

Nd is the most thoroughly-studied laser dopant in garnets, but optical applications for several other lanthanides have been demonstrated. Each ion has its own characteristic set of electron energy levels, and the various transitions among these levels have been shown useful not only for laser amplification, but for other optical functions, including the suppression of parasitic oscillation, modulation via saturable absorption, and even scintillation (see Chapter 2 for published examples). Experiments similar to the one reported in Chapter 5 could be used to determine the grain boundary diffusivity of other useful elements in YAG, and the methods could also be adapted to other garnet host materials. The ability to predict an element's overall diffusivity through the material would then allow the design of heat treatment procedures capable of achieving a controlled concentration profile in that element, which would add that element to the list of those available for incorporation into tailored ceramic devices.

As Cherniak observed in the context of single crystals, the chemical similarity among lanthanides means that the difference in their diffusivity through YAG can mostly be understood as a function of ion size[142]. Jimenez-Melendo *et al.* discussed Yb in the role of a proxy for Y, as a means of studying creep in YAG[132]. There is some size difference between Yb atoms and Y atoms, but there are potentially fifteen data points available (atomic numbers 57 through 71) if one wanted to use the lanthanides systematically. Thorough experimentation on the garnet lattice has the potential to develop a fuller picture of the effect of ion size

on diffusion in ceramic materials, offering a window into the relationship between the strain required for an atomic jump and the activation energy displayed by the overall process.

Creep is just one class of processes that can be illuminated by more careful study of atomic mobility. Densification and coarsening of YAG can also be illuminated by measuring the diffusion of rare-earth elements.

This project would not have been possible without the work on alumina that founded this field. Although few efforts can match the impact of the studies discussed in Subsection 2.1.1, there are ample opportunities to benefit from their example of science and technology reinforcing each other. Robert L. Coble worked both to explain the microstructural changes that occur in ceramics, and also to control them; both of these efforts contributed to a developing understanding. The dawn of transparent ceramic technology came, not coincidentally, shortly after a connection was made between the fundamentals of atomic mobility and their interplay with meso-scale phenomena such as grain structure and porosity.

Continued developments in the field of tailored ceramics are expected to further illuminate this connection. Just as identification of the mechanism of densification (bulk diffusion to grain boundaries) enabled the fabrication of PCA dense enough to be translucent, it is hoped that identification of the dominant mechanism for dopant transport during the fabrication of YAG ceramics (grain boundary diffusion, as shown in Section 4.1) will facilitate the fabrication of devices via tailoring of dopant profiles.

Appendix A

Parallels to semiconductor technology

This body of work determined the mechanism of material transport responsible for the re-distribution of Nd^{3+} during the sintering of YAG, under conditions expected to be relevant to the fabication of ceramic optical devices. Scientific inquiry into which mechanism explains this phenomenon was intertwined with technological imperatives to exert control over it.

The investigations presented in this dissertation offered the great privilege of addressing questions of pure science by developing methods of applying that science, such that theory and practice each informed the other's development. Preliminary evidence that diffusion through grain boundaries was the dominant mechanism motivated my efforts to carry out diffusion at reduced rates of coarsening. Achieving significant diffusion with negligible coarsening allowed me to measure diffusion kinetics, which ultimately confirmed the initial findings regarding the mechanism. These kinetics results also connected this work to studies of other materials systems.

The practical motivation for studying RE diffusion in YAG ceramics is an ambition to tailor the doping of solid-state laser amplifiers. Tailored doping would mean fabricating monolithic optical devices composed of multiple, functionally distinct regions. Rather than being fabricated, current technology only allows devices of this sort to be built, adjusted, and maintained by hand. The field

of semiconductor electronics underwent a similar shift when advances in science and technology allowed fabrication of P-N junctions via diffusion. For decades prior to that development, the only semiconductor electronic device was the cat's whisker detector, in which the user carefully moved the point of a thin metal wire against the surface of a semiconducting mineral in order to achieve and maintain a rectifying junction between the two materials.

Similar to a cat's whisker detector, a solid state laser of the sort currently available (commonly, a single-crystal Nd:YAG laser) has several components whose functional relationship to one another is achieved by careful preparation of their surfaces, followed by a careful and ongoing adjustment of their relative position and orientation. Ideally, devices would be fabricated by defining a controlled doping profile and carrying out diffusion, such that the final concentration gradient creates functional interfaces within the bulk of the material. Such a capability is expected to allow the development of higher-performance, lower-maintenance devices that directly replace those currently in use, much as germanium and then silicon diodes replaced cat's whisker detectors. Perhaps more importantly, a flexible device fabrication technology would allow for new functionality within a given solid-state device, analogous to the development of transistors and integrated logic gates.

In the case of semiconductor electronic devices, science advanced by explaining phenomena that had already been harnessed via cat's whisker detectors; the principles of device fabrication were scientifically understood, and only needed to be elaborated on a technical level. Solid-state lasers, by contrast, operate via well-understood principles, and the scientific barrier that was overcome in Chapter 4 had to do with phenomena observed during fabrication.

As this work began, the dissertation author was confident that the diffusion phenomena observed would fall within known theoretical categories, but undertaking these investigations involved preparation for complications due to simultaneous sintering processes. The major scientific obstacle to the fabrication of tailored laser ceramic devices seemed to be a lack of diffusion studies. No mechanism had yet been identified for the diffusion processes most relevant to laser ceramics (*i.e.*,

diffusion within the materials system and under the set of conditions expected to be technologically important). Grain boundary diffusion seemed likely to be important, especially late in the sintering process, but there was no guarantee that other mechanisms would not dominate the overall rate of material transport, by exploiting opportunities that are only available early in the sintering process. Grain boundary diffusivity of Yb^{3+} in YAG had been studied, but there was no published information on the kinetics of Nd^{3+} grain boundary diffusion in YAG.

This work is presented in the hope that it will offer control over the diffusion of Nd^{3+} in YAG, and a potential strategy for gaining the control of other dopants. This was done to allow the design of heat treatment methods for the fabrication of integrated solid-state laser devices. Important work toward that end remains, but the example of semiconductor technology is available to those ready to take it up.

Appendix B

Electron microprobe measurements: diffusion during sintering

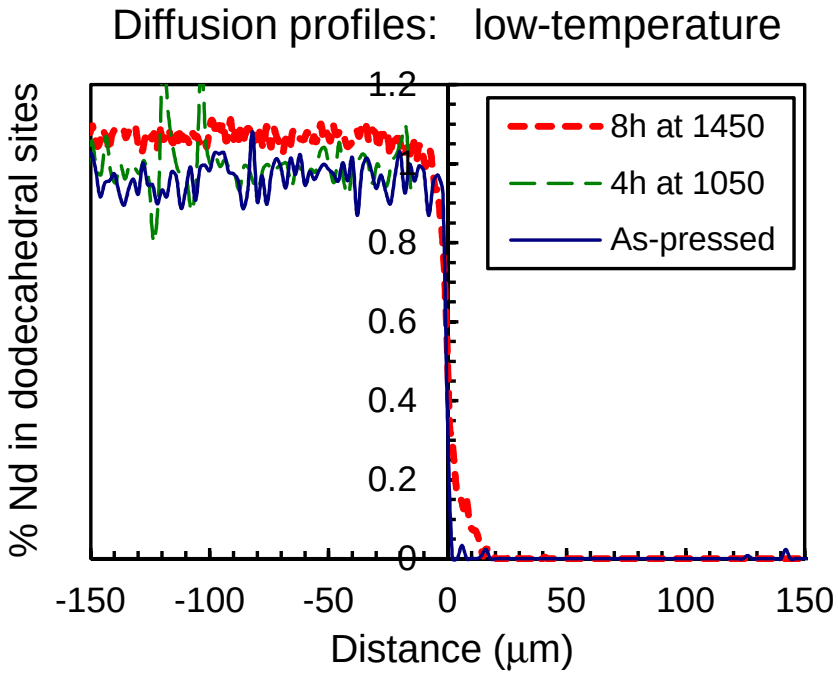

Figure B.1: EMP measurements of Nd concentration for YAG/Nd:YAG diffusion couples, measured without heat treatment (solid line), and following either of two heat treatment programs: 4 h at 1050 °C (narrow dashed line) and 8 h at 1450 °C. Concentration values represent a percentage of dodecahedral sites filled by Nd.

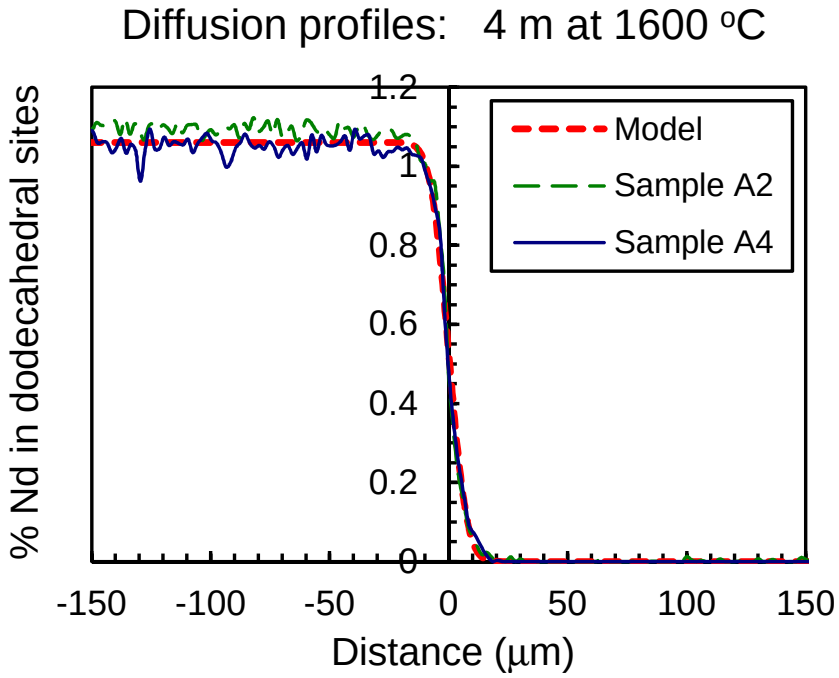

Figure B.2: EMP measurements of Nd concentration (narrow lines) and an error function fit (bold line) for YAG/Nd:YAG diffusion couples. Diffusion was carried out at 1600 °C for 4 min. Concentration values represent a percentage of dodecahedral sites filled by Nd.

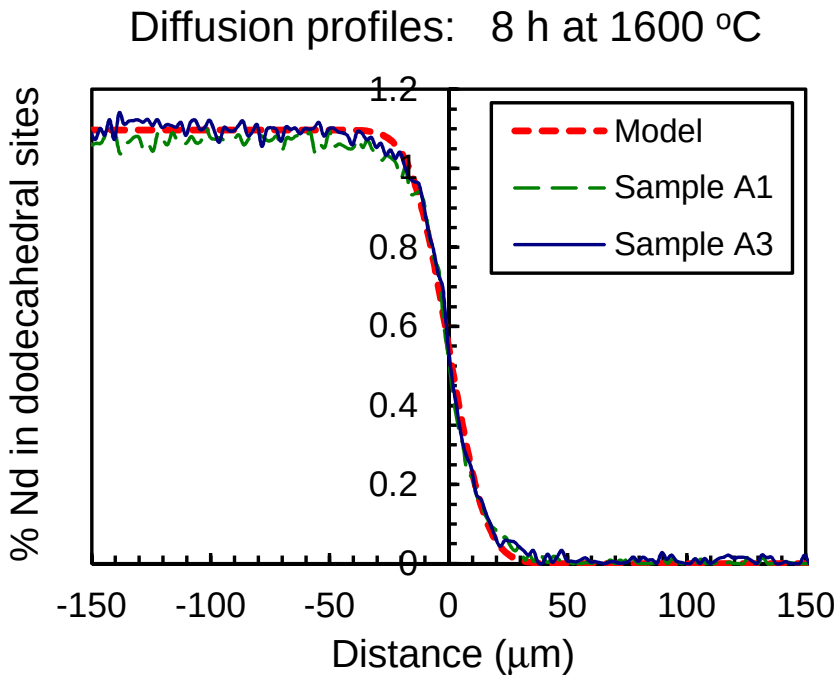

Figure B.3: EMP measurements of Nd concentration (narrow lines) and an error function fit (bold line) for YAG/Nd:YAG diffusion couples. Diffusion was carried out at 1600 °C for 8 h. Concentration values represent a percentage of dodecahedral sites filled by Nd.

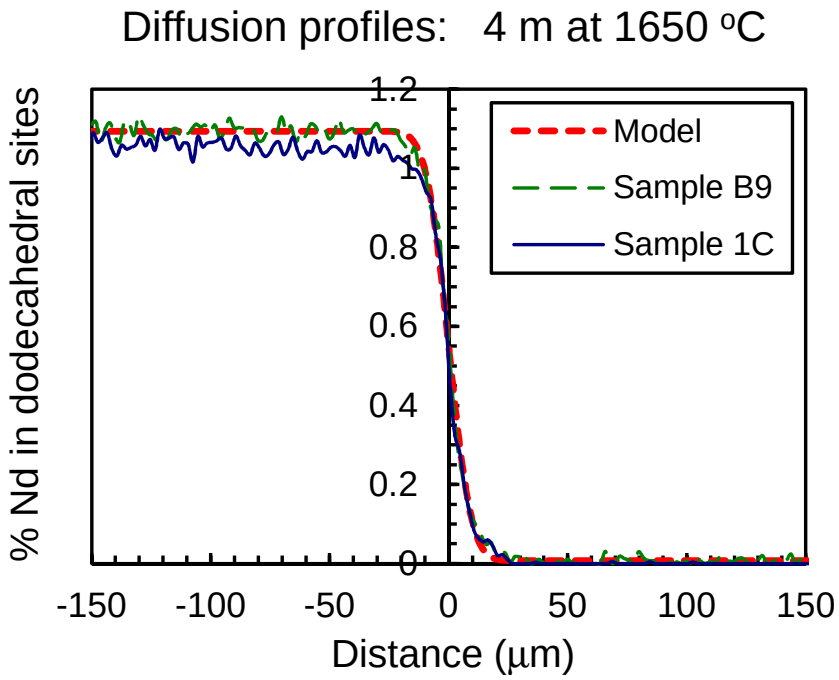

Figure B.4: EMP measurements of Nd concentration (narrow lines) and an error function fit (bold line) for YAG/Nd:YAG diffusion couples. Diffusion was carried out at 1650 °C for 4 min. Concentration values represent a percentage of dodecahedral sites filled by Nd.

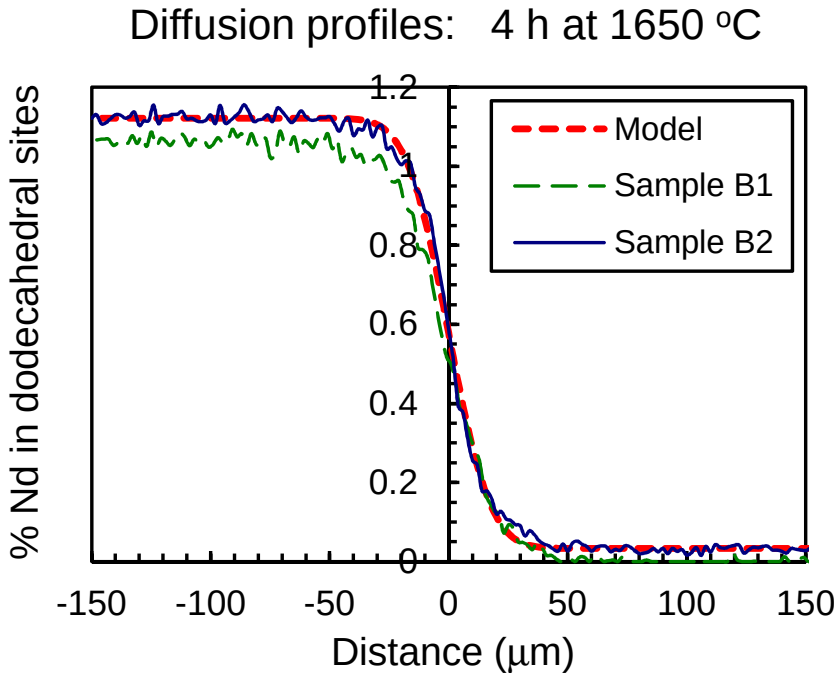

Figure B.5: EMP measurements of Nd concentration (narrow lines) and an error function fit (bold line) for YAG/Nd:YAG diffusion couples. Diffusion was carried out at 1650 °C for 4 h. Concentration values represent a percentage of dodecahedral sites filled by Nd.

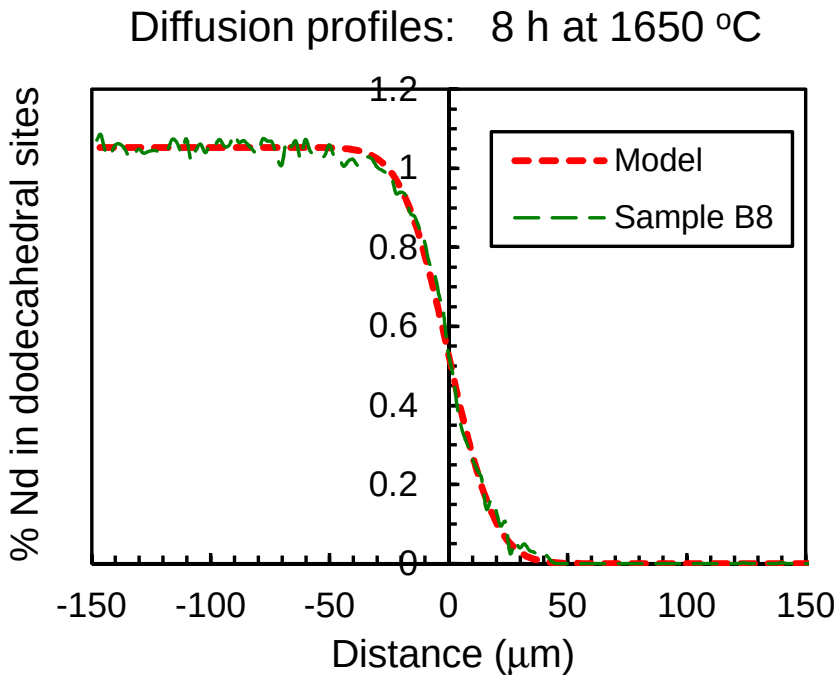

Figure B.6: EMP measurements of Nd concentration (narrow lines) and an error function fit (bold line) for YAG/Nd:YAG diffusion couples. Diffusion was carried out at 1650 °C for 8 h. Concentration values represent a percentage of dodecahedral sites filled by Nd.

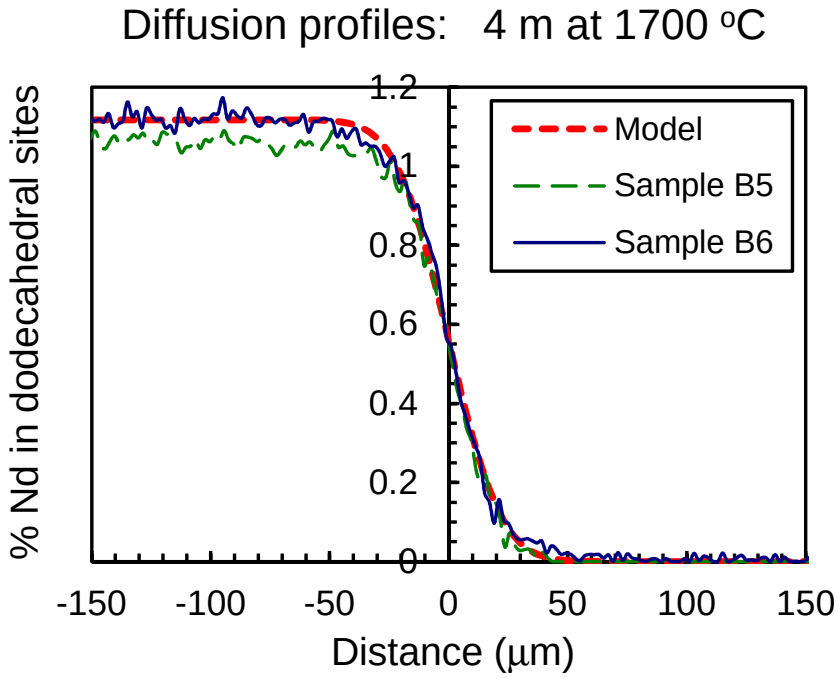

Figure B.7: EMP measurements of Nd concentration (narrow lines) and an error function fit (bold line) for YAG/Nd:YAG diffusion couples. Diffusion was carried out at 1700 °C for 4 min. Concentration values represent a percentage of dodecahedral sites filled by Nd.

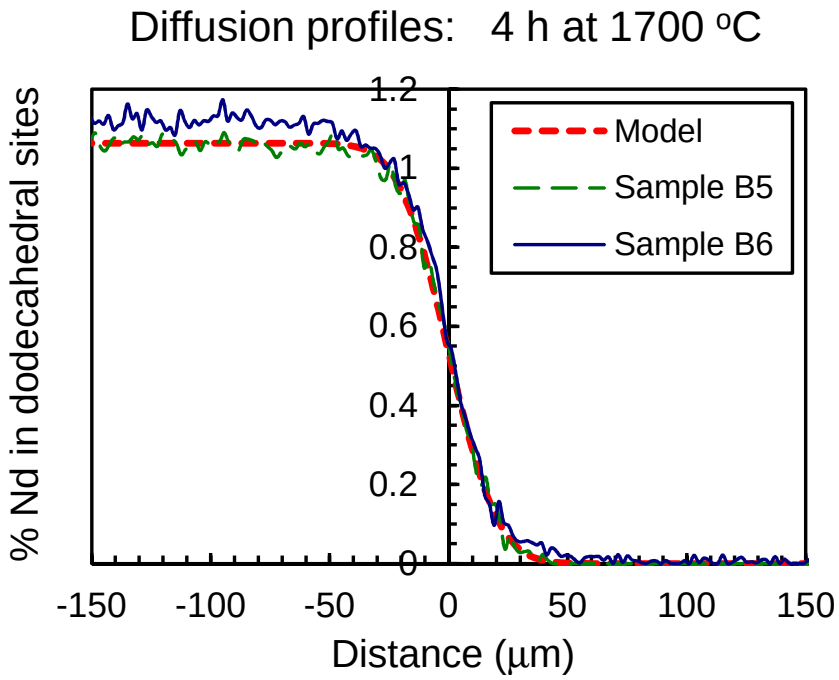

Figure B.8: EMP measurements of Nd concentration (narrow lines) and an error function fit (bold line) for YAG/Nd:YAG diffusion couples. Diffusion was carried out at 1700 °C for 4 h. Concentration values represent a percentage of dodecahedral sites filled by Nd.

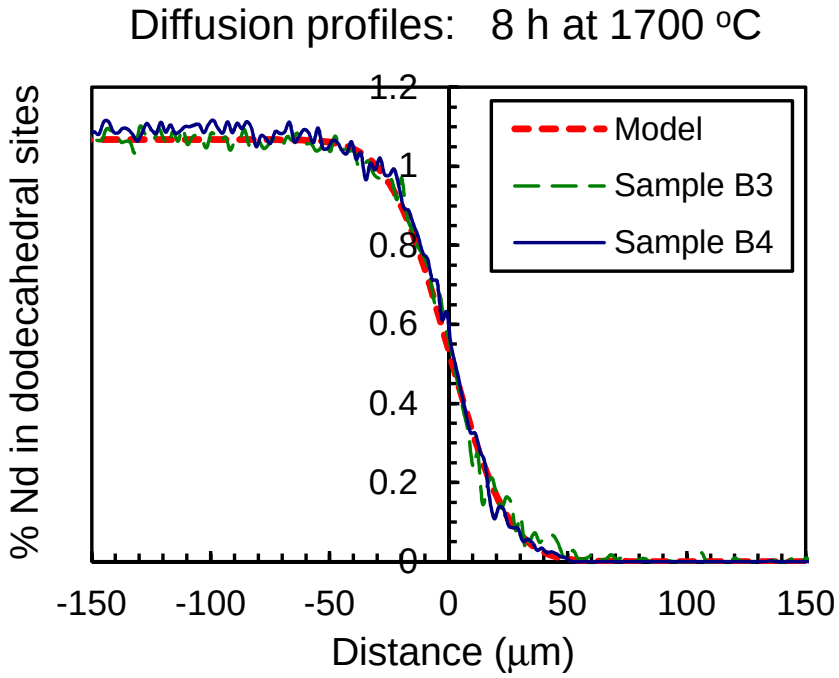

Figure B.9: EMP measurements of Nd concentration (narrow lines) and an error function fit (bold line) for YAG/Nd:YAG diffusion couples. Diffusion was carried out at 1700 °C for 8 h. Concentration values represent a percentage of dodecahedral sites filled by Nd.

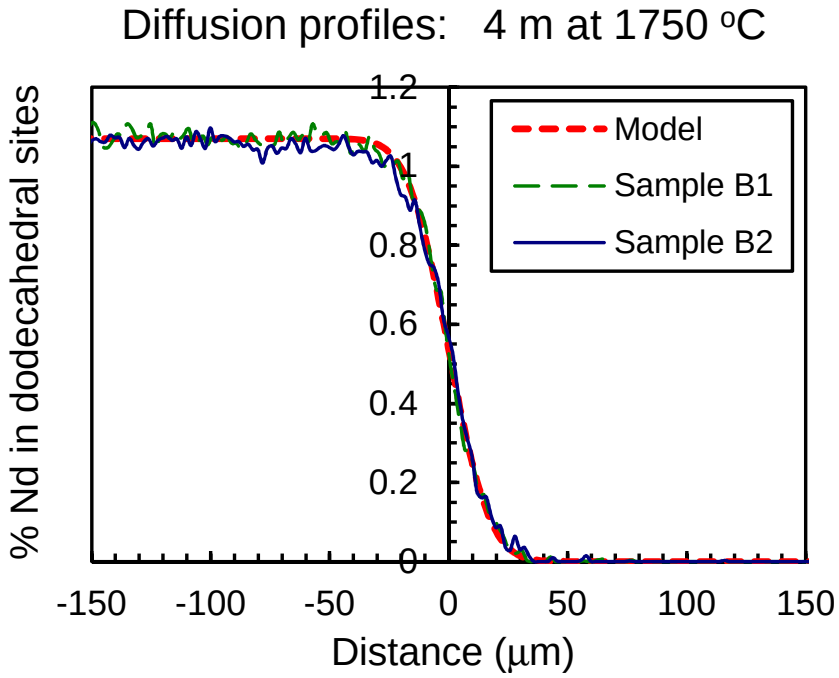

Figure B.10: EMP measurements of Nd concentration (narrow lines) and an error function fit (bold line) for YAG/Nd:YAG diffusion couples. Diffusion was carried out at 1750 °C for 4 min. Concentration values represent a percentage of dodecahedral sites filled by Nd.

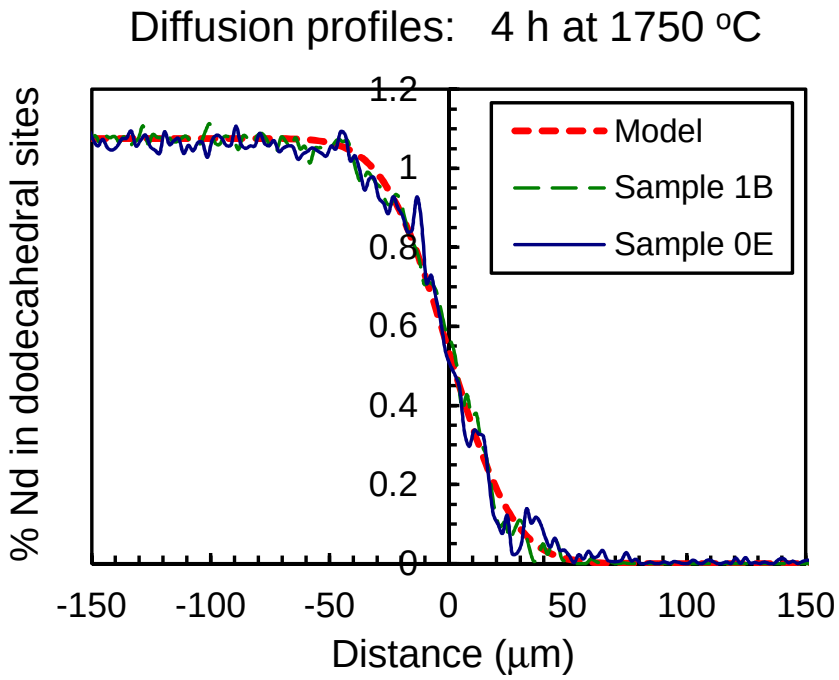

Figure B.11: EMP measurements of Nd concentration (narrow lines) and an error function fit (bold line) for YAG/Nd:YAG diffusion couples. Diffusion was carried out at 1750 °C for 4 h. Concentration values represent a percentage of dodecahedral sites filled by Nd.

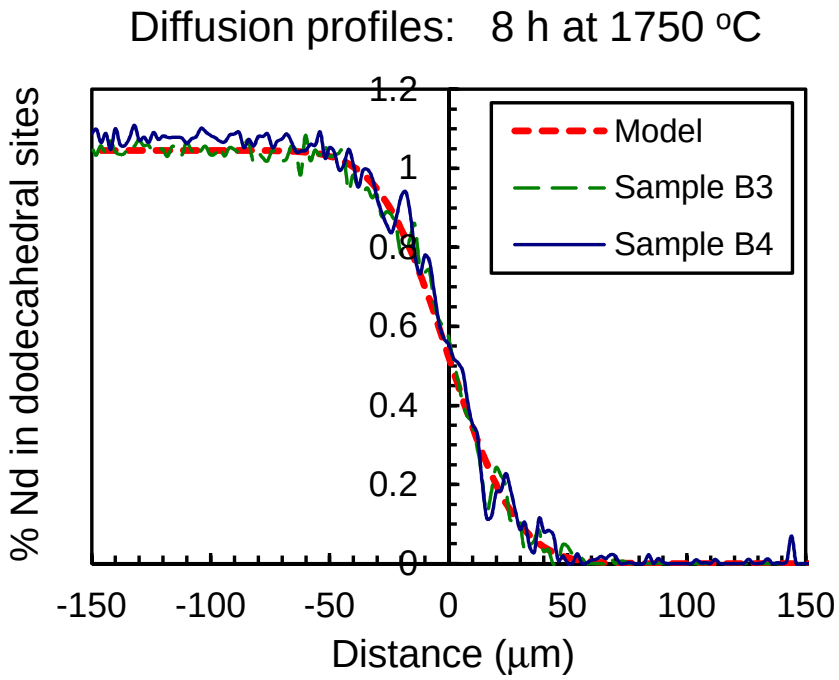

Figure B.12: EMP measurements of Nd concentration (narrow lines) and an error function fit (bold line) for YAG/Nd:YAG diffusion couples. Diffusion was carried out at 1750 °C for 8 h. Concentration values represent a percentage of dodecahedral sites filled by Nd.

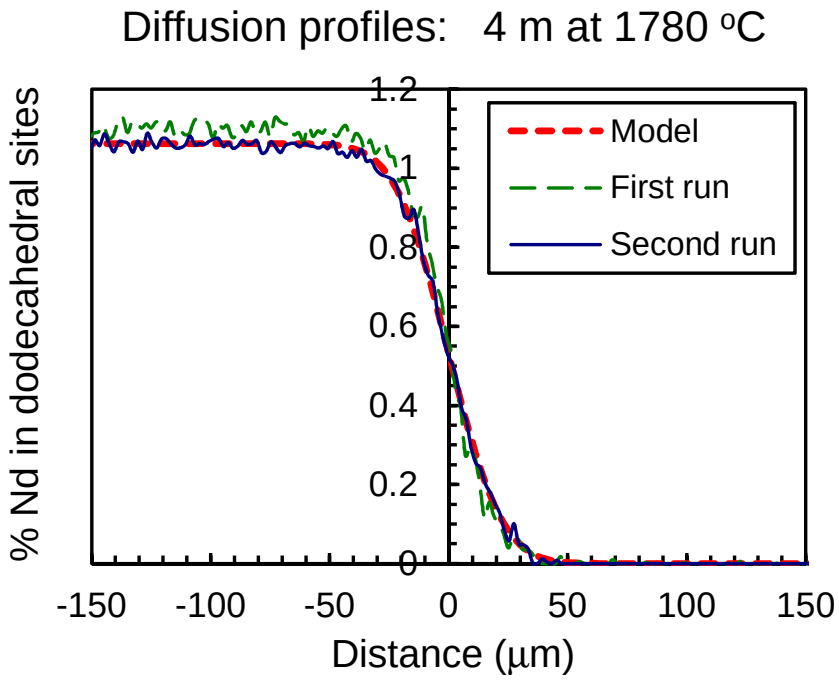

Figure B.13: EMP measurements of Nd concentration (narrow lines) and an error function fit (bold line) for YAG/Nd:YAG diffusion couples. Diffusion was carried out at 1780 °C for 4 min. Concentration values represent a percentage of dodecahedral sites filled by Nd.

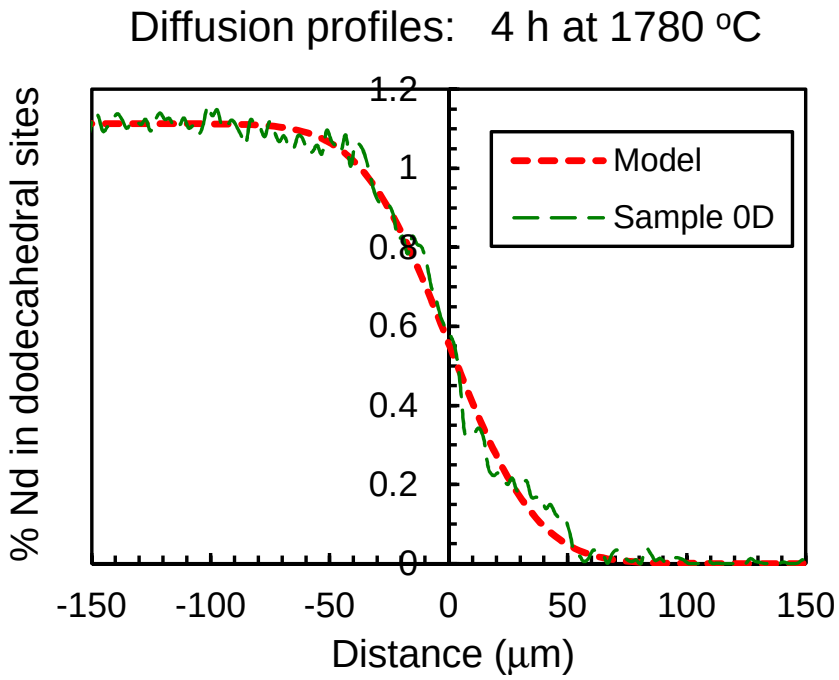

Figure B.14: EMP measurements of Nd concentration (narrow lines) and an error function fit (bold line) for YAG/Nd:YAG diffusion couples. Diffusion was carried out at 1780 °C for 4 h. Concentration values represent a percentage of dodecahedral sites filled by Nd.

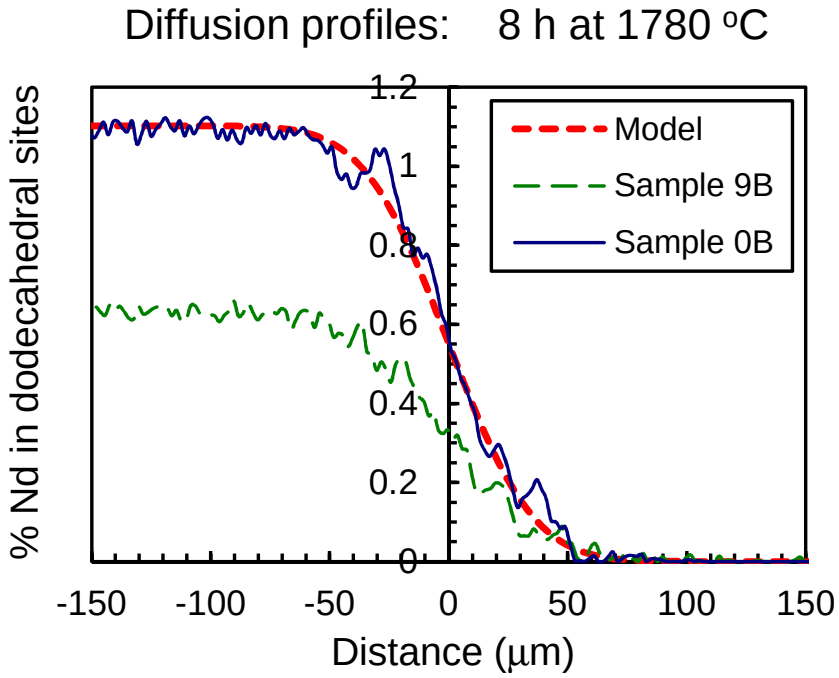

Figure B.15: EMP measurements of Nd concentration (narrow lines) and an error function fit (bold line) for YAG/Nd:YAG diffusion couples. Diffusion was carried out at 1780 °C for 8 h. Concentration values represent a percentage of dodecahedral sites filled by Nd.

Appendix C

Electron microprobe measurements: iso-structural diffusion

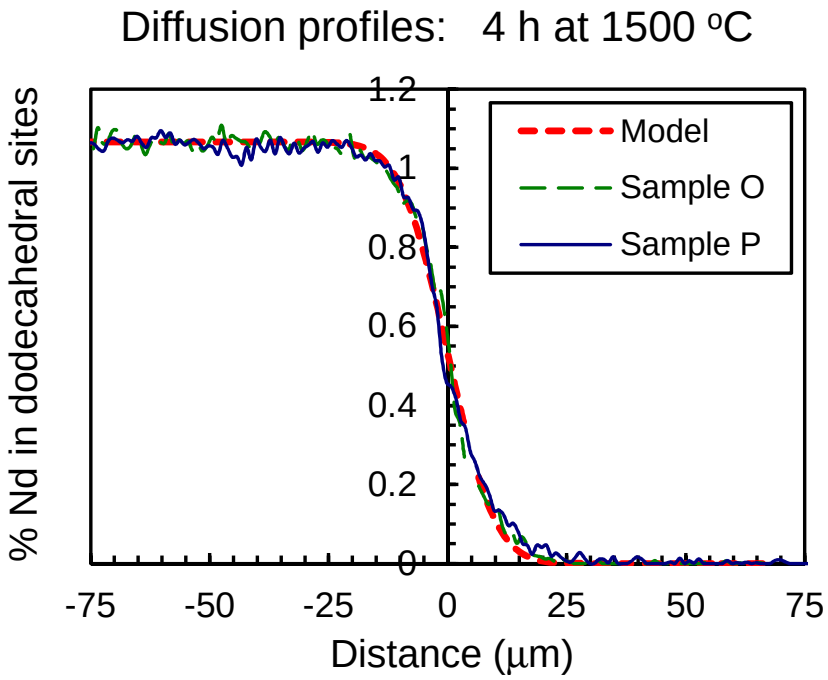

Figure C.1: EMP measurements of Nd concentration (narrow lines) and an error function fit (bold line) for YAG/Nd:YAG diffusion couples. Diffusion was carried out at 1500 °C for 4 h, following vacuum sintering at 1700 °C for 4 min. Concentration values represent a percentage of dodecahedral sites filled by Nd.

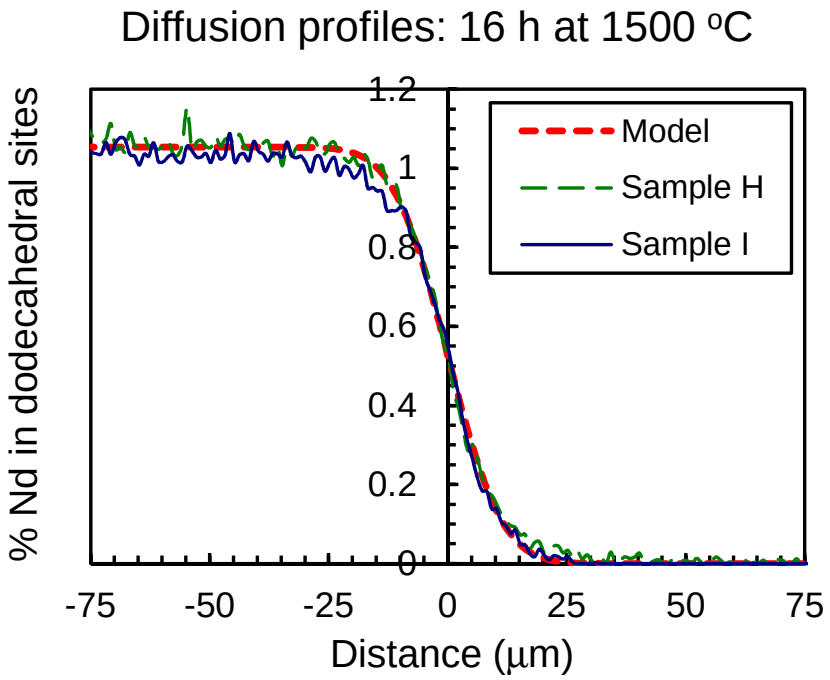

Figure C.2: EMP measurements of Nd concentration (narrow lines) and an error function fit (bold line) for YAG/Nd:YAG diffusion couples. Diffusion was carried out at 1500 °C for 16 h, following vacuum sintering at 1700 °C for 4 min. Concentration values represent a percentage of dodecahedral sites filled by Nd.

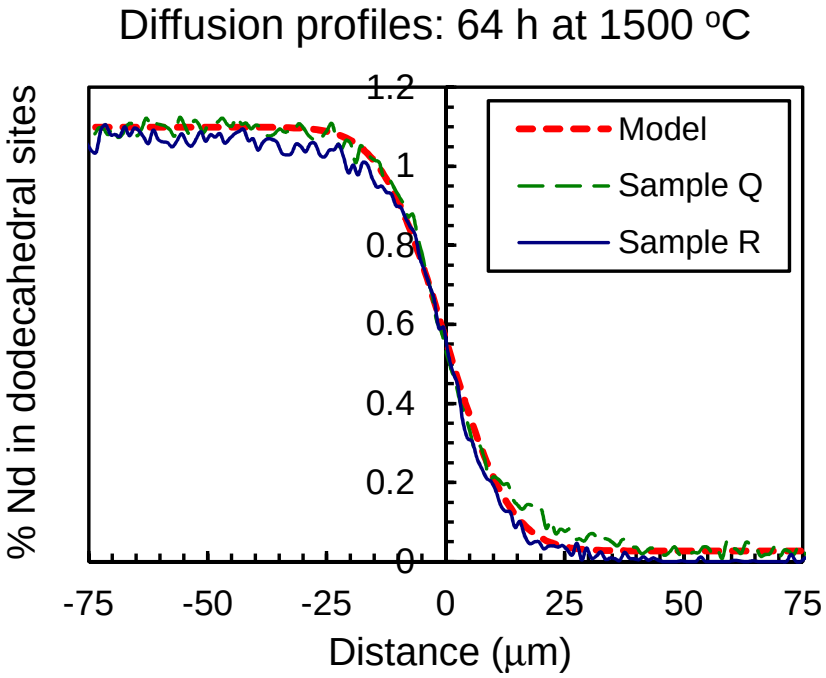

Figure C.3: EMP measurements of Nd concentration (narrow lines) and an error function fit (bold line) for YAG/Nd:YAG diffusion couples. Diffusion was carried out at 1500 °C for 64 h, following vacuum sintering at 1700 °C for 4 min. Concentration values represent a percentage of dodecahedral sites filled by Nd.

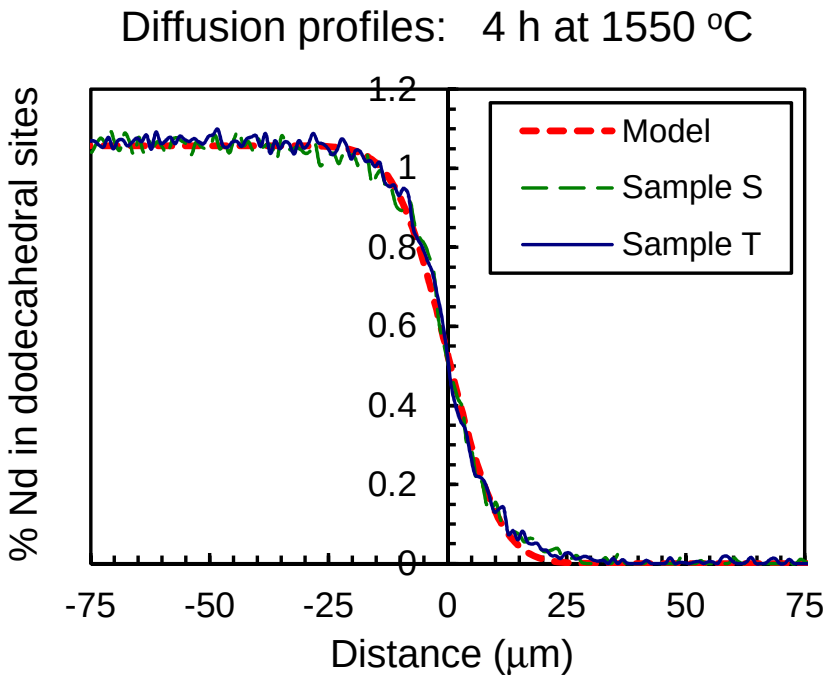

Figure C.4: EMP measurements of Nd concentration (narrow lines) and an error function fit (bold line) for YAG/Nd:YAG diffusion couples. Diffusion was carried out at 1550 °C for 4 h, following vacuum sintering at 1700 °C for 4 min. Concentration values represent a percentage of dodecahedral sites filled by Nd.

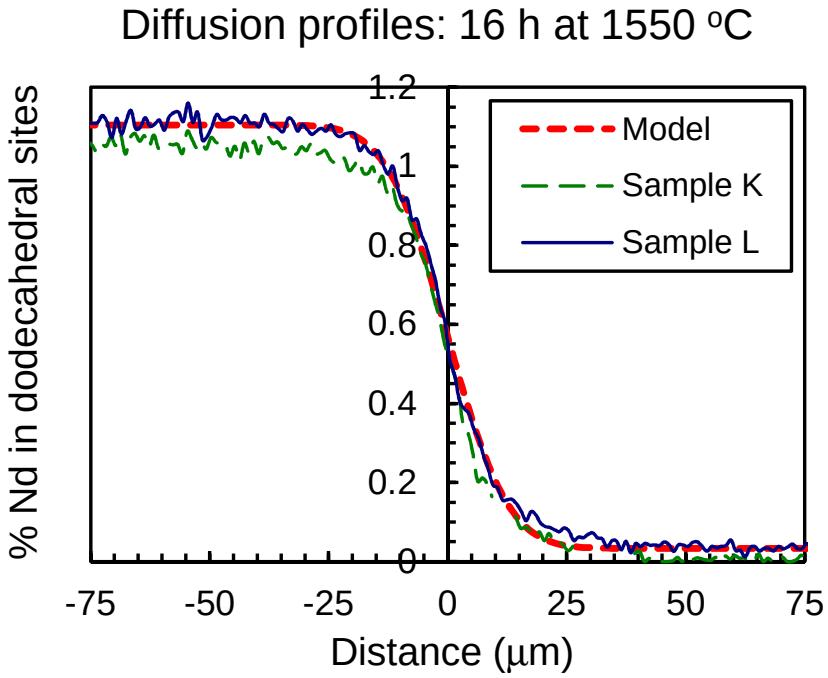

Figure C.5: EMP measurements of Nd concentration (narrow lines) and an error function fit (bold line) for YAG/Nd:YAG diffusion couples. Diffusion was carried out at 1550 °C for 16 h, following vacuum sintering at 1700 °C for 4 min. Concentration values represent a percentage of dodecahedral sites filled by Nd.

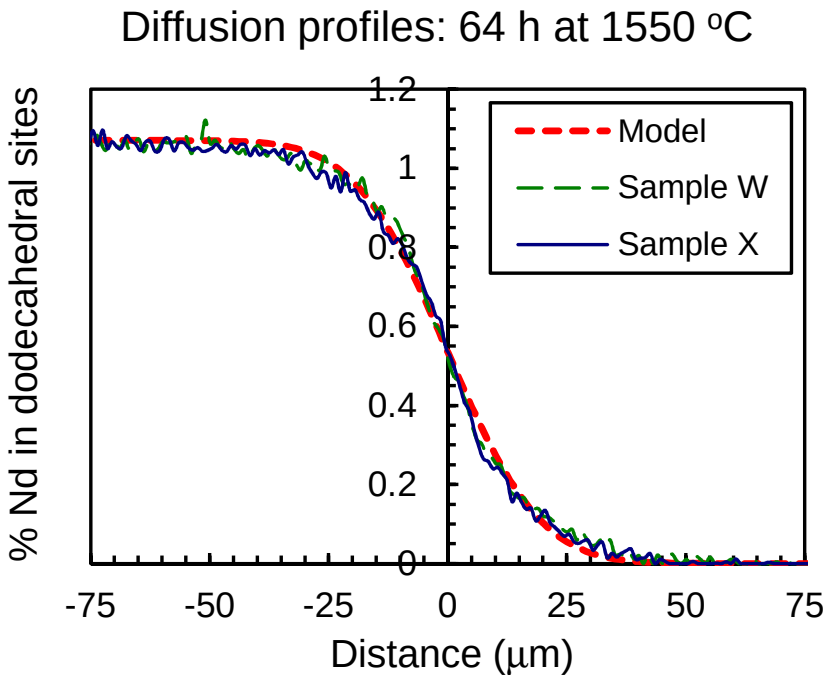

Figure C.6: EMP measurements of Nd concentration (narrow lines) and an error function fit (bold line) for YAG/Nd:YAG diffusion couples. Diffusion was carried out at 1550 °C for 64 h, following vacuum sintering at 1700 °C for 4 min. Concentration values represent a percentage of dodecahedral sites filled by Nd.

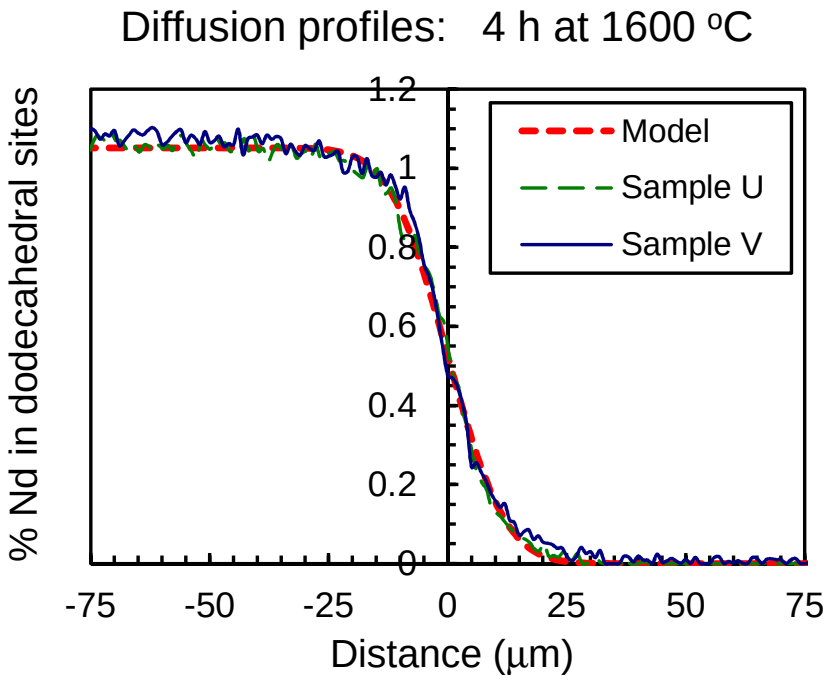

Figure C.7: EMP measurements of Nd concentration (narrow lines) and an error function fit (bold line) for YAG/Nd:YAG diffusion couples. Diffusion was carried out at 1600 °C for 4 h, following vacuum sintering at 1700 °C for 4 min. Concentration values represent a percentage of dodecahedral sites filled by Nd.

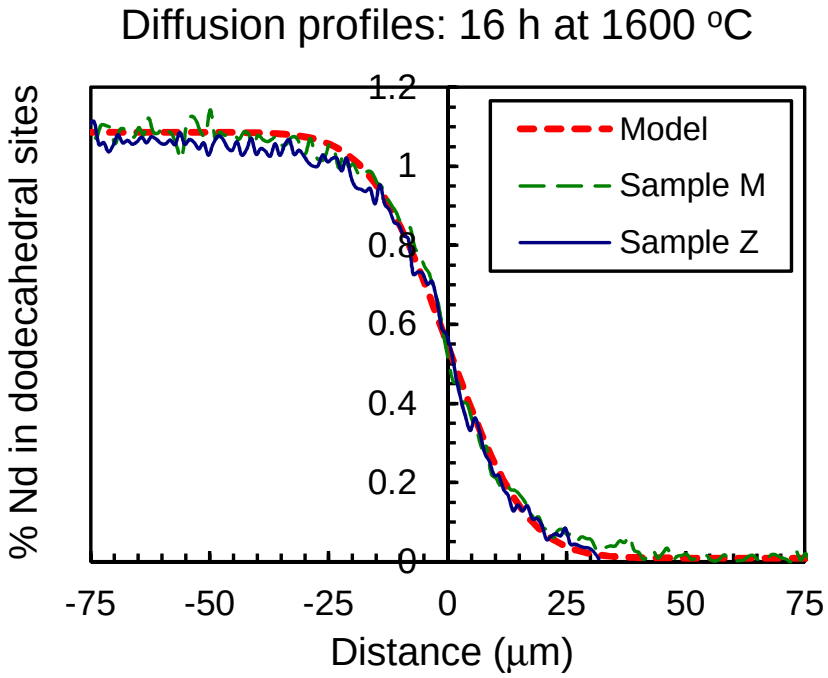

Figure C.8: EMP measurements of Nd concentration (narrow lines) and an error function fit (bold line) for YAG/Nd:YAG diffusion couples. Diffusion was carried out at 1600 °C for 16 h, following vacuum sintering at 1700 °C for 4 min. Concentration values represent a percentage of dodecahedral sites filled by Nd.

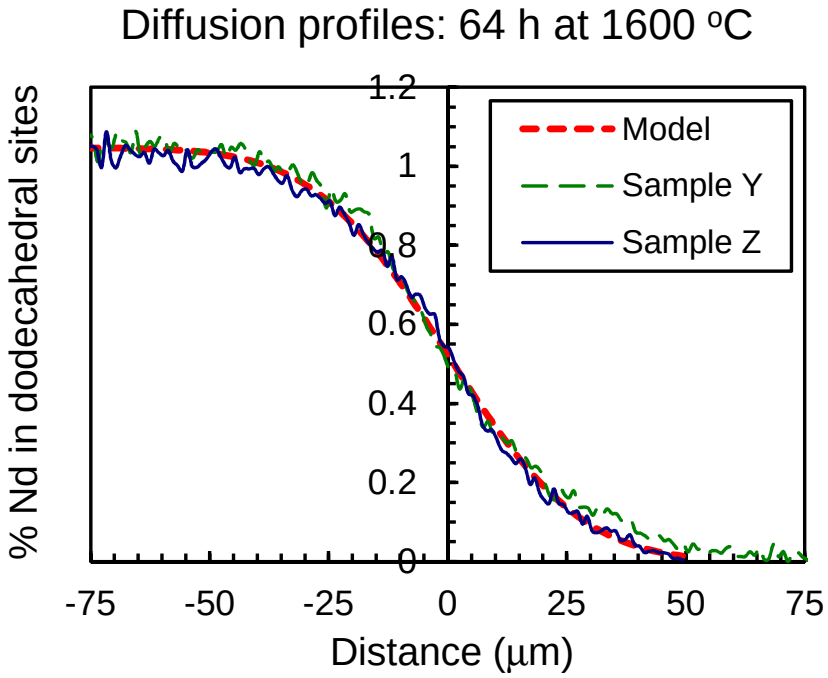

Figure C.9: EMP measurements of Nd concentration (narrow lines) and an error function fit (bold line) for YAG/Nd:YAG diffusion couples. Diffusion was carried out at 1600 °C for 64 h, following vacuum sintering at 1700 °C for 4 min. Concentration values represent a percentage of dodecahedral sites filled by Nd.

Bibliography

[1] A. Ikesue, Y. L. Aung, T. Taira, T. Kamimura, K. Yoshida, and G. L. Messing, "Progress in ceramic lasers," *Annual Review of Materials Research*, vol. 36, pp. 397–429, 2006.

[2] A. Kaminskii, M. Akchurin, V. Alshits, K. Ueda, K. Takaichi, J. Lu, T. Uematsu, M. Musha, A. Shirikawa, V. Gabler, H. Eichler, H. Yagi, T. Yanagitani, S. Bagayev, J. Fernandez, and R. Balda, "New data on the physical properties of $Y_3Al_5O_{12}$-based nanocrystalline laser ceramics," *Crystallography Reports*, vol. 48, pp. 515–519, May 2003.

[3] A. Ikesue and Y. L. Aung, "Synthesis and performance of advanced ceramic lasers," *Journal of the American Ceramic Society*, vol. 89, pp. 1936–1944, June 2006.

[4] R. R. Monchamp, "The distribution coefficient on neodymium and lutetium in Czochralski grown $Y_3Al_5O_{12}$," *Journal of Crystal Growth*, vol. 11, pp. 310–312, December 1971.

[5] J. Wisdom, *Design, characterization and fabrication of neodymium doping profiles in transparent YAG ceramics*. PhD thesis, Stanford University, 2008.

[6] D. J. Cherniak, "Rare earth element and gallium diffusion in yttrium aluminum garnet," *Physics and Chemistry of Minerals*, vol. 26, pp. 156–163, December 1998.

[7] C. Greskovich and J. P. Chernoch, "Improved polycrystalline ceramic lasers," *Journal of Applied Physics*, vol. 45, no. 10, pp. 4495–4502, 1974.

[8] R. L. Coble, "Transparent alumina and method of preparation," March 1962. US Pat. No. 3026210.

[9] R. L. Coble, "Sintering crystalline solids. II. Experimental test of diffusion models in powder compacts," *Journal of Applied Physics*, vol. 32, no. 5, pp. 793–799, 1961.

[10] R. L. Coble, "Initial sintering of alumina and hematite," *Journal of the American Ceramic Society Journal of the American Ceramic Society*, vol. 41, pp. 55–62, February 1958.

[11] J. E. Burke, "Role of grain boundaries in sintering.," *Journal of the American Ceramic Society*, vol. 40, no. 3, pp. 80–85, 1957.

[12] R. L. Coble, "Sintering crystalline solids. I. Intermediate and final state diffusion models," *Journal of Applied Physics*, vol. 32, no. 5, pp. 787–792, 1961.

[13] J. G. Peelen, *Alumina: Sintering and optical properties*. PhD thesis, Technische Hogeschool Eindhoven, Eindhoven, May 1977.

[14] T. F. Soules, "Light transmission through a Lucalox plate," tech. rep., General Electric, 1972.

[15] J. G. J. Peelen and R. Metselaar, "Light scattering by pores in polycrystalline materials: Transmission properties of alumina," *Journal of Applied Physics*, vol. 45, no. 1, pp. 216–220, 1974.

[16] E. Carnall, S. E. Hatch, L. S. Ladd, and W. F. Parsons, "Method of molding magnesium fluoride," December 1966. US Pat. No. 3294878.

[17] S. E. Hatch and R. J. Weagley, "Calcium fluoride optical elements and method for making same," December 1967. US Pat. No. 3359066.

[18] E. Carnall, "Lanthanum fluoride infrared transmitting optical elements," September 1961. US Pat. No. 3206279.

[19] E. Carnall and L. S. Ladd, "Process of hot pressing magnesium oxide infrared transmitting optical elements," April 1964. US Pat. No. 3131026.

[20] E. Carnall and S. E. Hatch, "Process of hot pressing magnesium oxide infrared transmitting optical elements," December 1968. US Pat. No. 3402226.

[21] E. Carnall and D. W. Roy, "Method of forming zinc oxide infrared transmitting optical element," December 1968. US Pat. No. 3416907.

[22] E. Carnall, P. B. Mauser, W. F. Parsons, D. W. Roy, and E. Kodak, "Process for molding zinc sulfide," April 1964. US Pat. No. 3131238.

[23] W. F. Parsons, "Optical materials research," *Appl. Opt.*, vol. 11, pp. 43+, January 1972.

[24] L. A. Brisette, P. L. Burnett, R. M. Spriggs, and T. Vasilos, "Thermomechanically deformed Y_2O_3," *Journal of the American Ceramic Society*, vol. 49, no. 3, pp. 165–166, 1966.

[25] R. A. Lefever and J. Matsko, "Transparent yttrium oxide ceramics," *Materials Research Bulletin*, vol. 2, pp. 865–869, September 1967.

[26] S. K. Dutta and G. E. Gazza, "Transparent Y_2O_3 by hot-pressing," *Materials Research Bulletin*, vol. 4, pp. 791–796, November 1969.

[27] R. C. Anderson, "Transparent yttria-based ceramics and method for producing same," December 1970. US Pat. No. 3545987.

[28] R. C. Anderson, "Transparent zirconia, hafnia-, and thoria-rare earth ceramics," February 1972. US Pat. No. 3640887.

[29] S. E. Hatch, W. F. Parsons, and R. J. Weagley, "Hot-pressed polycrystalline CaF_2:Dy^{2+} laser," *Applied Physics Letters*, vol. 5, no. 8, pp. 153–154, 1964.

[30] C. Greskovich and J. P. Chernoch, "Polycrystalline ceramic lasers," *Journal of Applied Physics*, vol. 44, no. 10, pp. 4599–4606, 1973.

[31] C. D. Greskovich and W. L. Roth, "Polycrystalline ceramic lasers," July 1975. US Pat. No. 3897358.

[32] C. Greskovich and K. N. Woods, "Fabrication of transparent ThO_2-doped Y_2O_3," *Ceramic Bulletin*, vol. 52, no. 5, pp. 473–478, 1973.

[33] G. Toda and I. Matsuyama, "Effect of BeO addition on sintering of transparent Y_2O_3," *Journal of the Japan Society of Powder and Powder Metallurgy*, vol. 35, pp. 486–491, 1988.

[34] W. H. Rhodes and J. F. Reid, "Transparent yttria ceramics containing magnesia or magnesium aluminate," November 1979. US Pat. No. 4174973.

[35] W. H. Rhodes, "Transparent yttria ceramics and method for producing same," April 1979. US Pat. No. 4147744.

[36] W. H. Rhodes, "Controlled transient solid second-phase sintering of yttria," *Journal of the American Ceramic Society*, vol. 64, no. 1, pp. 13–19, 1981.

[37] K. Majima, N. Niimi, M. Watanabe, S. Katsuyama, and H. Nagai, "Effect of LiF addition on the preparation and transparency of vacuum hot pressed Y_2O_3," *Materials Transactions*, vol. 35, no. 9, pp. 645–650, 1994.

[38] J. W. Mccauley and N. D. Corbin, "Phase relations and reaction sintering of transparent cubic aluminum oxynitride spinel (ALON)," *Journal of the American Ceramic Society*, vol. 62, no. 9-10, pp. 476–479, 1979.

[39] R. L. Gentilman, E. A. Maguire, and L. E. Dolhert, "Transparent aluminum oxynitride and method of manufacture," May 1985. US Pat. No. 4520116.

[40] R. J. Bratton, "Translucent sintered $MgAl_2O_4$," *Journal of the American Ceramic Society*, vol. 57, no. 7, pp. 283–286, 1974.

[41] D. Roy, "Hot-pressed $MgAl_2O_4$ for ultraviolet (UV), visible, and infrared (IR) optical requirements," in *Emerging Optical Materials* (S. Musikant, ed.), vol. 297, pp. 13+, Society of Photo-optical Instrumentation Engineers (SPIE), January 1981.

[42] D. W. Roy and F. J. Stermole, "Method for manufacturing a transparent ceramic body," August 1976. US Pat. No. 3974249.

[43] G. R. Villalobos, J. S. Sanghera, and I. D. Aggarwal, "Degradation of magnesium aluminum spinel by lithium fluoride sintering aid," *Journal of the American Ceramic Society*, vol. 88, no. 5, pp. 1321–1322, 2005.

[44] J.-G. Li, T. Ikegami, J.-H. Lee, and T. Mori, "Low-temperature fabrication of transparent yttrium aluminum garnet (YAG) ceramics without additives," *Journal of the American Ceramic Society*, vol. 83, no. 4, pp. 961–963, 2000.

[45] M. Shimada, T. Endo, T. Saito, and T. Sato, "Fabrication of transparent spinel polycrystalline materials," *Materials Letters*, vol. 28, pp. 413–415, October 1996.

[46] K. Tsukuma, "Transparent $MgAl_2O_4$ spinel ceramics produced by HIP post-sintering," *Nippon Seramikkusu Kyokai gakujutsu ronbunshi (Journal of the Ceramic Society of Japan)*, vol. 114, pp. 802–806, October 2006.

[47] C. R. Bickmore, K. F. Waldner, D. R. Treadwell, and R. M. Laine, "Ultrafine spinel powders by flame spray pyrolysis of a magnesium aluminum double alkoxide," *Journal of the American Ceramic Society*, vol. 79, no. 5, pp. 1419–1423, 1996.

[48] X. H. Chang, T. C. Lu, Y. Zhang, X. J. Lu, Q. Liu, C. B. Huang, J. Q. Qi, M. Y. Lei, C. X. Huang, and L. B. Lin, "$MgAl_2O_4$ transparent nano-ceramics prepared by sintering under ultrahigh pressure," *KEY ENGINEERING MATERIALS*, vol. 280-283, no. 1-2, pp. 549–552, 2005.

[49] T. Hartnett, M. Greenberg, and R. L. Gentilman, "Optically transparent yttrium oxide," August 1988. US Pat. No. 4761390.

[50] B. P. Borglum, "Method of producing optically transparent yttrium oxide," April 1991. US Pat. No. 5004712.

[51] A. Fujii and K. Shibata, "Light transmitting yttria sintered body and its preparation," December 1991. US Pat. No. 5075267.

[52] Belyakov, A., Lemeshev, D., Lukin, E., Valnin, G., Grinberg, and E., "Optically transparent ceramics based on yttrium oxide using carbonate and alkoxy precursors," *Glass and Ceramics*, vol. 63, pp. 262–264, July 2006.

[53] T. Stefanik, R. Gentilman, and P. Hogan, "Nano-composite optical ceramics for infrared windows and domes," in *Window and Dome Technologies and Materials X* (R. W. Tustison, ed.), vol. 6545A of *Proceedings of SPIE*, (Bellinghamton, WA), May 2007.

[54] M. Mitomo, Y. Moriyoshi, T. Sakai, T. Ohsaka, and M. Kobayashi, "Translucent beta-SiAlON ceramics," *Journal of Materials Science Letters*, vol. 1, pp. 25–26, January 1982.

[55] M.-A. Einarsrud and M. Mitomo, "Mechanism of grain growth of beta-SiAlON," *Journal of the American Ceramic Society*, vol. 76, no. 6, pp. 1624–1626, 1993.

[56] Z. Shen, M. Nygrenm, and U. Halenius, "Absorption spectra of rare-earth-doped alpha-SiAlON ceramics," *Journal of Materials Science Letters*, vol. 16, February 1997.

[57] X. Su, P. Wang, W. Chen, Y. Cheng, and D. Yan, "Effect of processing on microstructure and optical properties of Dy-alpha-SiAlON," *Materials Letters*, vol. 58, pp. 3340–3344, October 2004.

[58] M. I. Jones, H. Hyuga, K. Hirao, and Y. Yamauchi, "Highly transparent Lu-alpha-SiAlON," *Journal of the American Ceramic Society*, vol. 87, no. 4, pp. 714–716, 2004.

[59] J. Xue, Q. Liu, and L. Gui, "Lower-temperature hot-pressed Dy-alpha-SiAlON ceramics with an LiF additive," *Journal of the American Ceramic Society*, vol. 90, pp. 1623–1625, May 2007.

[60] D. Clay, D. Poslusny, M. Flinders, S. D. Jacobs, and R. A. Cutler, "Effect of $LiAl_5O_8$ additions on the sintering and optical transparency of LiAlON," *Journal of the European Ceramic Society*, vol. 26, no. 8, pp. 1351–1362, 2006.

[61] A. Granon, P. Goeuriot, and F. Thevenot, "Aluminum magnesium oxynitride: A new transparent spinel ceramic," *Journal of the European Ceramic Society*, vol. 15, no. 3, pp. 249–254, 1995.

[62] A. Pechenik, G. J. Piermarini, and S. C. Danforth, "Fabrication of transparent silicon nitride from nanosize particles," *Journal of the American Ceramic Society*, vol. 75, no. 12, pp. 3283–3288, 1992.

[63] R.-J. Sung, T. Kusunose, T. Nakayama, Y.-H. Kim, T. Sekino, S. Lee, and K. Niihara, "Mechanical properties of transparent polycrystalline silicon nitride," *Key Engineering Materials: The Science of Engineering Ceramics III*, vol. 317-318, pp. 305–308, 2006.

[64] Y. Xiong, Z. Fu, Y. Wang, and F. Quan, "Fabrication of transparent AlN ceramics," *Journal of Materials Science*, vol. 41, pp. 2537–2539, April 2006.

[65] N. Kuramoto and H. Taniguchi, "Transparent AlN ceramics," *Journal of Materials Science Letters*, vol. 3, pp. 471–474, June 1984.

[66] N. Kuramoto, H. Taniguchi, and I. Aso, "Translucent AlN ceramic substrate," *Components, Hybrids, and Manufacturing Technology, IEEE Transactions on*.

[67] N. Kuramoto, H. Taniguchi, and I. Aso, "Development of translucent aluminum nitride ceramics," *American Ceramic Society Bulletin*, vol. 68, no. 4, pp. 883–887, 1989.

[68] C. D. Greskovich, D. A. Cusano, and F. A. Dibianca, "Preparation of yttria-gadolinia ceramic scintillators by vacuum hot pressing," *United States Patent*, August 1984. US Pat. No. 4466929.

[69] J. Leppert, "Method for producing rare earth oxysulfide powder," October 2001. US Pat. No. 6296824.

[70] D. A. Cusano, C. D. Greskovich, and F. A. Dibianca, "Rare-earth-doped yttria-gadolina ceramic scintillators," May 1988. US Pat. No. 4747973.

[71] S. L. Dole and C. D. Greskovich, "Method of forming yttria-gadolinia ceramic scintillator from ammonium dispersed oxalate precipitates," March 1992. US Pat. No. 5100598.

[72] A. Lempicki, C. Brecher, P. Szupryczynski, H. Lingertat, V. V. Nagarkar, S. V. Tipnis, and S. R. Miller, "A new lutetia-based ceramic scintillator for X-ray imaging," *Nuclear Instruments and Methods in Physics Research Section A: Accelerators, Spectrometers, Detectors and Associated Equipment*, vol. 488, pp. 579–590, August 2002.

[73] N. Matsuda, M. Tamatani, and K. Yokota, "Method of manufacturing a rare earth oxysulfide ceramic," June 1988. US Pat. No. 4752424.

[74] C. D. Greskovich, W. P. Minnear, C. R. O'Clair, E. O. Gurmen, and R. J. Riedner, "Transparent polycrystalline garnets," January 1996. US Pat. No. 5484750.

[75] A. Lempicki, C. Brecher, H. Lingertat, and V. K. Sarin, "High-density polycrystalline lutetium silicate materials activated with ce," November 2005. US Pat. No. 6967330.

[76] Y.-K. Liao, D.-Y. Jiang, and J.-L. Shi, "Transparent lutetium aluminum garnet sintered from carbonate coprecipitated powders," *Materials Letters*, vol. 59, pp. 3724–3727, December 2005.

[77] H.-L. Li, X.-J. Liu, and L.-P. Huang, "Fabrication of transparent cerium-doped lutetium aluminum garnet (LuAG:Ce) ceramics by a solid-state reaction method," *Journal of the American Ceramic Society*, vol. 88, no. 11, pp. 3226–3228, 2005.

[78] J. D. Kuntz, J. J. Roberts, M. Hough, and N. J. Cherepy, "Multiple synthesis routes to transparent ceramic lutetium aluminum garnet," *Scripta Materialia*, vol. 57, pp. 960–963, November 2007.

[79] C. E. Land and P. D. Thacher, "Ferroelectric ceramic electrooptic materials and devices," *Proceedings of the IEEE*, vol. 57, no. 5, pp. 751–768, 1969.

[80] G. H. Haertling and C. E. Land, "Hot-pressed (Pb,La)(Zr,Ti)O_3 ferroelectric ceramics for electrooptic applications," *Journal of the American Ceramic Society*, vol. 54, no. 1, pp. 1–11, 1971.

[81] G. H. Haertling, "Improved hot-pressed electrooptic ceramics in the (Pb, La)(Zr, Ti)O_3 system," *Journal of the American Ceramic Society*, vol. 54, no. 6, pp. 303–309, 1971.

[82] G. Haertling and C. Land, "Recent improvements in the optical and electrooptic properties of PLZT ceramics," *Ferroelectrics*, vol. 3, pp. 269–280, 1972.

[83] G. S. Snow, "Improvements in atmosphere sintering of transparent PLZT ceramics," *Journal of the American Ceramic Society*, vol. 56, no. 9, pp. 479–480, 1973.

[84] K. K. Li and Q. Wang, "Electro-optic ceramic material and device," June 2004. US Pat. No. 6746618.

[85] H. Jiang, Y. K. Zou, Q. Chen, K. K. Li, R. Zhang, Y. Wang, H. Ming, and Z. Zheng, "Transparent electro-optic ceramics and devices," in *Optoelectronic Devices and Integration* (H. Ming, X. Zhang, and M. Y. Chen, eds.), vol. 5644, pp. 380–394, January 2005.

[86] A. S. S. de Camargo, Luiz, I. A. Santos, D. Garcia, and J. A. Eiras, "Structural and spectroscopic properties of rare-earth (Nd^{3+}, Er^{3+}, and Yb^{3+})

doped transparent lead lanthanum zirconate titanate ceramics," *Journal of Applied Physics*, vol. 95, no. 4, pp. 2135–2140, 2004.

[87] A. S. S. de Camargo, E. R. Botero, D. Garcia, J. A. Eiras, and L. A. O. Nunes, "Nd^{3+}-doped lead lanthanum zirconate titanate transparent ferroelectric ceramic as a laser material: Energy transfer and stimulated emission," *Applied Physics Letters*, vol. 86, no. 15, pp. 152905–152907, 2005.

[88] G. de With and H. J. A. van Dijk, "Translucent $Y_3Al_5O_{12}$ ceramics," *Materials Research Bulletin*, vol. 19, pp. 1669–1674, December 1984.

[89] A. Ikesue, T. Kinoshita, K. Kamata, and K. Yoshida, "Fabrication and optical properties of high-performance polycrystalline Nd:YAG ceramics for solid-state lasers," *Journal of the American Ceramic Society*, vol. 78, no. 4, pp. 1033–1040, 1995.

[90] A. Ikesue, K. Kamata, and K. Yoshida, "Synthesis of Nd^{3+},Cr^{3+}-codoped YAG ceramics for high-efficiency solid-state lasers," *Journal of the American Ceramic Society*, vol. 78, no. 9, pp. 2545–2547, 1995.

[91] K.-I. Ueda, "Advances in ceramic laser media," in *Frontiers in Optics*, Laser Science XXIII, (Vancouver, BC, Canada), 2007.

[92] A. Ikesue and K. Yoshida, "Scattering in polycrystalline Nd:YAG lasers," *Journal of the American Ceramic Society*, vol. 81, no. 8, pp. 2194–2196, 1998.

[93] A. Ikesue and K. Kamata, "Microstructure and optical properties of hot isostatically pressed Nd:YAG ceramics," *Journal of the American Ceramic Society*, vol. 79, no. 7, pp. 1927–1933, 1996.

[94] A. Ikesue, K. Kamata, and K. Yoshida, "Effects of neodymium concentration on optical characteristics of polycrystalline Nd:YAG laser materials," *Journal of the American Ceramic Society*, vol. 79, no. 7, pp. 1921–1926, 1996.

[95] A. Ikesue, T. Taira, Y. Sato, and K. Yoshida, "High-performance microchip lasers using polycrystalline nd:yag ceramics," *Journal of the Ceramic Society of Japan*, vol. 108, no. 4, pp. 428–430, 2000.

[96] V. Lupei, A. Lupei, S. Georgescu, T. Taira, Y. Sato, and A. Ikesue, "The effect of Nd concentration on the spectroscopic and emission decay properties of highly doped Nd:YAG ceramics," *Physical Review B*, vol. 64, no. 9, pp. 092102–092105, 2001.

[97] V. Lupei, A. Lupei, N. Pavel, T. Taira, I. Shoji, and A. Ikesue, "Laser emission under resonant pump in the emitting level of concentrated Nd:YAG ceramics," *Applied Physics Letters*, vol. 79, no. 5, pp. 590–592, 2001.

[98] M. Sekita, H. Haneda, T. Yanagitani, and S. Shirasaki, "Induced emission cross section of Nd:$Y_3Al_5O_{12}$ ceramics," *Journal of Applied Physics*, vol. 67, pp. 453–458, January 1990.

[99] J.-G. Li, T. Ikegami, J.-H. Lee, T. Mori, and Y. Yajima, "Co-precipitation synthesis and sintering of yttrium aluminum garnet (YAG) powders: The effect of precipitant," *Journal of the European Ceramic Society*, vol. 20, pp. 2395–2405, December 2000.

[100] J. Lu, M. Prabhu, J. Song, C. Li, J. Xu, K. Ueda, A. A. Kaminskii, H. Yagi, and T. Yanagitani, "Optical properties and highly efficient laser oscillation of Nd:YAG ceramics," *Applied Physics B: Lasers and Optics*, vol. 71, pp. 469–473, October 2000.

[101] J. Lu, M. Prabhu, J. Song, C. Li, J. Xu, K. I. Ueda, A. A. Kaminskii, H. Yagi, and T. Yanagitani, "Production of yttrium aluminum garnet fine powder (ittoriumu aruminiumu ganetto bifuntai no seizohoho)," 1998. Japan Patent #10-101333.

[102] J. Lu, M. Prabhu, J. Song, C. Li, J. Xu, K. I. Ueda, A. A. Kaminskii, H. Yagi, and T. Yanagitani, "Production of yttrium aluminum garnet powder (ittoriumu aruminumu ganetto funmatsu no seizohoho)," 1998. Japan Patent #10-101333.

[103] J. Lu, T. Murai, K. Takaichi, T. Uematsu, K. Misawa, M. Prabhu, J. Xu, K. Ueda, H. Yagi, T. Yanagitani, A. A. Kaminskii, and A. Kudryashov, "72 W Nd:$Y_3Al_5O_{12}$ ceramic laser," *Applied Physics Letters*, vol. 78, no. 23, pp. 3586–3588, 2001.

[104] Y. Qi, X. Zhu, Q. Lou, J. Ji, J. Dong, and Y. Wei, "Nd:YAG ceramic laser obtained high slope-efficiency of 62% in high power applications," *Optics Express*, vol. 13, pp. 8725–8729, October 2005.

[105] J. Lu, K.-I. Ueda, H. Yagi, T. Yanagitani, Y. Akiyama, and A. A. Kaminskii, "Neodymium doped yttrium aluminum garnet ($Y_3Al_5O_{12}$) nanocrystalline ceramics–A new generation of solid state laser and optical materials," *Journal of Alloys and Compounds*, vol. 341, pp. 220–225, July 2002.

[106] Y. Sato, T. Taira, and A. Ikesue, "Spectral parameters of Nd^{3+}-ion in the polycrystalline solid-solution composed of $Y_3Al_5O_{12}$ and $Y_3Sc_2Al_3O_{12}$," *Japan Journal of Applied Physics*, vol. 42, pp. 5071–5074, August 2003.

[107] *The spectroscopic properties and laser characteristics of polycrystalline Nd:$Y_3Sc_xAl_{(5-x)}O_{12}$ laser media*, vol. 83 of *OSA Trends in Optics and Photonics*, Optical Society of America, February 2003.

[108] H. Yagi, J. F. Bisson, K. Ueda, and T. Yanagitani, "$Y_3Al_5O_{12}$ ceramic absorbers for the suppression of parasitic oscillation in high-power Nd:YAG lasers," *Journal of Luminescence*, vol. 121, pp. 88–94, November 2006.

[109] T. Ikegami, T. Mori, and Y. Yajima, "Fabrication of transparent ceramics through the synthesis of yttrium hydroxide at low temperature and doping by sulfate ions," *Journal of the ceramic Society of Japan*, vol. 107, no. 1243, pp. 297–299, 1999.

[110] A. Fukabori, M. Sekita, T. Ikegami, N. Iyi, T. Komatsu, M. Kawamura, and M. Suzuki, "Induced emission cross section of a possible laser line in Nd:Y_2O_3 ceramics at 1.095 µm," *Journal of Applied Physics*, vol. 101, no. 4, 2007.

[111] J. Lu, J. Lu, T. Murai, K. Takaichi, T. Uematsu, K.-I. Ueda, H. Yagi, T. Yanagitani, and A. A. Kaminskii, "Nd^{3+}:Y_2O_3 ceramic laser," *Japan Journal of Applied Physics*, vol. 40, pp. L1277–L1279, December 2001.

[112] J. Lu, K. Takaichi, T. Uematsu, A. Shirakawa, M. Musha, K.-I. Ueda, H. Yagi, T. Yanagitani, and A. A. Kaminskii, "Yb^{3+}:Y_2O_3 ceramics - A novel solid-state laser material," *Japanese Journal of Applied Physics*, vol. 41, pp. L1373–L1375, December 2002.

[113] J. Kong, J. Lu, K. Takaichi, T. Uematsu, K. Ueda, D. Y. Tang, D. Y. Shen, H. Yagi, T. Yanagitani, and A. A. Kaminskii, "Diode-pumped Yb:Y_2O_3 ceramic laser," *Applied Physics Letters*, vol. 82, no. 16, pp. 2556–2558, 2003.

[114] J. Kong, D. Y. Tang, J. Lu, and K. Ueda, "Spectral characteristics of a Yb-doped Y_2O_3 ceramic laser," *Applied Physics B*, vol. 79, pp. 449–455, 2004.

[115] N. Saito, S.-I. Matsuda, and T. Ikegami, "Fabrication of transparent yttria ceramics at low temperature using carbonate-derived powder," *Journal of the American Ceramic Society*, vol. 81, pp. 2023–2028, August 1998.

[116] J.-G. Li, T. Ikegami, and T. Mori, "Fabrication of transparent Sc_2O_3 ceramics with powders thermally pyrolyzed from sulfate," *Journal of Materials Research*, vol. 18, pp. 1816–1822, May 2003.

[117] J. G. Li, T. Ikegami, and T. Mori, "Solution-based processing of Sc_2O_3 nanopowders yielding transparent ceramics," *Journal of Materials Research*, vol. 19, pp. 733–736, March 2004.

[118] J. Lu, J. F. Bisson, K. Takaichi, T. Uematsu, A. Shirakawa, M. Musha, K. Ueda, H. Yagi, T. Yanagitani, and A. A. Kaminskii, "Yb^{3+}:Sc_2O_3 ceramic laser," *Applied Physics Letters*, vol. 83, no. 6, pp. 1101–1103, 2003.

[119] J. Lu, K. Takaichi, T. Uematsu, A. Shirakawa, M. Musha, K. Ueda, H. Yagi, T. Yanagitani, and A. A. Kaminskii, "Promising ceramic laser material: Highly transparent Nd^{3+}:Lu_2O_3 ceramic," *Applied Physics Letters*, vol. 81, no. 23, pp. 4324–4326, 2002.

[120] A. A. Kaminskii, S. N. Bagayev, K. Ueda, K. Takaichi, A. Shirakawa, S. N. Ivanov, E. N. Khazanov, A. V. Taranov, H. Yagi, and T. Yanagitani, "New results on characterization of highly transparent nanocrystalline C-modification Lu_2O_3 nanocrystalline ceramics: Room-temperature tunable CW laser action of Yb^{3+} ions under LD-pumping and the propagation kinetics of non-equilibrium acoustic phonons," *Laser Physics Letters*, vol. 3, no. 8, pp. 375–379, 2006.

[121] P. Aubry, A. Bensalah, P. Gredin, G. Patriarche, D. Vivien, and M. Mortier, "Synthesis and optical characterizations of Yb-doped CaF_2 ceramics," *Optical Materials*, vol. 31, no. 5, pp. 750 – 753, 2009. Selected Papers from the 3rd Laser Ceramics Symposium: International Symposium on Transparent Ceramics for Photonic Applications.

[122] T. T. Basiev, M. E. Doroshenko, P. P. Fedorov, V. A. Konyushkin, S. V. Kuznetsov, V. V. Osiko, and Akchurin, "Efficient laser based on CaF_2-SrF_2-YbF_3 nanoceramics," *Opt. Lett.*, vol. 33, pp. 521–523, March 2008.

[123] A. Gallian, V. V. Fedorov, S. B. Mirov, V. V. Badikov, S. N. Galkin, E. F. Voronkin, and A. Lalayants, "Hot-pressed ceramic Cr^{2+}:ZnSe gain-switched laser," *Optics Express*, vol. 14, pp. 11694–11701, November 2006.

[124] D. Kracht, M. Frede, R. Wilhelm, and C. Fallnich, "Comparison of crystalline and ceramic composite Nd:YAG for high power diode end-pumping," *Optics Express*, vol. 13, pp. 6212–6216, August 2005.

[125] A. Strasser and M. Ostermeyer, "Improving the brightness of side pumped power amplifiers by using core doped ceramic rods," *Optics Express*, vol. 14, pp. 6687–6693, July 2006.

[126] J. Dong, A. Shirakawa, K. I. Ueda, H. Yagi, T. Yanagitani, and A. A. Kaminskii, "Ytterbium and chromium doped composite $Y_3Al_5O_{12}$ ceramics self-Q-switched laser," *Applied Physics Letters*, vol. 90, pp. 191106–191108, May 2007.

[127] N. Ter-Gabrielyan, L. D. Merkle, E. R. Kupp, G. L. Messing, and M. Dubinskii, "Efficient resonantly pumped tape cast composite ceramic Er:YAG laser at 1645 nm," *Opt. Lett.*, vol. 35, pp. 922–924, Apr. 2010.

[128] C. Scott, M. Kaliszewski, C. Greskovich, and L. Levinson, "Conversion of polycrystalline Al_2O_3 into single-crystal sapphire by abnormal grain growth," *Journal of the American Ceramic Society*, vol. 85, no. 5, pp. 1275–1280, 2002.

[129] W. D. Kingery and M. Berg, "Study of the initial stages of sintering solids by viscous flow, evaporation-condensation, and self-diffusion," *Journal of Applied Physics*, vol. 26, no. 10, pp. 1205–1212, 1955.

[130] M. I. Peters and I. E. Reimanis, "Grain boundary grooving studies of yttrium aluminum garnet (YAG) bicrystals," *Journal of the American Ceramic Society*, vol. 86, no. 5, pp. 870–872, 2003.

[131] I. Sakaguchi, H. Haneda, J. Tanaka, and T. Yanagitani, "Effect of composition on the oxygen tracer diffusion in transparent yttrium aluminium garnet (YAG) ceramics," *Journal of the American Ceramic Society*, vol. 79, no. 6, pp. 1627–1632, 1996.

[132] M. Jimenez-Melendo, H. Haneda, and H. Nozawa, "Ytterbium cation diffusion in yttrium aluminum garnet (YAG)—Implications for creep mechanisms," *Journal of the American Ceramic Society*, vol. 84, no. 10, pp. 2356–2360, 2001.

[133] S. Pratsinis, "Flame aerosol synthesis of ceramic powders," *Progress in Energy and Combustion Science*, vol. 24, no. 3, pp. 197–219, 1998.

[134] L. Madler, H. Kammler, R. Mueller, and S. Pratsinis, "Controlled synthesis of nanostructured particles by flame spray pyrolysis," *Journal of Aerosol Science*, vol. 33, pp. 369–389, February 2002.

[135] J. P. Hollingsworth, J. D. Kuntz, and T. F. Soules, "Neodymium ion diffusion during sintering of Nd : YAG transparent ceramics," *Journal of Physics D: Applied Physics*, vol. 42, pp. 052001+, Mar. 2009.

[136] J. P. Hollingsworth, J. D. Kuntz, F. J. Ryerson, and T. F. Soules, "Nd diffusion in YAG ceramics," *Optical Materials*, vol. 33, pp. 592–595, Feb. 2011.

[137] P. G. Shewmon, *Diffusion in Solids*, ch. Diffusion equations, pp. 19–22. In [147], 2 ed., Oct. 1989.

[138] P. G. Shewmon, *Diffusion in Solids*, ch. High diffusivity paths, pp. 202–203. In [147], 2 ed., Oct. 1989.

[139] F. C. Pampel, *Logistic Regression: A Primer (Quantitative Applications in the Social Sciences)*, pp. 54–60. SAGE Publications, Inc, 1 ed., May 2000.

[140] T. A. Parthasarathy, T.-I. Mah, and K. Keller, "Creep mechanism of polycrystalline yttrium aluminum garnet," *Journal of the American Ceramic Society*, vol. 75, no. 7, pp. 1756–1759, 1992.

[141] X.-H. Wang, P.-L. Chen, and I.-W. Chen, "Two-step sintering of ceramics with constant grain-size, I. Y_2O_3," *Journal of the American Ceramic Society*, vol. 89, no. 2, pp. 431–437, 2006.

[142] D. J. Cherniak, "Rare earth element and gallium diffusion in yttrium aluminum garnet," *Physics and Chemistry of Minerals*, vol. 26, pp. 156–163, Dec. 1998.

[143] J. A. Wisdom, R. Gaume, R. Route, Y. L. Aung, A. Ikesue, and R. L. Byer, "Design of transverse Nd doping profiles in transparent YAG ceramics for edge-pumped laser geometries," in *Solid State Lasers XVII: Technology and Devices* (W. A. Clarkson, A. V. Kudryashov, J. Broeng, S. J. Davis, S. Mecherle, P. E. Powers, M. S. Zediker, O. Korotkova, A. S. Holmes, W. Pfleging, J. Neev, S. Nolte, Y. Lu, M. C. Heaven, M. Meunier, C. Headley, A. H. Paxton, N. Hodgson, R. K. Shori, V. S. Ilchenko, C. B. Arnold, J. T. Schriempf, K. Washio, A. Heisterkamp, C. B. Schaffer, W. Hoving, H. Niino, D. B. Geohegan, J. Amako, F. Träger, and J. J. Dubowski, eds.), no. 6871, pp. 68711I–68711I–12, SPIE, Feb. 2008.

[144] M. O. Ramirez, J. Wisdom, H. Li, Y. L. Aung, J. Stitt, G. L. Messing, V. Dierolf, Z. Liu, A. Ikesue, R. L. Byer, and V. Gopalan, "Three-dimensional grain boundary spectroscopy in transparent high power ceramic laser materials," Mar. 2008.

[145] J. R. Hayes, G. W. Nyce, and J. D. Kuntz, "Filter casting nanoscale porous materials," Feb. 2013. US Pat. Application No. 20130037982.

[146] J. P. Hollingsworth, J. D. Kuntz, Z. M. Seeley, and T. F. Soules, "Transparent ceramics and methods of preparation thereof," Oct 2011. US Pat. No. 8039413.

[147] P. G. Shewmon, *Diffusion in Solids*. Wiley, 2 ed., Oct. 1989.